Imperial College London
Department of Civil and Environmental Engineering

Assessing the impacts of land-use change on the hydrology of the tropical Andes

Hsi-Kai Chou

2019

Submitted in part fulfilment of the requirements for the degree of
Doctor of Philosophy in Civil and Environmental Engineering of Imperial College London
and the Diploma of Imperial College London

Declaration of Originality

The contents of this report are all my own work, and any quotation from, or description of, the work of others is fully acknowledged by reference to the sources, whether published or unpublished.

Copyright Declaration

Abstract

Land-use and land-cover change (LUCC) has been identified as a major driver of change to the hydrological cycle. However, it is still a scientific challenge to quantify these effects. Land surface models are increasingly being used for such hydrological assessment because of their state-of-the-art representation of physical processes and versatility. A physically-based model has the advantage to map the modeller's knowledge about the hydrological impacts of land-use and land-cover change into physically meaningful parameters. This PhD thesis explores the use of a land surface model (Joint UK Land-Environment Simulator, JULES) in combination with high temporal resolution in-situ data on streamflow, precipitation, and several weather variables, collected by a grassroots hydrological monitoring initiative (called iMHEA) in the tropical Andes. I find that the in-situ data can improve the hydrological simulation substantially, mainly by reducing uncertainty inherent in using large-scale precipitation data. The commonly used soil parameters based on pedotransfer functions lead to an underestimation of the flow. Therefore, I modified the soil parameterisation with experimental data for a more accurate representation of subsurface flow generation. Subsequently, I assessed the potential impacts of watershed interventions (grazing, afforestation, cultivation) using the calibrated soil parameters. A reduction in water yield and water regulation ability under these land use scenarios was identified, which is in line with observed impacts and relevant for water resources managers. In a next step, I implemented an open source land use change model, the lulcc R package, to analyse the regional land cover changes in the Andean region, and to generate predictive land use maps that can be used to drive the JULES model. For this purpose, the JULES model has been implemented at a regional scale using multiple sources of global data. The use of the JULES model allows the effects of LUCC to be assessed using knowledge about physical processes. My results show a further 3.7% of deforestation occurring in the region, which changes the flow by ±17% consequently.

Acknowledgements

Funding for this PhD research was gratefully received from “Taiwan Top University Strategic Alliance PhD Scholarships – Imperial PhD Scholarships” of the Ministry of Education, Taiwan. I am very honoured to be educated with the pioneer knowledge and prosperous activity of hydrological research at Imperial College London.

I would like to express the deepest appreciation to my supervisor Dr Wouter Buytaert for sharing his expertise, giving advice on my research, and guiding me on pursuing scientific knowledge. My sincere thanks also go to Dr Ana Mijic and Dr Lina Mercado for providing precious feedbacks for finalising the PhD Thesis.

I am grateful to Dr Bert De Bièvre and the Water Protection Fund of Quito (FONAG) for their warm hospitality on my field study in Quito. I also thank all partners of the Regional Initiative for Hydrological Monitoring of Andean Ecosystems (iMHEA) for providing hydrometeorological data used in this research.

I am pleased to be a part of the Environmental and Water Resource Engineering section, especially thanks to my colleagues for bringing this research environment. My grateful recognition to Dr Boris Ochoa-Tocachi for collaborating ideas with his knowledge and expertise, to Dr Simon Moulds for his assistance on the application of lulccR package, and to Dr Jonathan Paul for his advice on my research activities. I would also like to mention Charles Zogheib, Anna Twomlow, Neeraj Sah, Yuting Chen, Jimmy O’Keeffe, Simon De Stercke, Greta Antonini for their companionship through the PhD study. I thank the support provided by my closest friends, Yueh Ho Chiu, Joanne Chiueh, Chunching Li, Chia-Han Yeh, and Greg Sheen.

I would like to appreciate the unlimited support from my family, Dr Tung-Sheng Chou, Yi-Ling Wu, and Chia-Ying Chou. None of these milestones could be completed without their unconditional love, support, and encouragement.

Contents

List of Tables

List of Figures

1 Introduction

1.1 Human impact on the hydrological cycle

1.1.1 Global hydrological cycle

The hydrological cycle refers to the water movements between different natural area of the global land surface (Figure 1.1). The upper boundary condition of the terrestrial hydrological cycle is precipitation in the form of rainfall or snow. Precipitation may be intercepted by the vegetation cover, infiltrate into soil, or directly run over the land surface to generate streamflow. The infiltrated water is stored in the soil column or drains as subsurface flow. Water is returned to the atmosphere as a result of evaporation from soil and vegetation interception, or as transpiration by the vegetation. As the volume of precipitation in many regions exceeds the evaporation in the terrestrial hydrological cycle, the excess is return to the oceans as runoff (Chahine, 1992). In this PhD research, I particularly focused on evaluating the terrestrial hydrological fluxes under changes of land use and land cover.

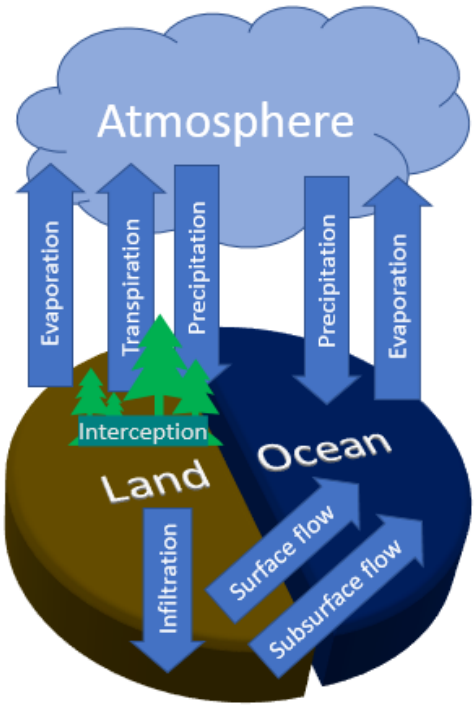

Figure 1.1 The Global Hydrological Cycle

1.1.2 Global dynamics of land use change

Land use change such as cultivation, livestock grazing, construction, timber extraction has considerably transformed global land cover (Turner, B. L., Meyer & Skole, 1994). Land cover can be prone to degradation (e.g. overgrazed grassland), conservation (e.g. restoration) or be converted to another land cover type (e.g. clearance of forest). These land use and land cover changes (LUCC) have cumulatively affected the global environment, in terms of climate, atmospheric composition, biodiversity, soil condition, water and sediment flows (Turner, B. L., Meyer & Skole, 1994). Of the different type of LUCC, deforestation and expansion of cropland are the major ones (Turner, B. L., Meyer & Skole, 1994) accelerated by the economic growth and globalization (Lambin & Meyfroidt, 2011).

The highest increase in deforestation (increased at 1021 km^2/year rate) was reported in Indonesia from 2000 (10000 km^2/year) through 2012 (over 20000 km^2/year). Globally, over 4 million km^2 of land cover has been changed between 2001 and 2012, which consisted of 3.3% changes of the total land identified with the available data covering 84.1% of the Earth's land surface (Borrelli et al., 2017). Deforestation is the biggest change, with 2.07 million km^2 of forest been converted to semi-natural vegetation (savannah, scrublands, grassland, transition forest) and 0.094 million km^2 been cultivated in this period. In the same time, 0.61 million km^2 of areas was afforested for propose such as carbon sequestration (Farley, Jobbágy & Jackson, 2005), which led to a combined 1.65 million km^2 of forest area decrease (Borrelli et al., 2017; Hansen et al., 2013).

Cultivation is the second largest driver of LUCC, which includes the transition from forest (0.094 million km^2), semi-natural vegetation (0.67 million km^2), and the contrary process (0.49 million km^2 cropland to semi-natural vegetation, and 0.055 million km^2

cropland to forest) which totally expend the cropland by 0.22 million km^2.

The expansion of cropland drives the deforestation in all continents within the subtropical regions, including South Africa, central Chile, southeastern Brazil, Uruguay, southern China, Australia, and New Zealand (Hansen et al., 2013). Forestry is the major driver of deforestation in temperate regions, including intensive forestry in the northwest United States, temperate Canada, Estonia and Latvia (Hansen et al., 2013). In boreal region, forestry is found in Sweden, Finland, eastern Canada, parts of European Russia, and central Siberia, Russia. The largest area of forest loss is found in Russia (Hansen et al., 2013). The tropical regions have experienced the major deforestation dynamics (32% of the total forest losses), which threatened the Brazilian rainforest, the Eurasian tropical rainforest, the African tropical moist deciduous forest, the South American dry tropical forest, the Eurasian tropical moist deciduous and the dry forests (Hansen et al., 2013).

1.1.3 Impacts on hydrological cycles

Hydrological evidence worldwide suggests that land use and land cover changes have a significant impact to the hydrological cycle (Table 1.1). The vegetation types, soil properties, and landscape of river basins can be considerably altered by increasing human activities, which consequently led to hydrological changes in transpiration, infiltration, and interception. These changes are particularly important in headwater catchments (Buytaert et al., 2006). Thus, understanding these hydrological processes is essential and contributes to successful water resource management.

Changes in vegetation types affect runoff directly by intercepting precipitation, transpiration extraction, and indirectly by affecting soil infiltration. Canopy interception is found to be low in grasslands, but is considerably higher for broadleaf trees (10-20% of precipitation) and conifers (20-40% of precipitation) (Le Maitre, Scott & Colvin, 1999). In Andean regions, 30% of forest interception was estimated, and 11% for grassland and cropland (Molina et al., 2012). The transpiration rate is determined by rooting characteristics, leaf area, stomatal response, plant surface albedo, and turbulence (Farley, Jobbágy & Jackson, 2005). A higher leaf area index and a deeper and better-developed root system of forest leads to higher transpiration than grassland (Buytaert, Iniguez & De Bievre, 2007). The evapotranspiration in forest catchment is typically higher than a grassland covered catchment (Zhang, Dawes & Walker, 2001). Therefore , a flow reduction is often found in afforested catchments (Buytaert, Iniguez & De Bievre, 2007; Farley, Jobbágy & Jackson, 2005; Ochoa-Tocachi et al., 2016), whereas a flow increment is found in deforested catchments (Guzha, Rufino et al., 2018b; Molina et al., 2012). The vegetation dynamics affect evapotranspiration not only because of the change in vegetation properties, but also tends to have an effect on the soil properties (Buytaert et al., 2006). Increasing soil

erosion has been observed in the transition from forests to cropland (Borrelli et al., 2017). Intensive sheep grazing can lead to crust formation, increase in runoff, erosion, and reduction in hydraulic conductivity in the Ecuadorian páramo (Buytaert et al., 2006). At the catchment scale a 40% loss of water regulation capacity has been found in intensively grazed and cultivated páramo catchments (Buytaert, 2004). Despite of these effects, soils have been drained and ploughed intensively for cultivation in Ecuador (Buytaert et al., 2005), which reduced the available water storage, hence reduced the evaporation.

The hydrological response can also be affected by changes at the larger landscape topography scale. Buytaert et al. (2006) indicated that a decrease in surface roughness and local depressions by the removal of the vegetation and the organic litter layer considerably affects the delay of surface runoff. Molina et al. (2007) found that degraded land with lower vegetation cover and lower soil organic matter content could transform the area to a saturation excess dominated flow regime by reducing infiltration capacity. In these conditions surface properties be more important for a saturation excess flow rather than an infiltration excess flow (Hortonian flow) (Buytaert et al., 2006). A faster hydrological response was observed under a cultivated land despite its higher saturated hydraulic conductivity, infiltration capacity, and water storage capacity (Buytaert et al., 2005).

Table 1.1 Overview of reviewed studies on the hydrological impacts of LUCC

LUCC	Hydrological impact	Location	References
Cultivation (potato) & grazing	Reducing hydrological regulation capacity Reducing runoff by 15% Increasing water storage capacity by 5 to 30% Increasing hydraulic conductivity by 31%	Huagrahuma & Soroche, Ecuador	(Buytaert, Iniguez & De Bievre, 2007) (Buytaert et al., 2005)
Cultivation	Reducing hydrological regulation capacity Reducing runoff by 12~15%	Paute, Ecuador Tiquipaya, Bolivia	(Ochoa-Tocachi et al., 2016)
Cultivation (soybean)	Increasing infiltrability from 100 to 469mm/h Enhancing subsoil compaction: decreased saturated hydraulic conductivity at 30cm from 122 to 80 mm/h	Mato Grosso, Brazil	(Scheffler et al., 2011)
Grazing	No significant impact on runoff	Piura & Huaraz, Peru	(Ochoa-Tocachi et al., 2016)
Burning and grazing	Increasing runoff Reducing saturated hydraulic conductivity	Pichincha, Ecuador	(Poulenard et al., 2001)
Afforestation	Reducing runoff by 30-40% (pine), 38-75% (Eucalypts)	Global data (India, the UK, Germany, Australia, New Zealand, South Africa)	(Farley, Jobbágy & Jackson, 2005)
Afforestation (Pine)	Reducing peak and base flows Reducing runoff by 64% Increasing hydrological regulation capacity Reducing runoff by 53~68%	Marianza, Ecuador Paute, Ecuador Chachapoyas & Tambobamba, Peru	(Buytaert, Iniguez & De Bievre, 2007) (Ochoa-Tocachi et al., 2016)
Deforestation	Increasing baseflow by 25 mm/year Increasing surface runoff by 4–90%	Jadan, Ecuador East Africa	(Molina et al., 2012) (Guzha, Rufino et al., 2018a)
Deforestation	Decreasing infiltrability from 1258 to 100mm/h Reducing saturated hydraulic conductivity	Mato Grosso, Brazil	(Scheffler et al., 2011)

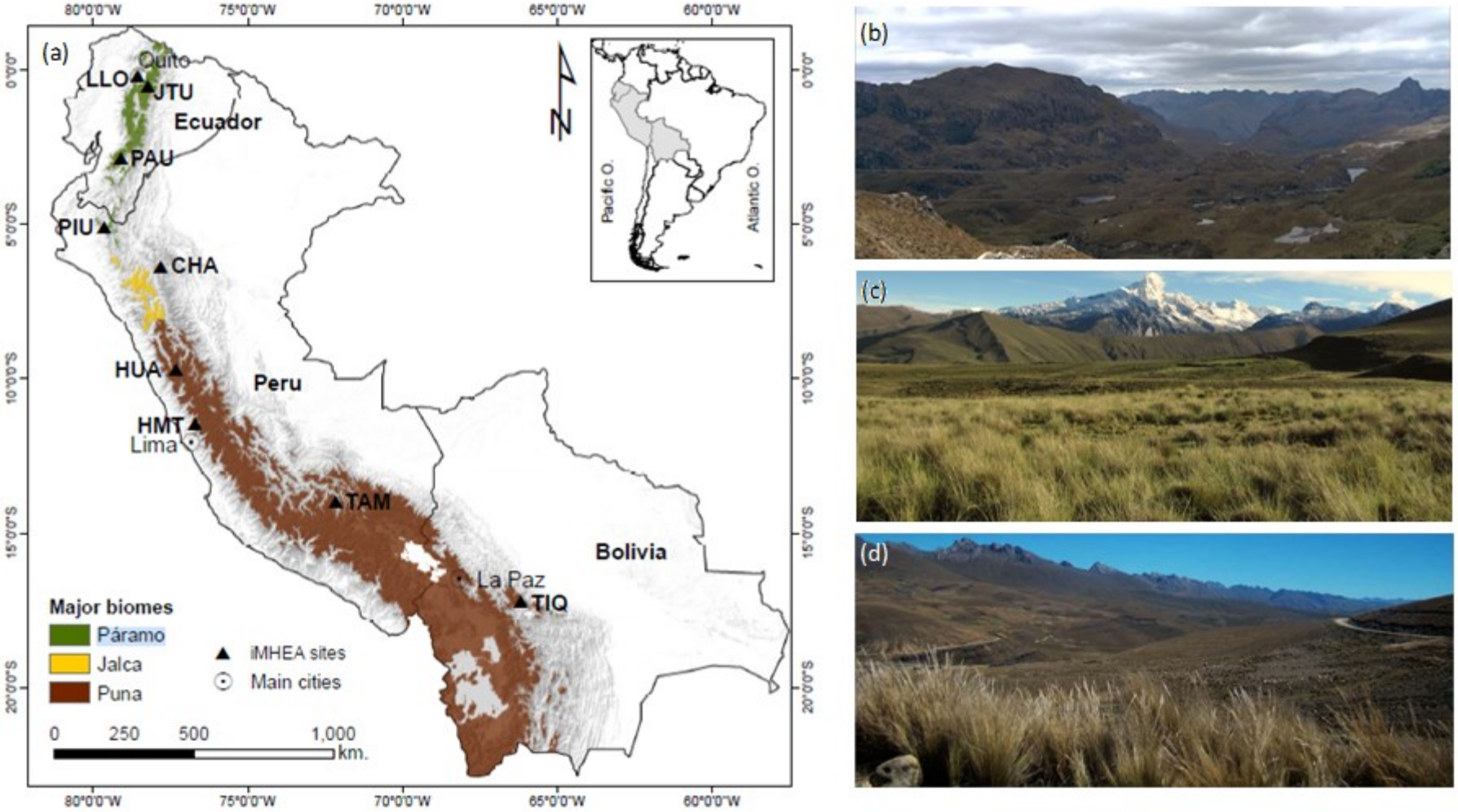

Figure 1.2 a) The distribution of major biomes of the tropical Andes, b) Humid páramo in southern Ecuador, c) Humid puna in central Perú, d) Dry puna in central Bolivia. Source: Ochoa-Tocachi et al. (2018)

1.2 Hydrology of the tropical Andes

The Andean region has been a hotspot of hydrological change, which warrants studying because of its important role in regional water supply and vulnerability to human activities. However, these effects are hard to identify and quantify due to the high data requirement to investigate how such changes propagate through the complex and interacting hydrological processes of a catchment (Viviroli et al., 2007).

In the tropical Andes, the major hydrological processes are defined by varying bio-physical properties within a variety of ecosystems. The páramo, jalca, and puna are high altitude neotropical ecosystems distributed within different latitude (Figure 1.2). Approximately 35,000 km^2 of areas in Northern Colombia and Venezuela to northern Perú are covered by a discontinuous belt of páramo, a collection of neotropical alpine ecosystems within the grassland biome, which is consisted of glacier formed valleys, a large variety of lakes, peat bogs, and wet grasslands with shrublands and low-statured forest patches (Buytaert et al., 2006). Jalca locates in the transition region from páramo to puna in the regions of northern to central Perú. Humid puna ranges from eastern Perú to the north-eastern Bolivian Cordillera, whereas dry puna could be found in its west side, from western Perú until the southwest of Bolivia and northern Argentina and Chile (Ochoa-Tocachi et al., 2016). Below those ecosystems, montane forests and cloud forests are characteristic forests that can be found at elevations above 1000 m in the Andes, classified by the presence of permanent could (Célleri et al., 2009).

The Andes provide a wide range of ecosystem services, including biodiversity conservation, nutrient recycling, carbon storage and sequestration, high quality water provision and hydrological regulation, with its complexity of landscapes (Buytaert, Cuesta-Camacho & Tobón, 2011). Of those, the provision of water may be the most

important service of Andean ecosystems. The Andean páramo is featured by its large water surplus, extreme water regulating capacity, and sustained base flow (Buytaert et al., 2006), which covers the headwaters of the major largest rivers of the Amazon basin (Célleri et al., 2009). It supports the water needs for major downstream Andean populations, smallholder irrigated agriculture, industrial consumption, and hydroelectricity production (Buytaert et al., 2014).

Despite its importance of water supply, these mountain areas are particularly vulnerable and prone to human impact. Drastic changes in the water cycle have been produced by human activities as a result of the rapid economic growth during the past half-century (Harden, 2006). Land-use and land-cover change (LUCC) led by deforestation, oil exploitation, mining, and hydropower production (Zulkafli et al., 2013), and the significantly increasing demand for páramo water for the purposes of intensive cattle grazing, cultivation, and pine planting (Buytaert et al., 2006) highlights the importance of water resources management. Therefore, the hydrology of these water sources requires to be assessed systematically.

Hydrological processes are usually poorly understood in these remote mountain regions since they are often determined by complex catchment characteristics (Viviroli et al., 2007). In addition, external drivers of change such as global warming (Bradley et al., 2006; Urrutia & Vuille, 2009) and population growth (Buytaert & De Bièvre, 2012), further complicate hydrological studies. In the Andean region, the water yield mechanism with small-scale, pristine and human-altered catchments related is explored by several research initiatives (Célleri et al., 2009). Buytaert et al. (2006) identified the effect of human activities on the páramo ecosystem by using a pairwise catchment approach. Breuer, Vache & Frede (2006) analysed the functioning of montane and cloud forests by applying a nested-approach.

Although a series of studies have been carried out, the hydrology and water

balance of these mountain basins are still poorly understood (Célleri et al., 2009). In order to extrapolate findings to non-monitored or data scarce catchments, further study and data is required (Wohl et al., 2012). However, the scarcity of data in both the spatial and temporal domains poses significant challenge for hydrological study which is usually characterised by a heterogenous and complex environment. The difficulties on the implementation and maintenance of research-grade observation networks has hindered the data collection on remote mountain area. This hinders the development of hydrological models and poses difficulty on model calibration. The advent of alternative methods for scientific data collection, and citizen science in particular, provides new opportunities to alleviate the issue of data scarcity, and additionally can promote public participation in hydrological science (Buytaert et al., 2014). As such, it can serve as a supplement to the traditional data collection, which is usually established within a professional environment (Buytaert et al., 2014; Herschy, 2014).

1.3 Citizen science in hydrology

Citizen science refers to the participation of general public in the research design, data collection and interpretation process together with scientists (Buytaert et al., 2014; Paul et al., 2018). Recently, innovations in sensing technology, data processing and visualization (Buytaert et al., 2014) have increased the potential of citizen science. It can be implemented in many forms such as community-based data collection, participatory data analysis or crowd-sourcing via internet (Buytaert et al., 2014). Newly developed sensing technology enables hydrological data to be collected by a participatory approach (Buytaert et al., 2014; Paul et al., 2018). The open-source Arduino platform is one example of low-cost technology that can be used to collect a wide range of data including temperature, soil-moisture, distance, and air pressure by combining it with different sensors (Fisher & Gould, 2012). These innovations have made citizen science an increasingly popular application in scientific research (Silvertown, 2009).

Buytaert et al. (2014) summarised the existing citizen science applications in the field of water resources management. The review indicated that most of the level of involvement of non-scientist is limited to data gathering and focused more on water quality monitoring (Buytaert et al., 2014). The major reason for this limited depth of engagement might be the geographical bias toward wealthy regions, instead of in areas where socio-ecological problems have more serious consequences (Buytaert et al., 2014). In developed regions, citizen science is regarded as supplement to tradition science approaches. In contrast, in developing regions it is more explored as a measure to reduce poverty and enhance the well-being of society (Gura, 2013). According to Buytaert et al. (2014), the variables commonly measured in the field of hydrological science, the current approaches of data collection, the challenges, and the

opportunities in the future are as follows:

- Precipitation: Widely measured in the context of citizen science as new sensor technology and more experiment methods are developed. For example, low-cost disdrometers are increasingly used for precipitation measurement as a cheap and robust device (Löffler-Mang & Joss, 2000). Traditional, low-cost rain gauges also allow precipitation to be observed in a non-professional environment. Continuous data can be recorded automatically by the electronic sensors such as tipping bucket rain gauge. Despite its advantages, a rain gauge can easily be blocked by vegetation or affected by local aerodynamic conditions in non-standard locations. Therefore, robust quality control protocols for installation, maintenance, and documentation of local environment should be implemented to ensure the data quality.
- Streamflow: Traditionally, streamflow is often measured by indirect methods, converting by measured flow velocity with cross section or river stage (Herschy, 2014). The construction of water level gauging stations is challenging due to the complexity of the river setting and the restriction of regulations. Nevertheless, streamflow is successfully measured by the iMHEA monitoring network in the Peruvian Andes (Célleri et al., 2009). This case study shows the possibility to monitoring streamflow in the context of citizen science. The potential of streamflow measurement could be extended by introducing new technology. For example, the application of camera-based water level measurement is an affordable and reliable approach for citizen science monitoring (Royem et al., 2012). Data coverage can be improved further by integrating remote sensing methods such as using high-resolution

digital elevation. Nevertheless, proper installation and maintenance of instruments should still be the most important consideration.

- Water quality: This is the most common hydrological property to be measured by citizen science. Newly developed technology make it possible to perform continuous sampling of variables such as temperature, dissolved oxygen, turbidity, conductivity, pressure, redox potential and pH value. However, water quality monitoring is often limited to the collection of water samples and the aforementioned basic hydrochemical parameters due to the high requirement of equipment and specialised knowledge (Overdevest, Orr & Stepenuck, 2004).

In the study of hydrology, citizen science can be a way to address the challenge of setting up repeated experiments. Controlled hydrological experiments are difficult to set up due to the large variety of uncontrolled boundary conditions such as land use change, and climate conditions. Using citizen science, it becomes possible to set up a large network of hydrological data collection through inexpensive, robust, and lower maintenance sensing equipment, thus covering larger variety of boundary conditions and hydrological variability. It also reduces the irreversible effects of perturbations to the water cycle posted by the control of experiments.

In addition to the supplement to data collection, citizen science can also be a method to pursue a more active role to engage the general public into the scientific process (Buytaert et al., 2014). It can be included in each stage of the scientific process. The Extreme Citizen Science framework classified the level of engagement into crowd-sourcing, distributed intelligence, participatory science, and extreme citizen science (Haklay, 2013). As the participation increases, non-scientists have more chance to be involved in the decision-making processes.

Local stakeholders often have a specific interest in hydrological studies since in many regions of the world, local development can be constrained if sustainable water resources management is unsuccessful (Célleri et al., 2009). This is particularly the case in the tropical Andes, where the initiative for Hydrological Monitoring of Andean Ecosystems (iMHEA in Spanish), was established in 2009 (Célleri et al., 2009). This citizen science-based hydrological monitoring effort is led by a regional NGO (Consortium for Sustainable Development of the Andean Ecoregion, CONDESAN). The network aims to increase data availability in the remote uplands which are not monitored by the standard national hydrometeorological network operated by the national hydrometeorological offices (e.g. SENAMHI in Perú) (Buytaert et al., 2014). The iMHEA network is a clear case of bottom-up initiative in response to the local awareness about the requirement for better understanding on watershed interventions (Ochoa-Tocachi et al., 2016). In order to identify the hydrological impacts of land-use change, including the benefits of restoration activities, the network focuses on pairwise catchment monitoring. Streamflow and precipitation are measured on 28 catchments distributed from Ecuador, Perú, to Bolivia (Ochoa-Tocachi et al., 2018). Such setup is ideal to study the relation between a catchment's land cover and its rainfall-runoff relation.

1.4 Hydrological models

Models are simplified and imperfect representations of a real-world system, which can nevertheless be useful to predict system behaviour and understand various processes. One of their main applications is to make predictions about the potential impact of changes. For the terrestrial water cycle, hydrological models are an essential tool in hydrological science and catchment management, to evaluate the hydrological impacts of instance climate change or land-use and land-cover change (Buytaert & Beven, 2011). A large variety of approaches exists: top-down (metric, empirical, or data-based), bottom-up (mechanistic or physically-based), or conceptual modelling, as summarised as followed:

- Top-down model (data-based): The hydrological response is entirely derived from observations of model input and output variables, such as rainfall and flow at the catchment-scale. Therefore, prediction of the hydrological response under LUCC can be difficult due to the inability to map the hydrological impact of change onto the model parameters.
- Bottom-up model (physically-based): These models are developed with understanding of the physics of hydrology. The effects of physical change can be explicitly represented once the physical properties of the catchment under existing and changed conditions can be determined (McIntyre et al., 2014). The physical properties have necessarily been derived from small-scale observations, and therefore calibration to the scale of interest is generally required. This can lead to problems of observation uncertainty and model identifiability.
- Conceptual model: This type of model is the combination of the top-down

and bottom-up approaches. The model structure is defined based on prior knowledge, then the parameter values are calibrated. A conceptual model is prone to the limitations of both top-down (detection of signals in the observations) and bottom-up approaches (prior specification and non-identifiability), makes it unsuitable for predicting proposes (McIntyre et al., 2014).

Physically based models can be used to detect and attribute change in hydrological observations, thus identifying the potential factors that affect the hydrological responses. They allow detailed mapping of the potential hydrological impacts of LUCC onto physically meaningful parameters, which can subsequently be used for scenario analysis in a land management context (McIntyre et al., 2014). Furthermore, the potential hydrological impact of different LUCC scenarios can be predicted by changing the model structure or parameter values that represent in the catchment properties. Despite the advantages of physically based models, conceptual models are commonly used for tropical basins e.g. (Buytaert & Beven, 2011) due to the data requirements to represent detailed hydrological processes accurately (Buytaert, Célleri & Timbe, 2009; Célleri & Feyen, 2009). However, in tropical Andean catchments, the novel hydrological monitoring data (Ochoa-Tocachi et al., 2018) opens new opportunity for hydrological studies. These data also allow physically based models to be applied for hydrological simulation.

1.5 Hydrological analysis using a land surface model, JULES

Land surface models were originally developed as lower boundary condition for Global Circulation Models (GCMs) and other atmospheric modelling (Best et al., 2011). Land surface models are increasingly used for hydrological assessment, given their advantage to map the modeller's knowledge about the hydrological impacts of land-use and land-cover change into physically meaningful parameters. One of such models, the Joint UK Land Environment Simulator (JULES) (Best et al., 2011; Clark, D. B. et al., 2011) is used in this study. JULES is a community land surface model developed from the Met Office Surface Exchange Scheme (MOSES) by the UK Met Office (Cox et al., 1999). It can be coupled to an atmospheric global circulation model, but is also used as a standalone land surface model which simulates the fluxes of carbon (Clark, D. B. et al., 2011) water, energy and momentum (Best et al., 2011) between the land surface and the atmosphere in continuous time series. It has been applied successfully for a range of applications such as weather forecasting, climate change prediction, earth system modelling, and has been increasingly used for hydrological assessment (Le Vine et al., 2016; Zulkafli et al., 2013). The JULES model is driven by a large dataset of hydrometeorological variables. It simulates the energy exchanges between various physical processes such as photosynthesis, carbon and nutrient cycles, irrigation, and crop growth. This makes it possible to investigate the interaction between hydrology and other land surface processes. (Zulkafli et al., 2013).

JULES can be used to detect and attribute change in hydrological observations, thus identifying the potential factors affecting the change. This makes it possible to identify the potential hydrological impact under anthropogenic interventions (Centre for Ecology & Hydrology, 2018) by changing the model structure or parameter values

which represents in the catchment properties.

JULES uses a tiled model to present the sub-grid heterogeneity consisting of 5 vegetated and 4 non-vegetated surfaces (Figure 1.3). Distinct parameters are used to calculate the energy balance of surface temperatures, short-wave and long-wave radiative fluxes, sensible and latent heat fluxes, ground heat fluxes, canopy moisture contents, snow masses and snow melting rates for each surface type in a grid-box. A shared 4-layer soil column with thickness of 0.1, 0.25, 0.65, and 2.0 m from the top to the bottom is used for individual tile.

In JULES, the precipitation is intercepted by the canopy storage, then partitioned into surface flow and infiltration into the soil based on the Hortonian infiltration excess mechanism. An instantaneous redistribution of soil moisture is assumed for the infiltration following the Darcy–Richards diffusion equation. The subsurface flow is generated by the gravity drainage at the lower boundaries. Saturation excess flow is calculated with a Probability Distributed Model (PDM) described by Moore (1985). The sub-grid distribution of soil moisture (θ) is described by a probability function (eq. 1.1), and the shape parameter B is modified to better represent the subsurface flow (Clark, Douglas B. & Gedney, 2008). The parameter is initially set as 1, whereas values of 0.1/0.5 can be used for a more subsurface flow dominated hydrology, and a value of 10 for a more flash hydrological response.

$$\mathrm{f}_{sat} = 1 - \left[1 - \frac{\theta}{\theta_s}\right]^{\frac{B}{B+1}} \qquad (1.1)$$

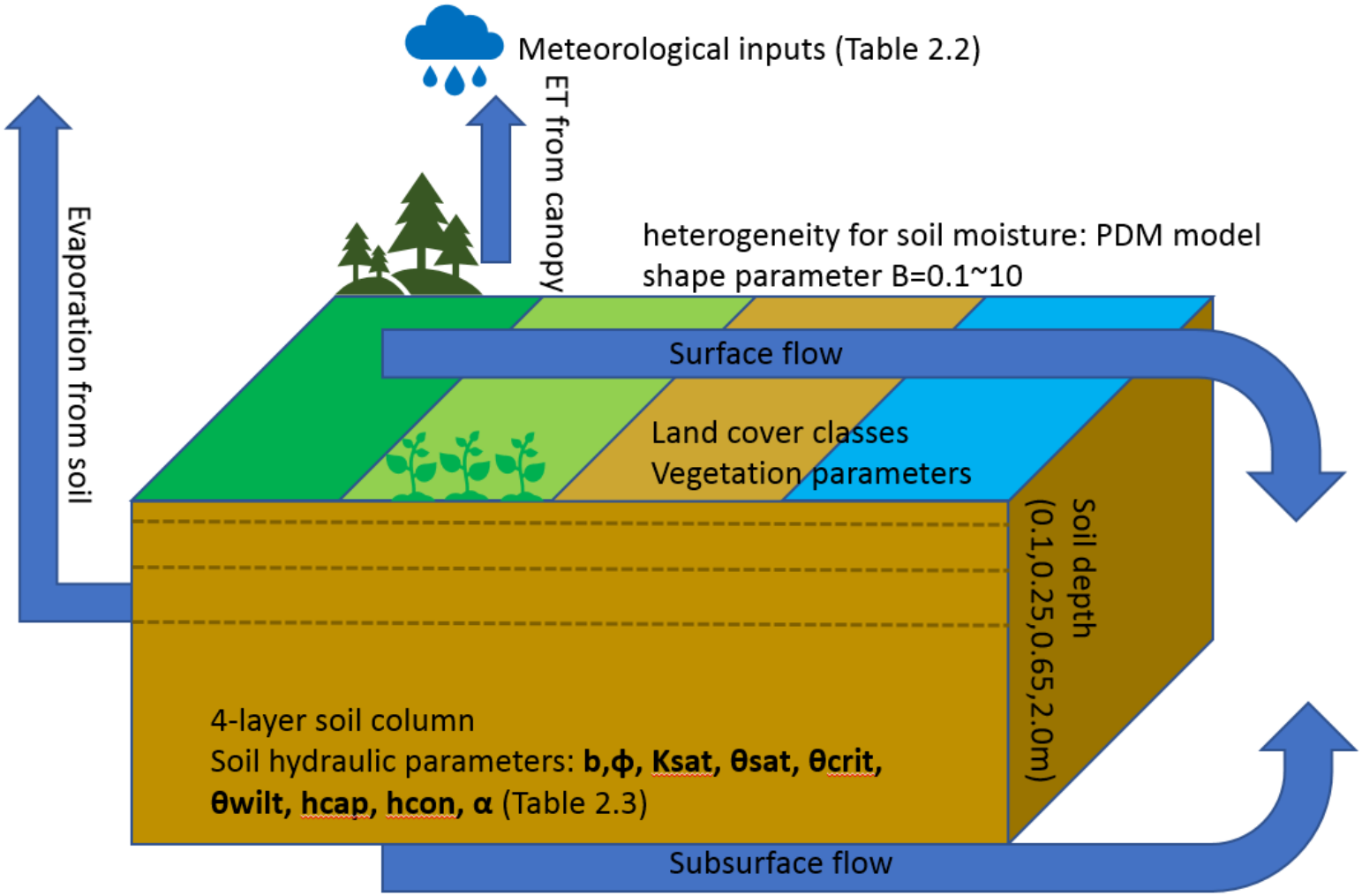

Figure 1.3 Overview of JULES

This research focuses particularly on addressing the uncertainty in precipitation, the soil parameterisation, and the vegetation parameters. The iMHEA citizen science network has opened new opportunities for the model development. In which, the highly uncertainty in precipitation could be reduced by using these participatory data. The required soil parameters are commonly developed using pedotransfer functions (PTFs) (Marthews et al., 2014), which estimate unavailable soil parameters from soil properties such as texture and dry bulk density (Cosby et al., 1984; Tomasella & Hodnett, 1998). In the study region, water retention properties from the local experiment data (Buytaert et al., 2005; Crespo et al., 2011) are considerably higher than the values derived from PTFs (Marthews et al., 2014), which could be attributed to the inability of the PTFs to present the high water retention caused by the high organic matter content in these soils (Buytaert et al., 2006). Therefore, this research modifies the soil water retention properties using data from local in-situ experiments.

The JULES model is used to assess the hydrology under LUCC impact. The analysis marks LUCC as the only contributor to affect the flow generation while other influencing factors such as meteorological influences have been kept constant. This approach reduces the uncertainty induced by changing catchment characteristics and meteorological drivers.

1.6 Thesis structure

The aim of this PhD research is to explore the changing Andean hydrology under land-use and land cover changes using three analytical components: quantifying land use change; quantifying the impact of hydrology by means of a land surface model, and using citizen science data to calibrate and validate the hydrological model (Figure 1.4). The research has focused on the impacts of grazing, cultivation, and afforestation in the upper-Andean region, and impacts of the forest dynamic in the Andes of Ecuador and Perú. First, the current state of the global LUCC and hydrological impacts, Andean hydrology, the challenges posed by land-use and land cover change, and the emergence of citizen science for data collection, and hydrological models are reviewed (Chapter 1). In a next step, the hydrological data obtained with citizen science are integrated into a land surface model, JULES, to simulate the hydrological fluxes under a variety of land use conditions (Chapter 2). The JULES model is then examined and calibrated at a headwater catchment scale (Chapter 3), and the potential impact of land use change on hydrology is further assessed by using this model approach (Chapter 4). The extent of regional land use and land cover changes are then assessed and predicted using a land use change model, lulcc R (Chapter 5). Lastly, the JULES model is implemented at a regional scale using multiple sources of global reanalysis data (Chapter 6) and the potential hydrological impacts posed by land use and land cover changes are then assessed. The main findings throughout the thesis and future works are then concluded.

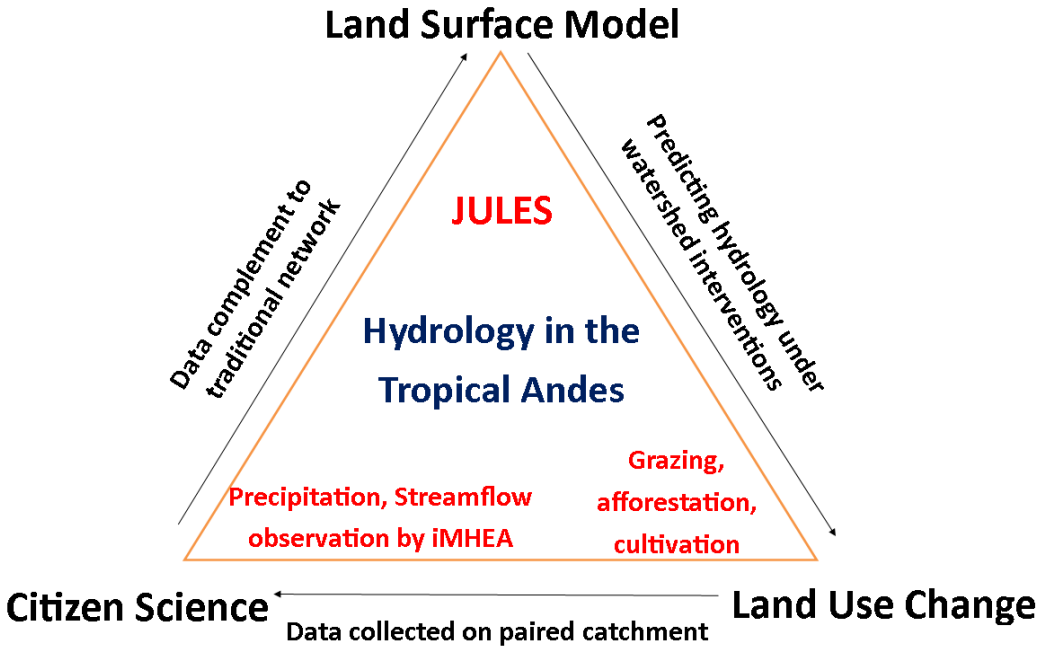

Figure 1.4 Conceptual representation of the approach implemented in this thesis.

2 Hydrological evaluation of JULES for the tropical Andes using citizen-science generated rainfall data

2.1 Introduction

Land surface models were originally developed as lower boundary condition for Global Circulation Models (GCMs) and other atmospheric modelling (Best et al., 2011). They simulate the fluxes of carbon (Clark, D. B. et al., 2011) water, energy and momentum (Best et al., 2011) between the land surface and the atmosphere, and have been applied successfully for a range of applications such as weather forecasting, climate change prediction, earth system modelling. They are also increasingly used for hydrological assessment (Le Vine et al., 2016; Zulkafli et al., 2013). In this chapter, the Joint-UK Land Environment Simulator (JULES) is applied for hydrological evaluation in the tropical Andes. It simulates the energy exchanges between various physical processes such as photosynthesis, carbon and nutrient cycles, irrigation, and crop growth. This makes it possible to investigate the interaction between hydrology and other land surface processes by mapping the modeller's knowledge about the hydrological impacts of land-use and land-cover change into physically meaningful parameters.

The JULES model is driven by a large dataset of hydrometeorological variables using a physically-based simulation approach. Globally available reanalysis datasets are commonly used for the setup, i.e. NCEP-DOE Reanalysis 2 (Kanamitsu et al., 2002), TRMM_3B42.7 (Huffman et al., 2007). However, the high uncertainty in the precipitation data makes it unreliable for small scale hydrological studies (Buytaert, Célleri & Timbe, 2009; Sheffield, Goteti & Wood, 2006). In this chapter, I evaluate the capacity of JULES to simulate streamflow using in-situ observational precipitation data

obtained from the participatory iMHEA network (Ochoa-Tocachi et al., 2018). The simulated results are evaluated with the streamflow observations obtained from the iMHEA network as well.

2.2 Methods

2.2.1 JULES setup

In this chapter, the setup of the land surface model, JULES vn5.3 (JULES, 2018) is explored using the analysis framework shown in Figure 2.1. The required time series of meteorological data, i.e. downward short-wave and long-wave radiation, temperature, specific humidity, wind speed, and surface pressure (as specific in Table 2.2), are extracted from the globally available NCEP-DOE Reanalysis II dataset (Kanamitsu et al., 2002). The JULES model was driven by three sources of precipitation data. The simulated flow among using the iMHEA precipitation data/ NCEP-DOE Reanalysis II/ TRMM_3B42.7 were evaluated for their capacity to better represent the flow in small catchment. The land cover is parameterised with the local survey data (Ochoa-Tocachi et al., 2018). The soil data is parameterised by using a pedotransfer function approach. Required soil composition and chemical variables are obtained from the Harmonized World Soil Database version 1.21 (Fao/Iiasa/Isric/Isscas/Jrc, 2012). The soil properties are assumed to be evenly distributed over the 4-layer soil column with thickness of 0.1, 0.25, 0.65, and 2.0 m from the top to the bottom. The simulated flows are routed with using a simple delayed function, then be further compared and evaluated with the iMHEA monitoring flow (Ochoa-Tocachi et al., 2018).

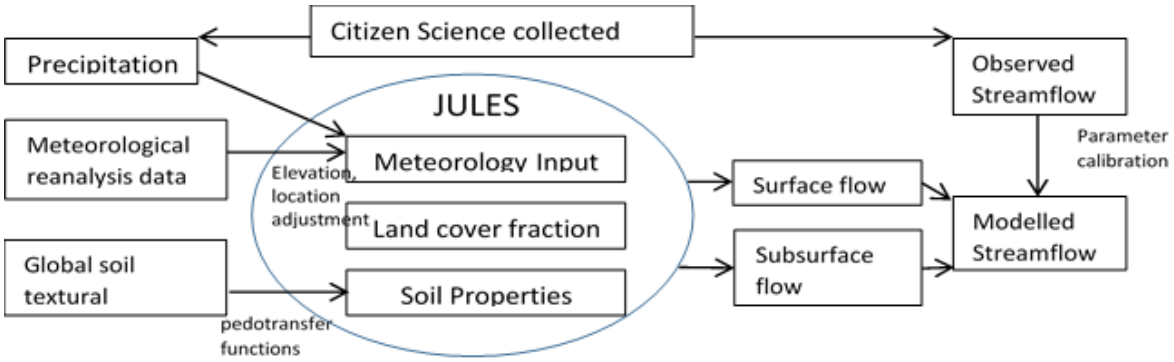

Figure 2.1 Conceptual overview of the hydrological modelling approach using JULES driven by input data from citizen science and conventional sources.

2.2.2 Citizen science-based data collection

Hydrological monitoring data is obtained from a regional citizen science-based initiative (Ochoa-Tocachi et al., 2018). The network is known as the Regional Initiative for Hydrological Monitoring of Andean Ecosystems (iMHEA) and is part of a grassroots initiative to characterize the hydrological response of different Andean ecosystems in Perú, Ecuador, and Bolivia. It collects data on streamflow, precipitation, and several weather variables at a high temporal resolution with using the cheap and robust technology (Buytaert et al., 2014). This monitoring is implemented in small and homogenous catchments, distributed from 0 and 17 °S, which covers three major high-elevation biomes, páramo, puna, and jalca in the tropical Andes (Figure 2.2). The 22 monitoring sites are described in Table 2.1. Most of the catchments are rural area covered by tussock and other grasses, wetlands, shrubs, and patches of native forest. These regions are not affected by urbanisation, water abstractions, and stream alterations.

The iMHEA monitoring setup relies on monitoring a set of paired catchments with similar physical and climatic characteristics, and geographically close to each other (Brown et al., 2005), in order to characterise the impacts of a variety of human alterations on the watershed response (Célleri et al., 2009). For example, impacts of grazing and burning are assessed by comparing the hydrological response of catchment LLO_01 (Lloa, Ecuador, Figure 2.3), to that of its adjacent restored catchment LLO_02. The hydrological benefits of pasture restoration in HUA_01 are evaluated by comparison with the adjacent grazed catchment HUA_02 (Huaraz, Perú, Figure 2.3). As an example, Figure 2.4, shows the impacts of grazing compared to both páramo covered catchments (natural PIU_01, and grazed PIU_02), and forest covered puna catchments (natural PIU_04, and grazed PIU_07).

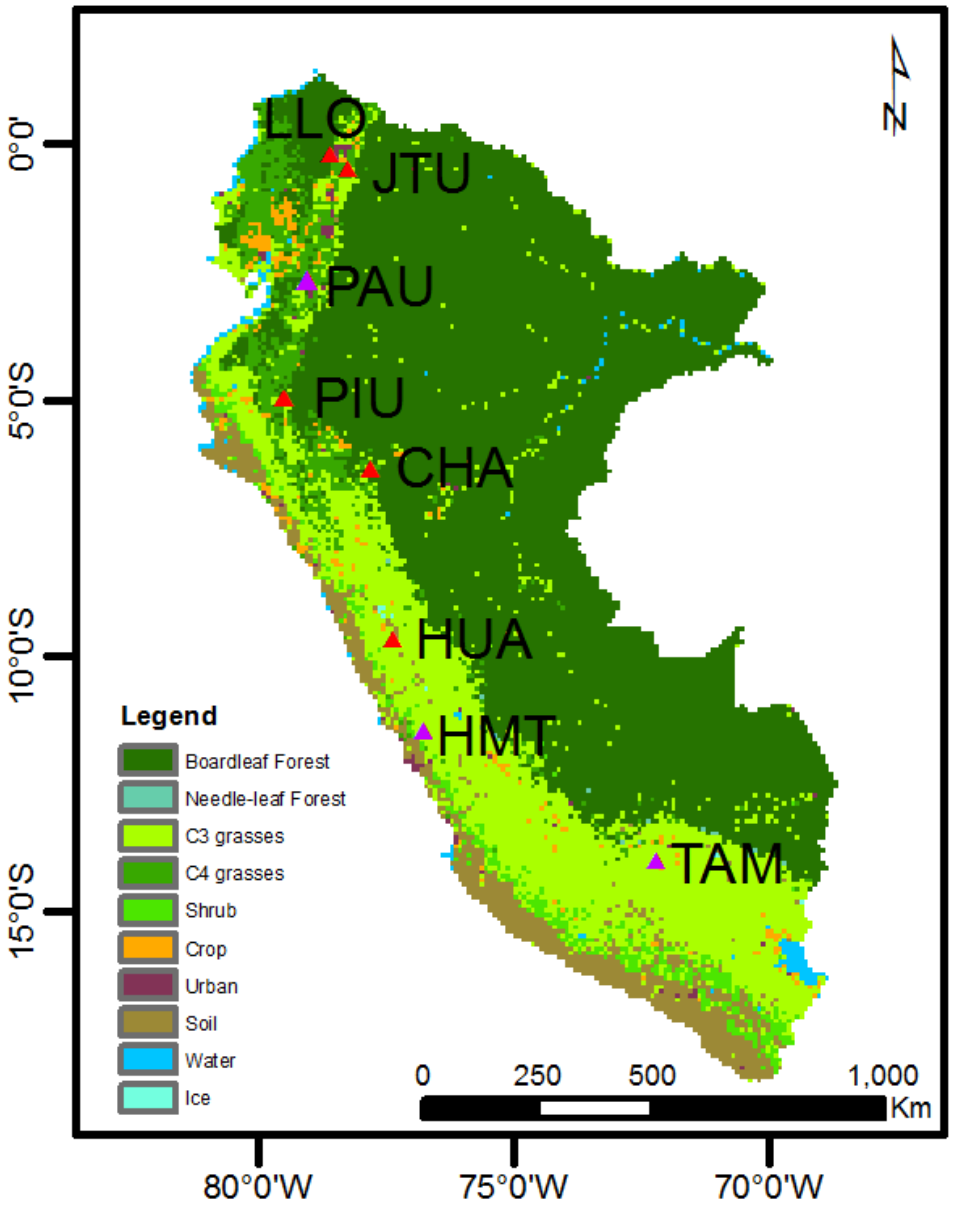

Figure 2.2 The location of the iMHEA sites within the major land cover types of the tropical Andes

Table 2.1 Description of the monitored catchments. BF: Broadleaf Forest, NF: Needleleaf Forest, CR: crop, C4: C4 grasses, SH: Shrub, BS: Bare soil.

Code	Ecosystem	Land Use	Altitude [m]	Area [km^2]	Soil	Land cover
PIU_01	Páramo	Natural	3112-3900	6.60	Andosol, Histosol	0.15 BF, 0.85 C4
PIU_02	Páramo	Grazing	3245-3610	0.95	Andosol, Histosol	0.15 BS, 0.85 C4
PIU_04	Forest	Natural	2682-3408	2.32	Andosol, Cambisol	0.80 BF, 0.20 C4
PIU_07	Dry puna	Grazing, cultivation	3110-3660	7.80	Andosol	0.35 CR, 0.45 C4, 0.2 SH
CHA_02	Jalca	Natural	3000-3450	1.63	Andosol, Inceptisol	0.10 BF, 0.90 C4
CHA_01	Jalca	Afforestation	2490-3200	0.95	Andosol, Inceptisol	0.80 NF, 0.20 C4
HUA_01	Humid puna	Natural	4280-4840	4.22	Andosol, Histosol	0.75 C4, 0.25 BS
HUA_02	Humid puna	Grazing	4235-4725	2.38	Andosol, Histosol	0.70 C4, 0.30 BS
LLO_02	Páramo	Grazing, restoration	4088-4680	2.21	Andosol, Histosol	0.10 BF, 0.90 C4
LLO_01	Páramo	Grazing, burning	3825-4700	1.79	Andosol	0.10 SH, 0.90 C4
JTU_03	Páramo	Natural	4144-4500	2.25	Andosol, Histosol	0.80 C4, 0.20 SH
JTU_02	Páramo	Grazing	4085-4322	2.42	Andosol	1.00 C4
PAU_01	Páramo	Natural	3665-4100	2.63	Andosol	1.00 C4
PAU_04	Páramo	Cultivation, grazing	3560-3721	1.55	Andosol	0.70 C4; 0.30 CR
PAU_02	Páramo	Natural, grazing	2970-3810	1.00	Andosol, Histosol	0.80 C4; 0.20 BF
PAU_03	Páramo	Afforestation	3245-3680	0.59	Andosol, Histosol	0.10 C4; 0.90 NF
HMT_01	Dry puna	Grazing	4025-4542	2.09	Leptosol, Inceptisol	0.75 C4; 0.10 SH, 0.15 BS
HMT_02	Dry puna	Grazing	3988-4532	1.67	Leptosol, Inceptisol	0.85 C4, 0.05 SH; 0.10 BS
TAM_02	Humid puna	Natural	3650-4360	1.67	Leptosol, Inceptisol	0.60 C4; 0.40 BF
TAM_01	Humid puna	Afforestation, grazing	3835-4026	0.82	Leptosol, Inceptisol	0.80 C4; 0.20 NF
TIQ_02	Humid puna	Natural	4182-4489	1.73	Leptosol, Inceptisol	0.95 C4; 0.05 BS
TIQ_01	Humid puna	Cultivation, grazing	4140-4353	0.69	Leptosol, Inceptisol	0.35 C4; 0.35 CR; 0.30 BS

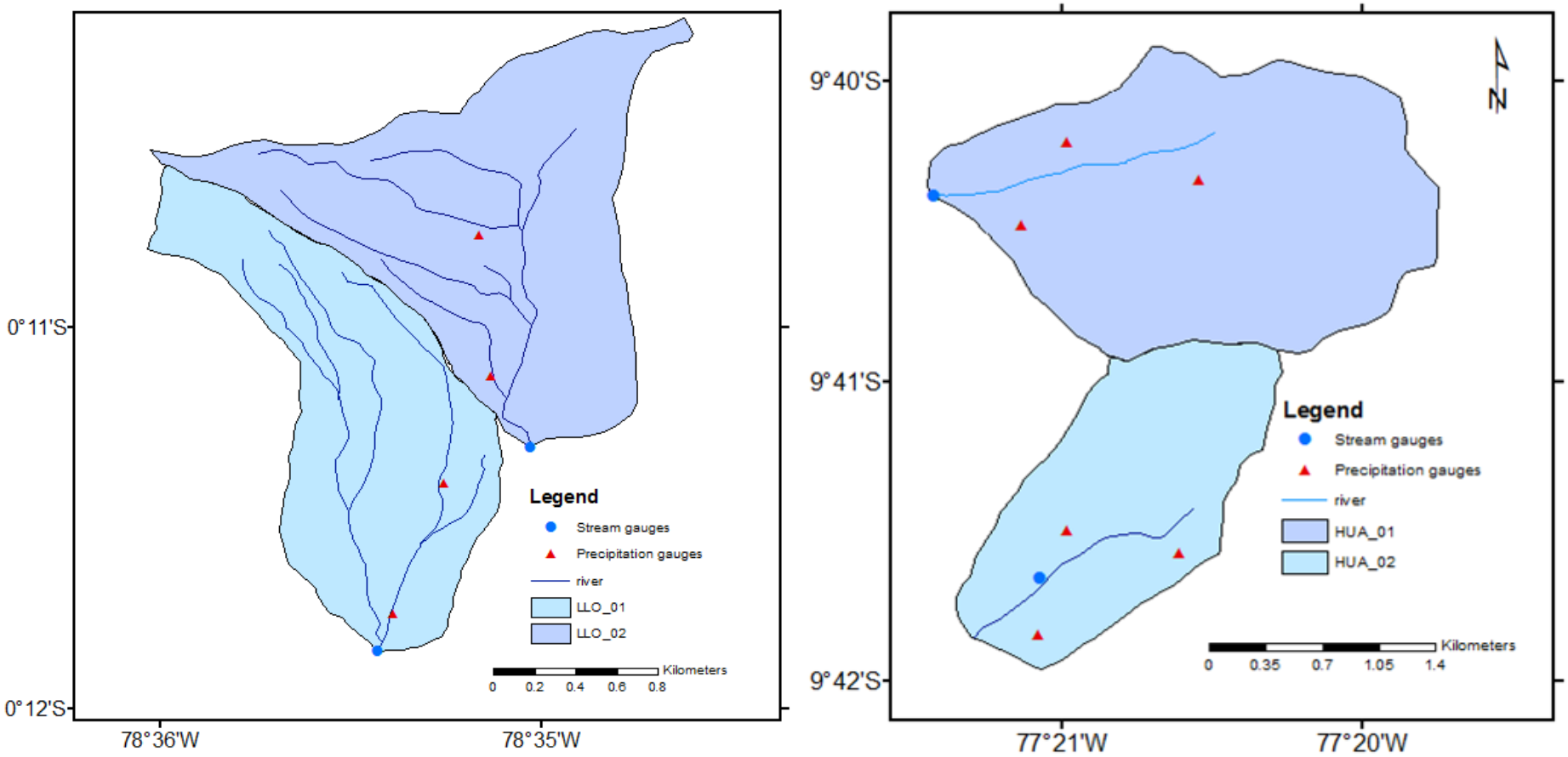

Figure 2.3 Example of paired catchments monitored at the iMHEA site LLO (Lloa, Ecuador) and HUA (Huaraz, Perú)

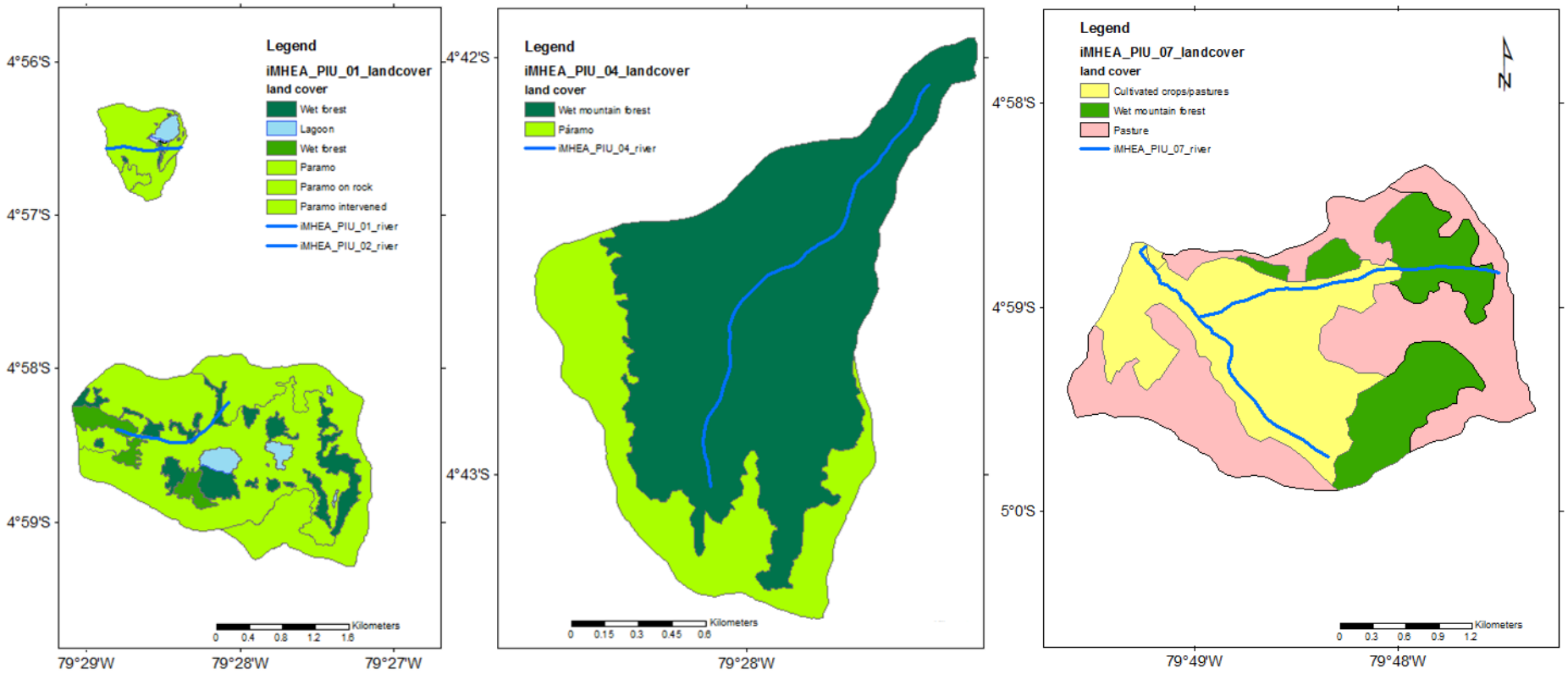

Figure 2.4 Example of paired catchments monitored at the iMHEA site PIU (Piura, Perú)

Precipitation data (referred as “iMHEA precipitation”) has been recorded in each catchment with a minimum of two tipping-bucket rain gauges at an installed height of 1.50m (resolutions of 0.254, 0.2 or 0.1mm) distributed over the catchment areas (Ochoa-Tocachi et al., 2016). Figure 2.5 shows the precipitation measurement site installed in JTU, Ecuador.

Figure 2.5 Precipitation observation in Antisana (JTU, Ecuador)

Figure 2.6 shows a streamflow monitoring site at the outlet of catchment in LLO, Ecuador, using a compound sharp-crested weir (a V-shaped section for low flows and a triangular–rectangular section for high flows) equipped with a pair of pressure transducers. The water level has been recorded at a regular interval of 5/15 min by iMHEA (Ochoa-Tocachi et al., 2018).

Figure 2.6 Streamflow observation in Pichincha (LLO, Ecuador)

Table 2.2 Meteorological forcing data required to drive the JULES model

Data	Units
Downward component of shortwave radiation at the surface	W m^{-2}
Downward component of longwave radiation at the surface	W m^{-2}
Precipitation	kgm^{-2} s^{-1}
Wind speed	m s^{-1}
Atmospheric temperature	K
Atmospheric specific humidity	kg kg^{-1}
Surface pressure	Pa

Source: (Best et al., 2011)

2.2.3 Non-iMHEA forcing data

The required time series of meteorological data that are not available from the iMHEA network, i.e. downward short-wave and long-wave radiation, temperature, specific humidity, wind speed, and surface pressure (as specific in Table 2.2), are extracted from the globally available NCEP-DOE Reanalysis II data set (Kanamitsu et al., 2002). The dataset is available on a T62 Gaussian grid with 192 x 94 points (approximately 2° scales) and provides 6-hourly temporal resolution form 1979/01 up to the present. This large-scale data is interpolated in space to a point scale with the nearest-neighbour interpolation method. An elevation adjustment was made for Temperature (T, °K) and pressure (P, Pa), from the record level (T_0, P_0) to the site level (T_Z, P_Z) using the environmental lapse rate (γ) and the gas constant of air (R). γ is between 0.5 and 0.7 °C per 100 meters (Buytaert et al., 2006) (eq. 2.1 and 2.2):

$$T_z = T_0 + \gamma z; \gamma = -0.0065 \frac{^\circ K}{m} \tag{2.1}$$

$$P_z = P_0 \left(\frac{T_z}{T_0}\right)^{\left(\frac{g}{\gamma R}\right)}; R = \frac{287J}{kg * ^\circ \mathrm{K}} \tag{2.2}$$

Specific humidity (q, kg/kg) is elevation adjusted assuming that the relative humidity (RH) remains constant with altitude (Cosgrove et al., 2003). By calculating saturated vapor pressure (e_{sat}, hPa) using Wexler's saturated water vapor pressure equation, saturated specific humidity (q_{sat}) can be obtained using the definition of specific humidity (eq. 2.3 – 2.6):

$$\mathrm{RH} = 100 \left(\frac{q_0}{q_{sat,0}}\right) \tag{2.3}$$

$$\mathrm{q}_z = \left(\frac{RH * q_{sat,z}}{100}\right) \tag{2.4}$$

$$\mathrm{q}_{sat,x} = \frac{0.622 \mathrm{e}_{sat,x}}{p_x - 0.378 \mathrm{e}_{sat,x}}; x = z, 0 \tag{2.5}$$

$$\mathrm{e}_{sat,x} = 6.112exp\left[\frac{17.67(T_x - 273.15)}{(T_0 - 273.15) + 243.5}\right]; x = z, 0 \quad (2.6)$$

Using the Stefan-Boltzmann law, downward longwave radiation (L, W/m^2) is also elevation adjusted (eq. 2.7 – 2.8), ε is the emissivity of the grey body, which depends on the wavelength, σ is the Stefan–Boltzmann constant:

$$\mathrm{L}_z = \frac{\varepsilon_z \sigma}{\varepsilon_0 \sigma}\left(\frac{T_z}{T_0}\right)^4 L_0 \quad (2.7)$$

$$\varepsilon_x = 1.08\left\{1 - exp\left[-e_x^{\left(\frac{T_x}{2016}\right)}\right]\right\}; \mathrm{e}_x = {}^{\mathrm{p}_x \mathrm{q}_x}/_{0.622}; \mathrm{x} = \mathrm{z}, 0 \quad (2.8)$$

Lastly, the wind speed (u) is elevation adjusted using a power law wind profile, assuming $\alpha = 0.143$ under neutral stability conditions: (eq. 2.9):

$$u = u_0\left(\frac{z}{z_0}\right)^{\alpha} \quad (2.9)$$

Shortwave radiation data is used directly from the NCEP Reanalysis II dataset without adjustment. The 6-hourly was disaggregated to hourly data with linear interpolation.

In addition to the iMHEA precipitation, which was used as the major data source, two alternative large-scale precipitation datasets are used for comparison: the NCEP-DOE Reanalysis II data and the remote sensing product TRMM_3B42.7 (Huffman et al., 2007) developed by the Global Precipitation Measurement (GPM) mission (Hou et al., 2014). TRMM_3B42.7 provides a higher spatial resolution (0.5° scales) and temporal resolution (3-hourly) than the NCEP-DOE Reanalysis II data, which has shown good performance over the Peruvian Andes–Amazon (Zulkafli et al., 2013) .

2.2.4 The upper-Andean soils

The study region is the upper Andean region of Perú and Ecuador, which mainly covered by the Andean páramo (Buytaert et al., 2006). Volcanic soils are the dominant soil types, in particular soils that are classified as Andosol, Leptosol, Histosol, Cambisol and Regosols (Fao/Iiasa/Isric/Isscas/Jrc, 2012). Andosols are particularly common, which are a dark, humic and acid soils with an open pore structure, in which organic matter and volcanic ash accumulate (Crespo et al., 2011). This type of soil covers the páramo ecosystem in large parts of the tropical Andean mountain belt between 3500 and 4500 m altitude (Buytaert et al., 2005). It has extremely high water retention capacity (0.64-0.93 cm^3/cm^3 at saturation) (Buytaert, 2004) with its large organic carbon content (13-36%), and low bulk density (0.2-0.8 g/cm^3). The soil is prone to irreversible changes and degradation (Dorel et al., 2000), which leads to volume change, lowering of water retention and increases in hydraulic conductivity (Buytaert et al., 2005). Leptosols are characterised by a shallow horizon with lower organic matter content (6-20%), and bulk density between the range of 0.5-1.0 g/cm^3. Histosols in the páramo belt contain a high fraction of non-decomposed plant fibers (Beck et al., 2008). It has very high organic matter (21-66%), low bulk density (0.1-0.3 g/cm^3), and high water retention between saturation and field capacity (Crespo et al., 2011). Cambisols have lower organic matter content, which leads to a lower water retention capacity than Andosols and Histosols. The soil properties of Regosol are similar to the properties of the Cambisol.

2.2.5 Soil parameterisation

Darcy's law describes the water flux (W) through saturated soil as the product of a gradient in hydraulic potential (φ) and the soil hydraulic conductivity (k) (eq. 2.10):

$$\mathrm{W} = \mathrm{k}\left(\frac{\partial \varphi}{\partial z} + 1\right) \tag{2.10}$$

The relations between soil water content (θ), suction (φ) and hydraulic conductivity (k) are described by Brooks and Corey (1964), or a more robust formula van Genuchten (1980) using the soil water retention curve (eq. 2.11):

$$\theta(\varphi) = \theta_r + \frac{\theta_s - \theta_r}{[1 + (\alpha\varphi)^n]^m} \; ; m = 1 - \frac{1}{n} \tag{2.11}$$

where θ_r is the residual water content, θ_s is the saturated water content, the parameter n measures the uniformity of pore sizes in the soil, and α indicates the air entry suction described by Van Genuchten (1980).

In JULES, the critical point (θ_{crit}; field capacity) is defined by a matrix water potential of −33 kPa (φ = −3.366m) (Cox et al., 1999), which enables vegetation to maintain an un-water stressed transpiration at values below field capacity with a soil moisture availability factor (β) (eq. 2.12). θ_{wilt} is the wilting point defined by matrix water potential = −1500 kPa (φ = −153 m). The vegetation cannot extract water if the water retention drops below this point.

$$\beta = \begin{cases} 1 & for\ \theta \geq \theta_{crit} \\ \dfrac{\theta - \theta_{wilt}}{\theta_{crit} - \theta_{wilt}} & for\ \theta_{wilt} < \theta < \theta_{crit} \\ 0 & for\ \theta \leq \theta_{wilt} \end{cases} \tag{2.12}$$

The soil parameters (Table 2.3) required by JULES are not been commonly available in the soil dataset (Best et al., 2011). Therefore, these parameters are developed using pedotransfer functions (PTFs) from Cosby et al. (1984), Hodnett & Tomasella (2002), with thermal properties (h_{cap} and h_{con}) described by Dharssi et al. (2009) as summarised in Table 2.4. The PTFs of Hodnett & Tomasella (2002) are more

robust and recommend for general use in tropical South America (Marthews et al., 2014) than the texture-based Cosby et al. (1984) PTFs, and Tomasella & Hodnett (1998) PTFs. The required soil composition and chemical variables are obtained from the Harmonized World Soil Database version 1.21 (Fao/Iiasa/Isric/Isscas/Jrc, 2012). The soil hydraulic parameter maps derived from the PTFs are shown in resp. Figure 2.7 (Van Genuchten parameters and hydraulic conductivity) and Figure 2.8 (water retention content).

Table 2.3 Soil hydraulic parameters in JULES

symbol	Description	Units
b	Exponent in soil hydraulic characteristics	
ϕ	Saturated soil water pressure	m
K_{sat}	Hydraulic conductivity at saturation	kg m^{-2} s^{-1}
θ_{sat}	Soil moisture content at saturation	m^3 m^{-3}
θ_{crit}	Soil moisture content at the critical point	m^3 m^{-3}
θ_{wilt}	Soil moisture content at the wilting point	m^3 m^{-3}
h_{cap}	Dry heat capacity	J m^{-3} K^{-1}
h_{con}	Dry thermal conductivity	W m^{-1} K^{-1}
α	Bare soil albedo	

Source: (Best et al., 2011)

Table 2.4 Soil parameterization using pedotransfer functions

Soil data	Pedotransfer function	Source
b=1/(n-1)	$\mathrm{n} = \exp\big((62.986 - 0.833CL - 0.529SOC + 0.593pH + 0.007CL^2 - 0.014SA * SI)/100\big)$	Hodnett & Tomasella (2002)
$1/\alpha$ (unit: m^{-1})	$\alpha = 1000 * 9.80665/\Big(1000/exp\big((-2.294 - 3.526SI + 2.440SOC - 0.076CEC - 11.331pH + 0.019SI^2)/100\big)\Big)$	
Saturation point (pF=0)	$\theta_{sat} = 0.01(81.799 + 0.099CL - 31.42DBD + 0.018CEC + 0.451pH - 0.0005SA * CL)$	
Wilting point (pF=4.2)	$\theta_{wilt} = 0.01(22.733 - 0.164SA + 0.235CEC - 0.831pH + 0.0018CL^2 + 0.0026SA * CL)$	
Critical point (pF=2.5)	$\theta_{crit} = \theta_{wilt} + \frac{\theta_{sat} - \theta_{wilt}}{[1 + (\alpha\lvert\varphi\rvert)^n]^{1-1/n}}$	Van Genuchten (1980)
Saturated hydraulic conductivity	$\mathrm{K}_{sat} = \frac{25.4}{3600} * 10^{(-0.60-0.0064CL+0.0126SA)}$	Cosby et al. (1984)
Saturated heat conductivity	$\mathrm{hcon} = \lambda_{air}^{\theta\mathrm{sat}}\left(\lambda_c^{Fc}\lambda_s^{Fs}\lambda_{si}^{Fsi}\right)^{1-\theta\mathrm{sat}}$ $\lambda\mathrm{s} = \lambda\mathrm{si} = 1.57025\ {}^{\mathrm{W}}/_{mK}\,; \lambda\mathrm{c} = 1.16025\ {}^{\mathrm{W}}/_{mK}; \lambda\mathrm{air} = 0.025\ {}^{\mathrm{W}}/_{mK}$	Dharssi et al. (2009)
heat capacity	$\mathrm{hcap} = (1 - \theta\mathrm{sat})(\mathrm{FcCc} + \mathrm{FsCs} + \mathrm{FsiCsi})$ $\mathrm{Cs} = \mathrm{Csi} = 2.133 * 10^6\ {}^{\mathrm{J}}/_{m^3K}\,; \mathrm{Cc} = 2.373 * 10^6\ {}^{\mathrm{J}}/_{m^3K}$	

CL: clay fraction, SA: sand fraction, SI: silt fraction, DBD: dry bulk density (g/cm^3), SOC: soil organic carbon (% weight), CEC: carbon exchange capacity (cmol/kg), pH: hydrogen ion activity

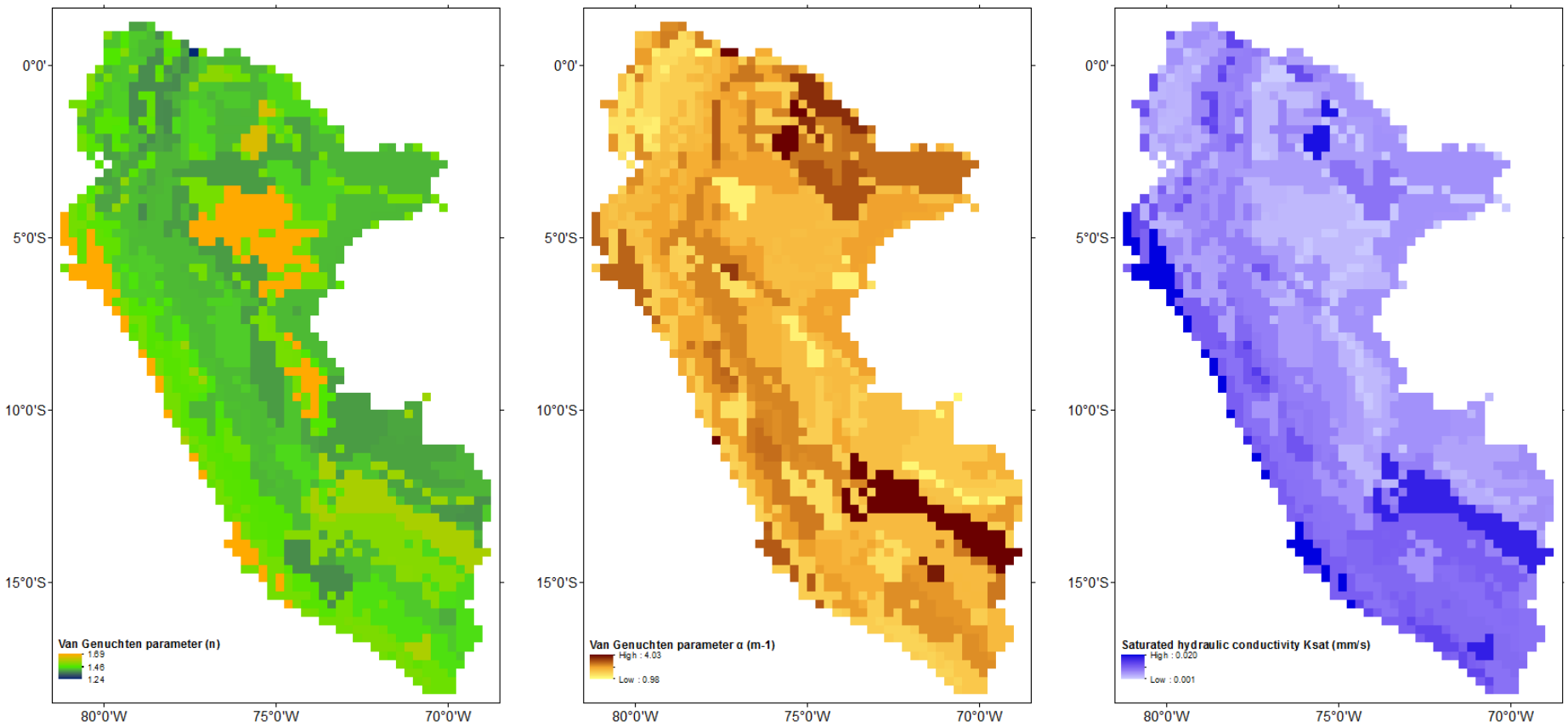

Figure 2.7 Soil hydraulic parameter maps for Perú and Ecuador derived from the PTFs

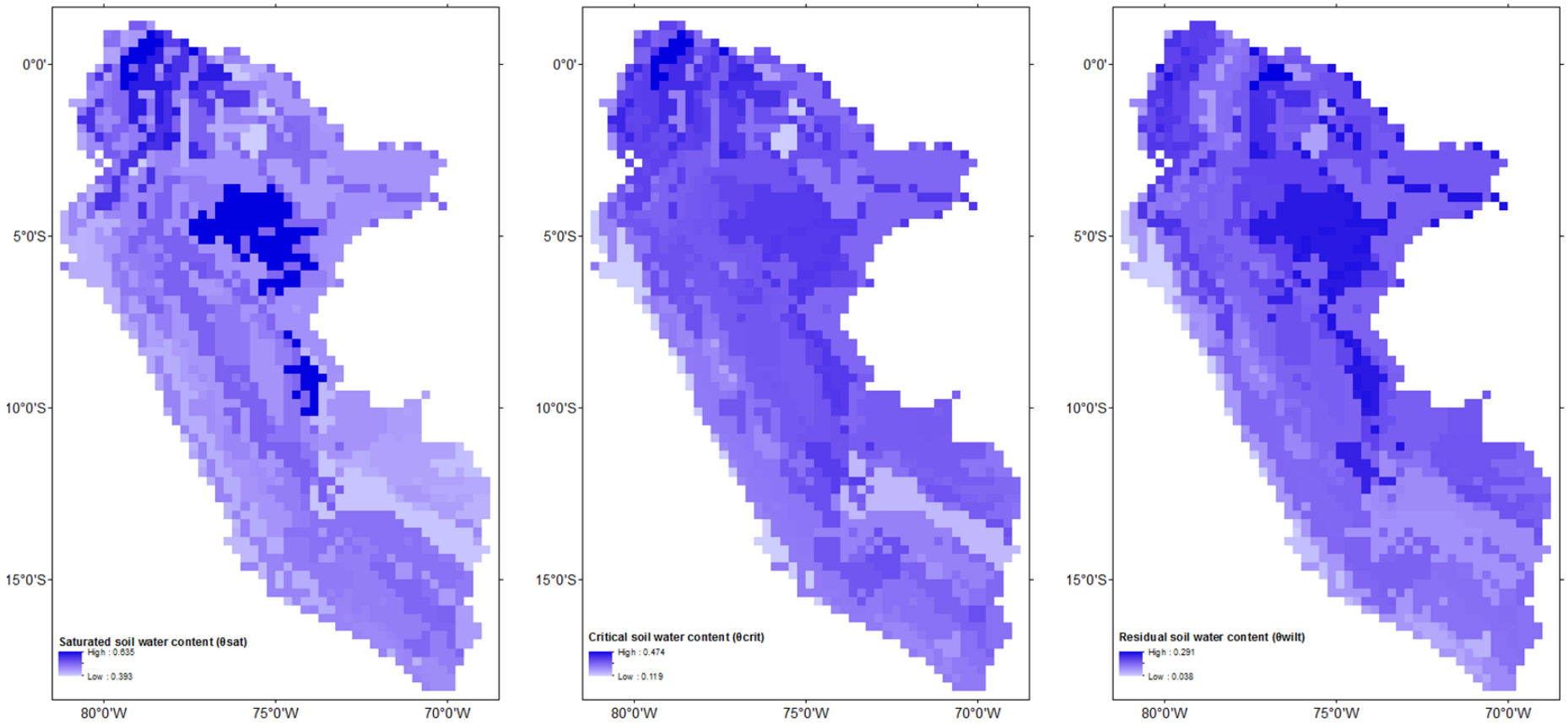

Figure 2.8 Soil hydraulic parameter maps for Perú and Ecuador derived from the PTFs (Soil water retention points)

2.2.6 Routing in catchment

The surface ($Q_{surface}$) and sub-surface ($Q_{subsurface}$) runoff fluxes simulated by the JULES model require an external river routing model for a reasonable comparison to observed river flows (Best et al., 2011). In this study, I applied a simple delayed function to account for the routing delay in the river discharge (Q_{sim}) in each timestep (t) (eq. 2.13).

$$Q_{sim,t} = \sum_{i=1}^{n} \left(Q_{surface,t-t_{i1}} + Q_{subsurface,t-t_{i2}} \right); t_{i1} = \frac{d_i}{C_{surface}}; t_{i2} = \frac{d_i}{C_{subsurface}} \quad (2.13)$$

The distribution of the distance (d) of each point (i) in the catchment to the outlet (Figure 2.9) was calculated using GIS software and D8 flow routine (Figure 2.10).

The lag time was obtained empirically by analysing the time interval between the maximum rainfall and the peak discharge of the observed hydrograph. A longer lag time up to 11.2 hours is found in PIU1 (Figure 2.11), whereas a shorter lag time 1.8 hours is found in PIU4 (Figure 2.12). The flood wave velocity (celerity, C) is then calculated by dividing the mean distance by the travel time (eq. 2.14), which ranges between 0.421 m/s to 0.040 m/s as summarised in Table 2.5.

$$C = \frac{Mean\ Distance}{Travel\ Time} \quad (2.14)$$

Table 2.5 Wave velocity for the delay function

	Mean distance to outlet (m)	Time to peak (hr)	Wave velocity (m/s)	(hr/m)
PIU1	1627.0	11.2	0.040	145
PIU2	545.7	3.4	0.045	161
PIU4	1511.3	1.8	0.233	840
PIU7	2017.5	1.3	0.421	1517
JTU2	1275.2	5.3	0.067	240
JTU3	1659.0	4.6	0.101	363
HUA1	1712.1	2.9	0.165	594
HUA2	851.5	1.3	0.189	681
CHA1	1135.9	2.1	0.148	531
CHA2	850.1	3.0	0.079	283

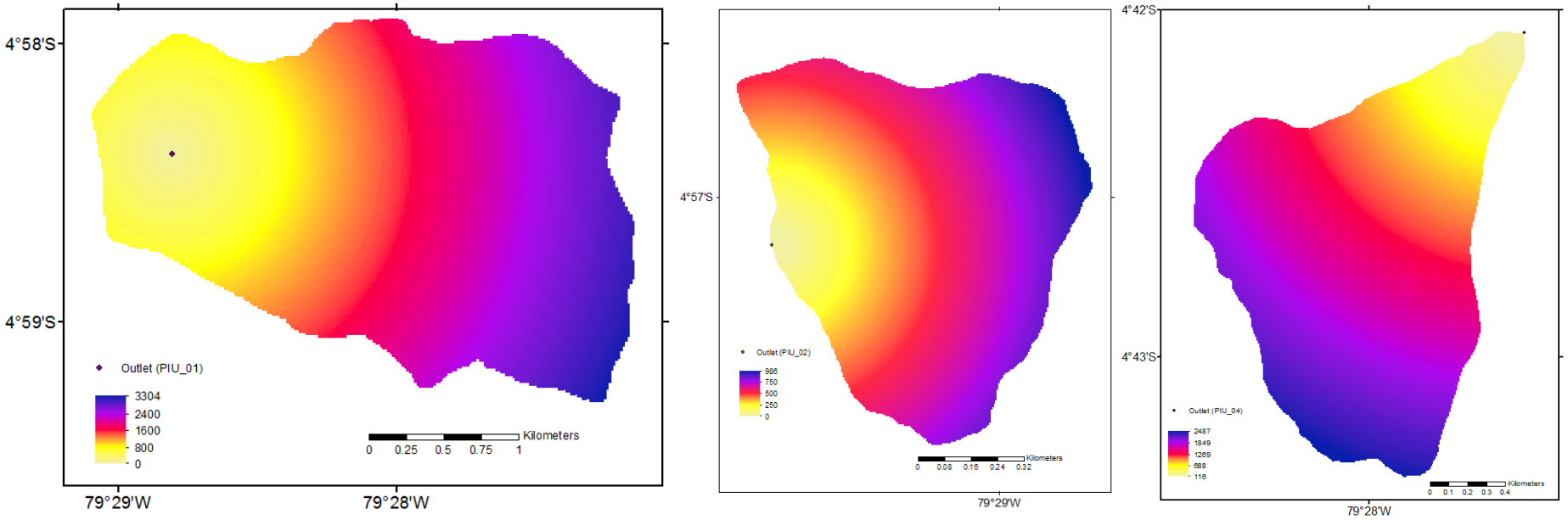

Figure 2.9 Maps of the distance to the outlet of three example iMHEA catchments, PIU1 (left), PIU2 (mid), and PIU4 (right).

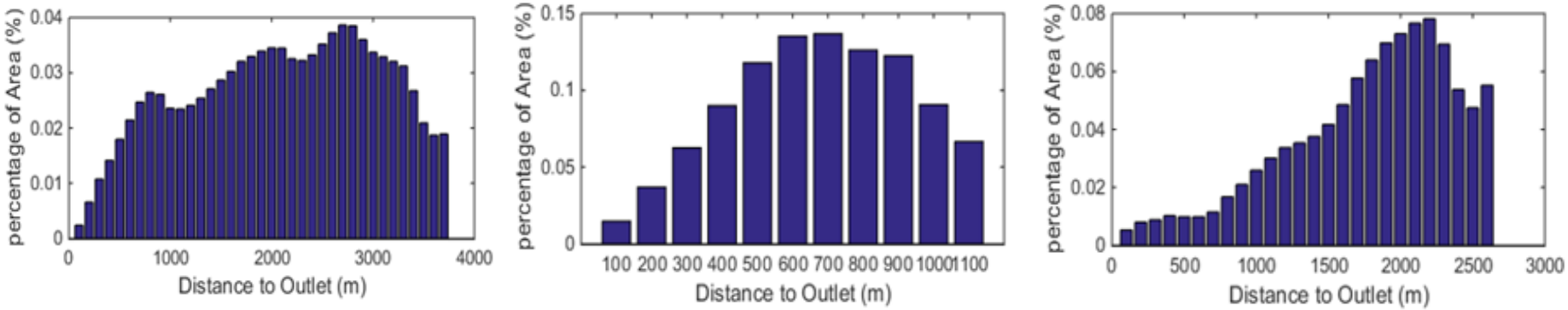

Figure 2.10 Histogram of the distance to the outlet of three example iMHEA catchments, PIU1 (left), PIU2 (mid), and PIU4 (right).

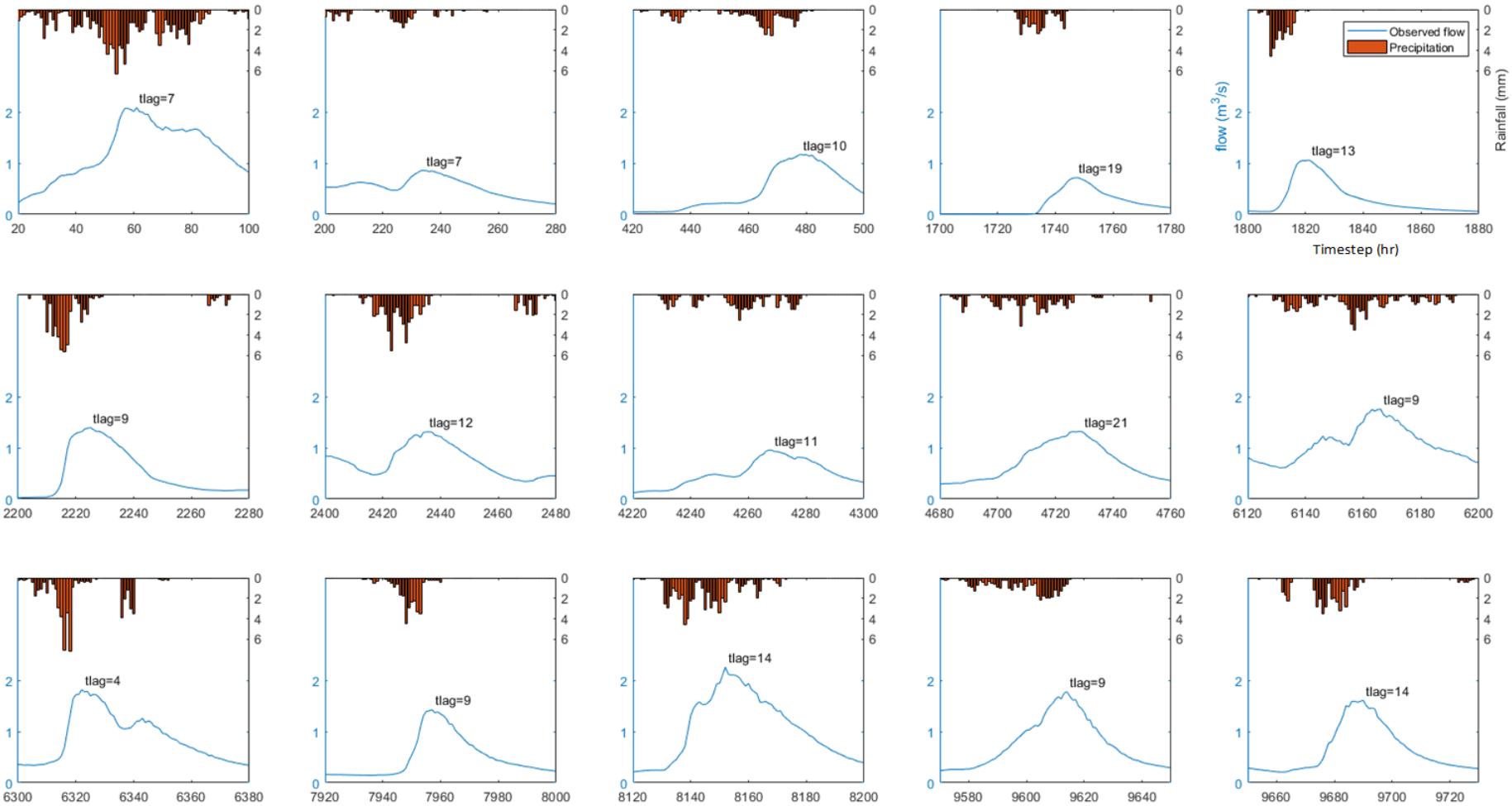

Figure 2.11 Time to peak identified by using hydrograph (mean value of tlag is 11.2 hr in PIU_01, label shown as the top-right figure)

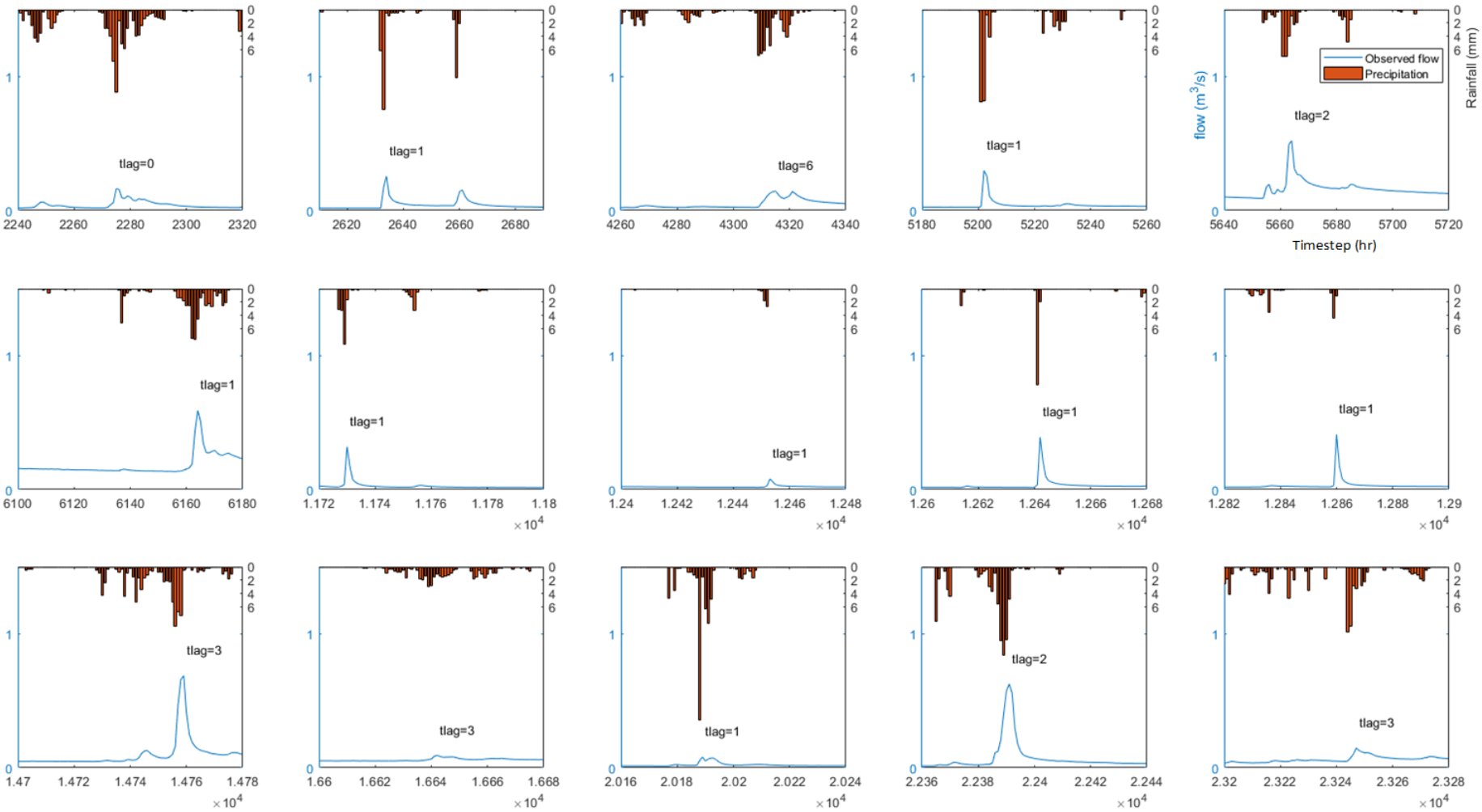

Figure 2.12 Time to peak identified by using hydrograph (mean value of tlag is 1.8 hr in PIU_04, label shown as the top-right figure)

2.2.7 Model evaluation

The hydrological response was simulated for 5 catchments (PIU_01, CHA_02, HUA_01, LLO_02, JTU_03). The selected catchments are natural catchments with no human intervention, distributed in the Upper Andean region. For each catchment, the JULES model was driven with the iMHEA precipitation dataset, and two alternative precipitation datasets from NCEP-DOE Reanalysis II, and TRMM_3B42.7, within the period of available iMHEA precipitation data (Table 2.6). The variability in three precipitation dataset was summarised using the annual ratio of days with zero precipitation (DAYP0) and daily rainfall variability (PVAR), which is the standard deviation (σ_P) divided by its mean value (P_{mean}) (eq. 2.15).

$$\text{Pvar:} \frac{\sigma_P}{P_{mean}} \tag{2.15}$$

The model performance was assessed by summarizing the simulated time series into hydrological indices, including rainfall-runoff ratio (RR), Baseflow index (BFI), daily flow variation (Qvar), skewness in daily flows (Qskew), the slope of the flow duration curve (R2FDC), and Nash–Sutcliffe model efficiency (NSE).

RR marks the ratio between the total flow (Q) and the total rainfall volume (P) over the monitored period, which gives direct indication of the water yield (eq. 2.16).

$$\text{RR} = \frac{Q}{P} \tag{2.16}$$

Table 2.6 Modelling period for the 5 catchments for rainfall data evaluation

Site	Modelling started	Modelled concluded	Duration (Years)
PIU_01	2013/7/6	2016/5/10	2.81
CHA_02	2012/1/1	2013/12/31	1.97
HUA_01	2011/2/27	2014/6/19	3.27
LLO_02	2013/1/11	2015/12/31	2.93
JTU_03	2013/11/21	2016/2/10	2.19

The baseflow sustaining the ecosystem between rainfall events was assessed using BFI as short-term indicator, and R2FDC as long-term indicator. BFI defines the ratio of baseflow (Q_{base}) to the total flow (eq. 2.17). For dry weather runoff assessment, the baseflow was separated from the total flow with using the two-parameter algorithm from Chapman (1999) with a filter parameter of 0.085 (Ochoa-Tocachi, Buytaert & De Bièvre, 2016).

$$\mathrm{BFI} = \frac{Q_{base}}{Q} \tag{2.17}$$

R2FDC is the slope in the middle third (between Q_{66} and Q_{33}) of the flow duration curve in logarithmic scale (eq. 2.18), which was used to assess the long-term hydrological regulation capacity (Olden & Poff, 2003). Flatter slope (value close to 0) indicates higher water hydrological regulation capacity with lower change in flow between 33% and 66% exceedance flow:

$$\mathrm{R2FDC} = \frac{\log_{10} Q_{66} - \log_{10} Q_{33}}{0.66 - 0.33} \tag{2.18}$$

The flow stability was assessed by using Qvar, which is the standard deviation (σ_Q) divided by its mean value (Q_{mean}) (eq. 2.19).

$$\mathrm{Qvar}: \frac{\sigma_Q}{Q_{mean}} \tag{2.19}$$

Q_{skew} flows provides an estimate of the third moment (eq. 2.10).

$$\mathrm{Q}_{skew} = \frac{E(x-\mu)^3}{\sigma^3} \tag{2.20}$$

The overall model performance was evaluated using the Nash Sutcliffe Efficiency (NSE):

$$\mathrm{NSE} = \frac{\sum_t^N \left(Q_{mod,t} - Q_{obs,t}\right)}{\sum_t^N \left(Q_{obs,t} - Q_{obs,mean}\right)} \tag{2.21}$$

where $Q_{obs,mean}$ is the mean of observed flow, $Q_{obs,t}$ and $Q_{mod,t}$ is the observed flow and modelled flow at timestep t (eq. 2.21). NSE can range from $-\infty$ to 1, as 1 marks a perfect match between the modelling flow and the observation, an efficiency of 0 denote that model predictions are as accurate as using the mean of the observed data (Nash & Sutcliffe, 1970).

2.3 Results and discussion

2.3.1 Uncertainty in precipitation data

The precipitation characteristics of the iMHEA precipitation dataset, and two alternate precipitation datasets from NCEP-DOE Reanalysis II, and TRMM_3B42.7 were compared using annual rainfall, DAYP0, and PVAR (Table 2.7) in 5 study catchments (PIU_01, CHA_02, HUA_01, LLO_02, JTU_03).

It is found that NCEP precipitation data is not reliable for site study in all five catchments due to the high difference in the magnitude of rainfall, ranging from 48.8% to 346.8% compared to the iMHEA data. In PIU_01, the variability (DAYP0, and PVAR) is close to the iMHEA rainfall. However, the magnitude of rainfall is far lower than the iMHEA precipitation (NCEP data is 48.8% of the iMHEA data). In HUA_01, the NCEP precipitation is 80.9% of the iMHEA value with lower variability (DAYP0: NCEP=0.02, iMHEA=0.32; PVAR: NCEP=1.23, iMHEA=1.46). In CHA_02, considerably higher rainfall is estimated by NCEP data (261.2% of the iMHEA data), LLO_02 (210.3% of the iMHEA data) and JTU_03 (346.8% of the iMHEA data).

The TRMM data underestimate the precipitation in PIU_01 (33.9% of the iMHEA data), and HUA_01 (68.5% of the iMHEA data). Reasonable estimation of the magnitude of rainfall can be found in CHA_02 (105.7% of the iMHEA data), and LLO_02 (99.9% of the iMHEA data). In CHA_02, the TRMM rainfall estimates are close to the iMHEA data, whereas the variability is higher (PVAR: TRMM=2.33, iMHEA=1.38). DAYP0 shows that 25% of days with zero precipitation in iMHEA, with the higher ratio using TRMM data (40%). In LLO_02, the difference in total rainfall between TRMM and iMHEA is merely 0.01%, DAYP0 has also indicated similar precipitation characteristic (TRMM:0.45, iMHEA:0.47). In JTU_03, higher precipitation has been suggested by the TRMM data (140.2% of the iMHEA data).

Table 2.7 Comparison of the three sets of rainfall data assessed in this study

Site	Data	Rainfall [mm/year]	PVAR	DAYP0
PIU_01	iMHEA	2012.0	1.52	0.20
	NCEP	983.6	1.54	0.26
	TRMM	681.3	2.67	0.63
CHA_02	iMHEA	887.3	1.38	0.25
	NCEP	2318.2	1.15	0.09
	TRMM	938.1	2.33	0.40
HUA_01	iMHEA	1210.0	1.46	0.32
	NCEP	978.6	1.23	0.02
	TRMM	828.8	1.38	0.04
LLO_02	iMHEA	1059.7	1.87	0.47
	NCEP	2228.9	1.83	0.14
	TRMM	1058.8	2.03	0.45
JTU_03	iMHEA	845.5	1.69	0.13
	NCEP	2932.6	1.72	0.03
	TRMM	1185.7	2.08	0.32

2.3.2 Modelling flow with iMHEA/NCEP/TRMM precipitation data

The hydrological response of 5 catchments (PIU_01, CHA_02, HUA_01, LLO_02, JTU_03) was simulated by driving the JULES model for each catchment using the iMHEA precipitation datasets, and two alternate precipitation datasets, NCEP-DOE Reanalysis II, and TRMM_3B42.7. Model performance is evaluated using the hydrological indices as summarised in Table 2.8.

The magnitude of flow is the major concern when comparing three sets of simulations. Runoff was considerably overestimated in JTU_03 (686.9% of the observation flow; Figure 2.13) using NCEP precipitation. Large gaps also exist in the other 4 catchments which could be attributed to the high difference in the magnitude of rainfall.

In LLO_02, the TRMM precipitation is closer to the iMHEA observations. Two simulations generated similar flow duration curve and hydrological indices, but both flows are significantly higher than the observed values. The gap could be attributed to the unobserved subsurface and groundwater preferential flow from deep soil layers (Buytaert et al., 2006; Ochoa-Tocachi et al., 2016), which was not observed by the monitoring network.

In CHA_02, the TRMM precipitation is 5% higher than the iMHEA precipitation. Both modelling results considerably underestimate the average flow with a marked difference in flow pattern. Higher peak flow was simulated using TRMM precipitation (Qskew: TRMM=8.59; iMHEA=3.46).

Among these three sets of rainfall input data, the modelling results using iMHEA data is the closest to the observed values in PIU_01 and HUA_01. As shown in Figure 2.14, most of the peak flow is well captured for the two sites. The largest gap between

the modelling results and the observation could be found in recession process of the modelled hydrograph. Lower water yield is generated, with faster recessions, using iMHEA precipitation data. Zulkafli et al. (2013) already showed that TRMM precipitation data (TRMM 3B42.6) has better model performance over the NCEP Reanalysis data (Kalnay et al., 1996) for large basins (> 4640 km^2) in the Peruvian Andes–Amazon study. In this Chapter, the NSE value suggests that better site-scale hydrological estimation can be obtained by using participatory data compared to the use of large-scale reanalysis data.

Table 2.8 Comparison of modelling results among using three set of rainfall data

	Rainfall [mm/year]	Runoff [mm/year]	RR	BFI	Qvar	Qskew	R2FDC	NSE
PIU_01								
Observation		1379.6	0.686	0.425	1.09	2.19	-1.29	
iMHEA	2012.0	944.0	0.469	0.406	1.37	3.03	-1.50	0.57
NCEP	983.6	336.5	0.342	0.360	1.73	3.87	-1.92	-0.64
TRMM	681.3	217.6	0.319	0.288	2.54	5.20	-0.78	-0.59
CHA_02								
Observation		714.8	0.806	0.550	1.26	4.73	-0.53	
iMHEA	887.3	157.4	0.178	0.247	1.72	3.46	-4.30	0.05
NCEP	2318.2	1094.4	0.472	0.543	1.08	4.52	-1.33	-1.57
TRMM	938.1	214.2	0.228	0.195	2.68	8.59	-3.43	-0.47
HUA_01								
Observation		774.1	0.640	0.674	1.30	1.64	-3.23	
iMHEA	1210.0	653.8	0.540	0.561	1.13	2.35	-1.44	0.55
NCEP	978.6	374.8	0.383	0.553	1.06	3.17	-1.06	0.04
TRMM	828.8	281.6	0.340	0.393	1.21	3.47	-1.34	-0.14
LLO_02								
Observation		146.6	0.138	0.880	0.60	1.72	-0.69	
iMHEA	1059.7	513.9	0.485	0.863	0.68	0.93	-1.05	-26.8
NCEP	2228.9	1600.7	0.718	0.811	1.19	2.64	-1.26	-670
TRMM	1058.8	509.2	0.481	0.862	0.71	1.12	-1.16	-28.2
JTU_03								
Observation		310.5	0.368	0.742	0.90	4.53	-0.58	
iMHEA	845.5	162.6	0.192	0.726	0.83	1.93	-0.91	0.040
NCEP	2932.6	2132.8	0.727	0.803	1.10	2.48	-1.33	-115
TRMM	1185.0	473.0	0.399	0.818	0.64	2.73	-0.78	-0.57

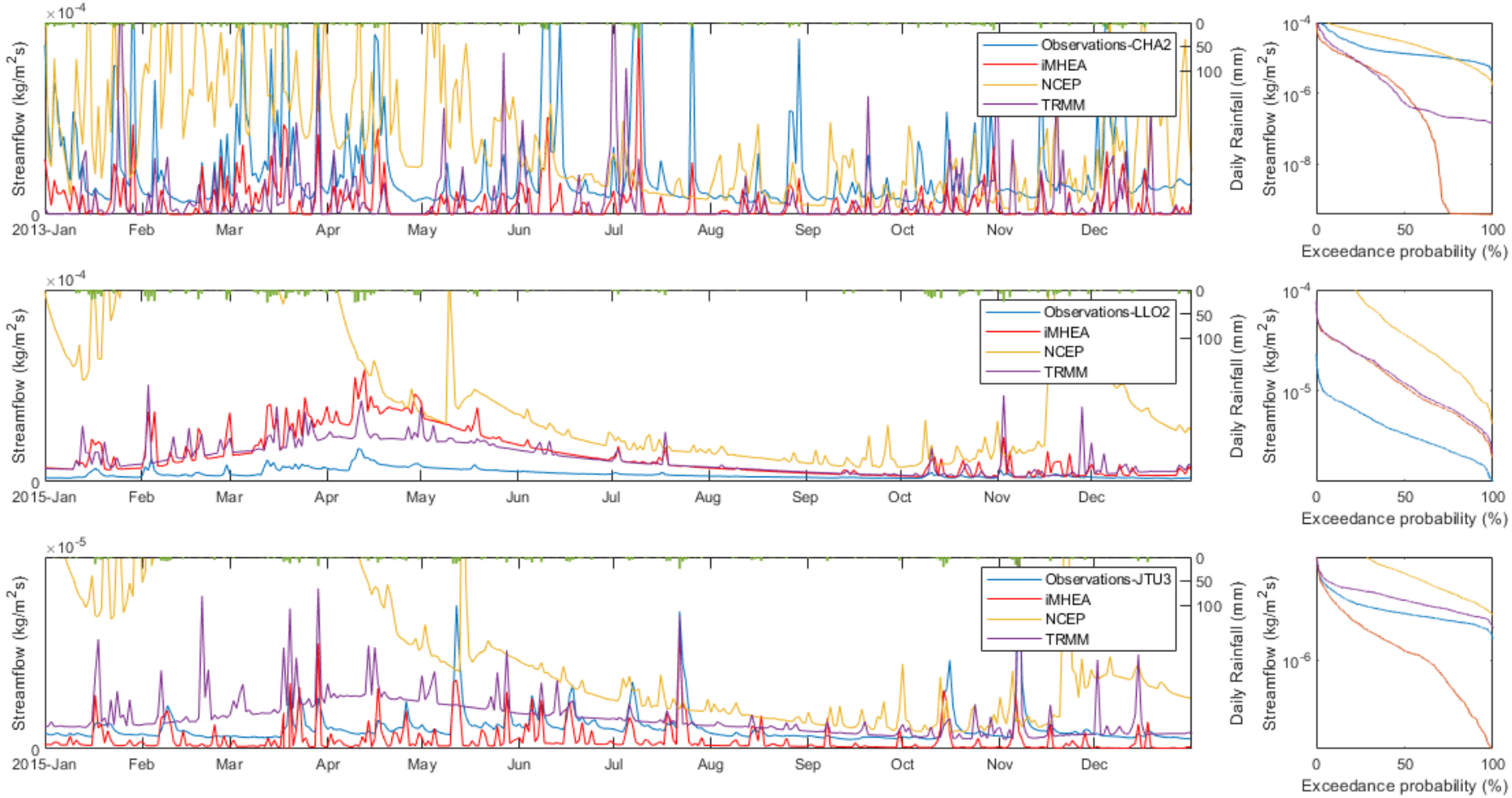

Figure 2.13 Simulated discharge time series (left) and flow duration curves (right) using resp. iMHEA/NCEP/TRMM precipitation data in CHA2/LLO2/JTU3

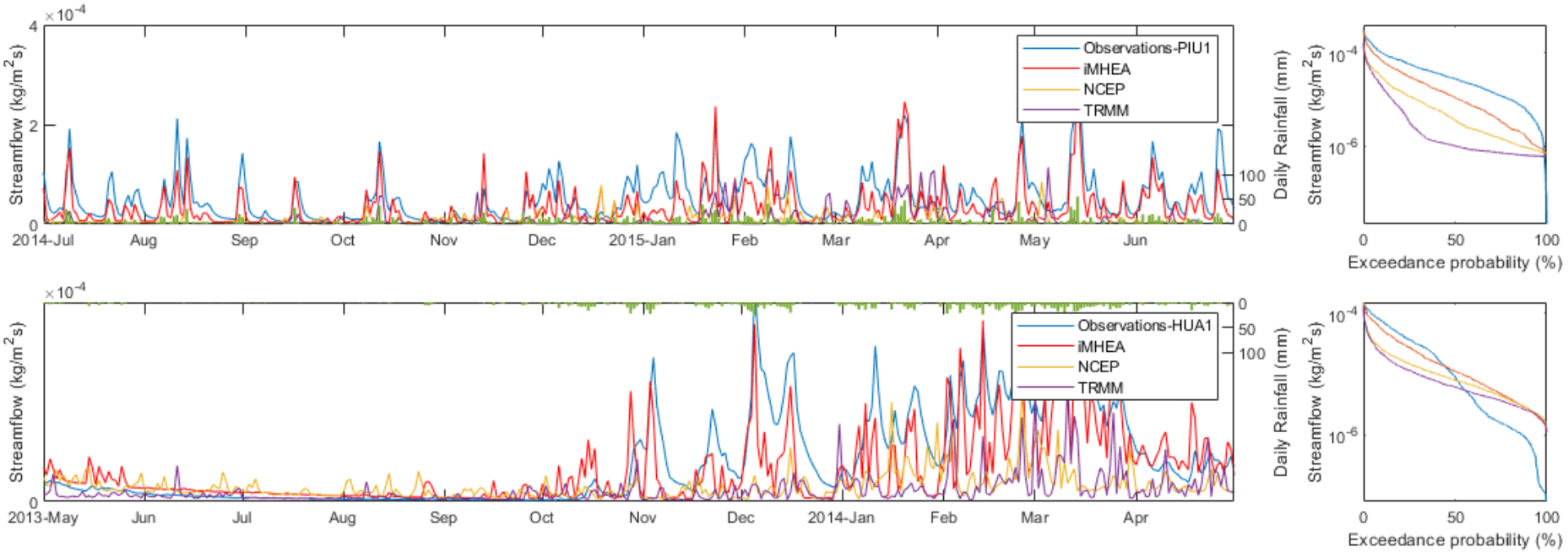

Figure 2.14 Simulated discharge time series (left) and flow duration curves using resp. iMHEA/NCEP/TRMM precipitation data in PIU1/HUA1

2.4 Conclusions

Land surface models have been increasingly used for hydrological assessment. The JULES model used in this study, has been successfully implement in regional hydrological assessment (e.g. Zulkafli et al., 2013). Precipitation data is the most important driver in the hydrological model. However, it could be highly uncertain for small scale hydrological studies (Buytaert, Célleri & Timbe, 2009). In the five selected tropical Andean catchments, I found that there is considerable difference in the rainfall characteristic, both in magnitude and variability, among participatory data (iMHEA), and two large-scale reanalysis data (NCEP and TRMM). Evaluations of flow simulations were made by driven the JULES model using the iMHEA/NCEP/TRMM precipitation dataset, respectively. At the scale of catchments no larger than 7.8 km^2, I therefore conclude that participatory collected data (iMHEA) are more capable to simulate the flow. There are still gaps between the simulation and observation, which might be attributed to the uncertainty in soil and vegetation representatio. These issues are further investigated in the following Chapters.

3 Parameterization of JULES land surface types for the tropical Andes using a network of monitored catchments

3.1 Introduction

Physically-based hydrological models are often used to predict the impact of change, such as catchment interventions and land-use and land-cover change (LUCC), because it is possible to map the modeller's knowledge about the hydrological impacts of LUCC into physically meaningful parameters. Soil hydraulic models determinate the water movement by using soil parameters (see Section 2.2.5). A major weakness of JULES and other land surface models is the limited number of land surface parameterizations that is available in the default setup. In JULES, land cover representation is simplified into five plant functional types, and the required soil parameters are commonly derived from large scale soil textual database (Cosby et al., 1984; Tomasella & Hodnett, 1998) using pedotransfer functions (PTFs). The availability of sets of parameterizations greatly simplifies setting up JULES for large scale applications and data-scarce regions, but it comes at the expense of a highly simplified representation and coarse classification of surface hydrological processes. Marthews et al. (2014) concluded that the availability of soil data is still low in the tropical South America. For the study sites, I found considerably higher values of water retention properties investigated from the local experimental data (Buytaert et al., 2005; Crespo et al., 2011) than the values derived from the commonly use PTFs. This is problematic if JULES is used for LUCC evaluation, because of the high variability of land-use types and related hydrological processes. The common PTFs approach generates the same soil parameters for nearby catchments with different LUC due to the coarse resolution

of available soil properties. To avoid the issues related to parameterization of individual land-use types in a complex physically-based model such as JULES on the one hand, and the limited number of predefined land cover classes in JULES on the other, I posit the idea of the creation of parameter "libraries" of land cover classes for models such as JULES. The parameter libraries extend directly the default setup in JULES to 12 represented land-cover types (Table 3.1) in the tropical Andes from a network of upland catchments designed to characterise of different LUC types (Ochoa-Tocachi et al., 2018). These selected catchments feature Andosols (Ochoa-Tocachi et al., 2018), and are characterised by the highest availability of recent hydrological monitoring data (from 2012 to 2017). I use these data to assess the effects of soil parameterisation on JULES's simulation of streamflow and evaluate the impact of allowing for the more fine-grained representation of LUCC on hydrological evaluation.

Table 3.1 The parameter libraries for the represented land-cover types in the tropical Andes. BF: Broadleaf Forest, NF: Needleleaf Forest, C3: C3 grasses, C4: C4 grasses, SH: Shrub, BS: Bare soil.

Site	Land cover	Default setup	Major soil class (FAO)
PIU_01	Natural páramo	0.15 BF, 0.85 C4	60% Cambisols; 40% Regosols
PIU_02	Grazed páramo	0.15 BS, 0.85 C4	
PIU_04	Puna forest	0.80 BF, 0.20 C4	
PIU_07	Cultivated puna	0.35 CR, 0.45 C4, 0.20 SH	
JTU_03	Natural páramo	0.80 C4, 0.20 SH	100% Andosols
JTU_02	Grazed páramo	1.00 C4	
LLO_02	Restored páramo	0.10 BF, 0.90 C4	50% Phaeozems;30% Andosols; 20% Regosols
LLO_01	Grazed páramo	0.10 SH, 0.90 C4	
CHA_02	Natural jalca	0.10 BF, 0.90 C4	45% Leptosols; 40% Cambisols; 15% Regosols
CHA_01	Afforested jalca	0.80 NF, 0.20 C4	
HUA_01	Natural puna	0.75 C4, 0.25 BS	100% Leptosols
HUA_02	Grazed puna	0.70 C4, 0.30 BS	

3.2 Methods

3.2.1 Parameterisation of high-Andean soils

The pedotransfer functions (PTFs) of Hodnett & Tomasella (2002) are commonly used (Marthews et al., 2014) to estimate the unavailable soil parameters of land surface models from a large-scale soil database (Fao/Iiasa/Isric/Isscas/Jrc, 2012). In the experimental catchments, the high-Andean soils (Andosol, Leptosol, Histosol, Cambisol and Regosol) are characterised high water retention capacity (Buytaert et al., 2005; Crespo et al., 2011), which is not well represented by the PTF-based estimations (Figure 3.1). This could be attributed to the inability of the PTFs to present the high water retention caused by the presence of amorphous clay minerals such as allophane and imogolite (Buytaert et al., 2006). Therefore, I explore the use of in-situ experiment data of Histic Andosols obtained by Buytaert et al. (2005) as a complement to the PTF-based soil water retention data.

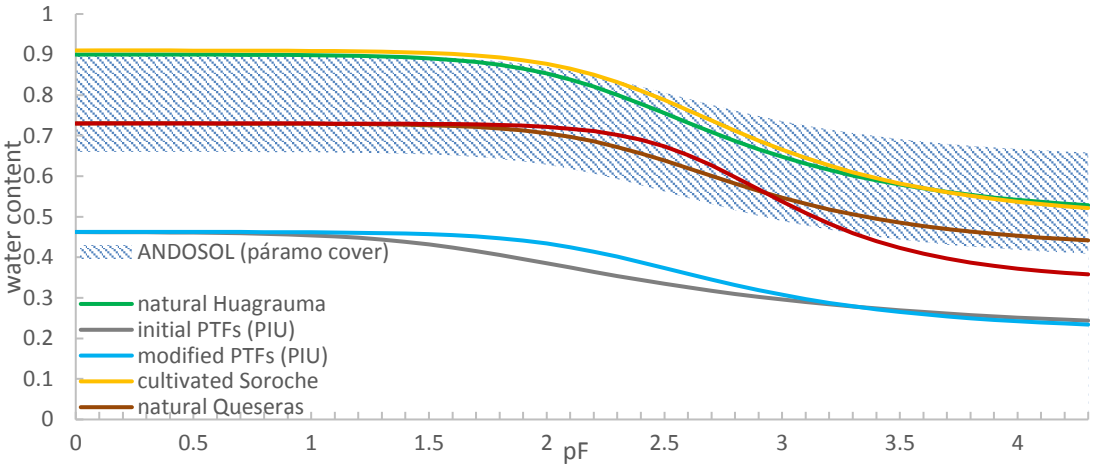

Figure 3.1 Water retention curves obtained from 1) PTFs estimation 2) in-situ investigation at three locations: Huagrauma, Soroche and Queseras.

Table 3.2 Four combinations of soil parameters.

Parameter estimation method	Van Genuchten parameters (n, α)	Water retention (θsat, θcrit, θwilt)	Thermal properties (hcon, hcap)	Saturated hydraulic conductivity (Ksat)
initial PTFs	FAO+PTFs	FAO+PTFs	FAO+PTFs	FAO+PTFs
initial Huagrauma	Histic	Histic	Histic+PTFs	Histic
modified Huagrauma	Histic	Modified Histic	Histic+PTFs	Histic
modified PTFs	Histic	FAO+PTFs	FAO+PTFs	FAO+PTFs

I parameterise the soil data using four different combination as shown in Table 3.2 since these parameters are independently derived from others. The first one “initial PTFs” is the most common approach, which obtains the parameters using PTFs (Table 2.4) with the FAO soil data (Table 3.3).

The second one “initial Huagrauma” uses the water retention properties and saturated hydraulic conductivity from the in-situ experiment data at the Huagrauma catchment in the south Ecuadorian páramo (Buytaert et al., 2005). The Van Genuchten parameters are numerically fitted using the least-squares method with the available water retention data (using eq. 2.11).

The water retention data in Huagrauma were found to vary within a range (θsat : 0.66-0.90; θcrit:0.39-0.64) (Crespo et al., 2011). Therefore, the third combination “modified Huagrauma” lowered the wilting point to a level found in the páramo covered Andosol (Figure 3.1). I use the same Van Genuchten parameters from the second combination due to the insufficient data for numerical fitting (only the ranges of θsat, θcrit, θwilt are available).

The fourth combination “modified PTFs” is similar to the first one, but has replaced the Van Genuchten parameters to the values of the second combination, which shown gradually decrease under increasing pressure compared to the first combination (Figure 3.2). A higher value of θcrit is obtained with this approach compared to “initial PTFs”.

Table 3.3 Soil properties obtained from FAO soil database. CL: clay fraction, SA: sand fraction, SI: silt fraction, DBD: dry bulk density (g/cm^3), SOC: soil organic carbon (% weight), CEC: carbon exchange capacity (cmol/kg), pH: hydrogen ion activity.

Catchment	Sand	Silt	Clay	DBD	SOC	CEC	pH
PIU	0.392	0.270	0.338	1.308	12.62	19.2	5.6
CHA	0.508	0.282	0.211	1.164	24.64	13.8	4.7
HUA/HMT	0.551	0.255	0.195	1.395	8.87	18.0	5.6
LLO	0.623	0.307	0.070	1.226	14.49	7.9	6.2
JTU	0.426	0.466	0.108	0.914	45.28	14.0	5.2
TAM	0.416	0.385	0.199	1.293	20.34	20.6	7.3
PAU	0.484	0.348	0.168	1.004	30.26	11.4	5.4
TIQ	0.211	0.521	0.269	1.231	16.63	5.0	5.2

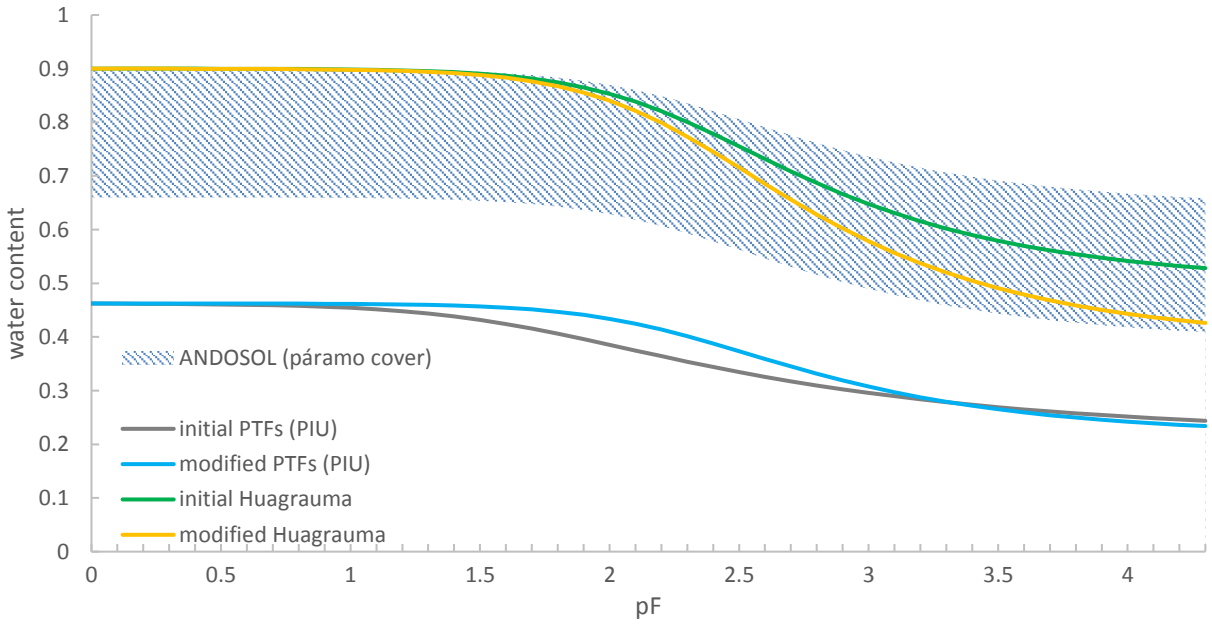

Figure 3.2 Water retention curves of the soil as generated by each of the parameter estimation methods.

3.2.2 Model evaluation

The performance of the model using four combinations of soil parameters was assessed by summarizing the simulated time series into hydrological indices, including rainfall-runoff ratio (RR), Baseflow index (BFI), daily flow variation (Qvar), skewness in daily flows (Qskew), the slope of the flow duration curve (R2FDC), and the Nash–Sutcliffe model efficiency (NSE) as described in detail in Section 2.2.7. In addition to the hydrological indicators, the hydrograph is used to compare the peak flow (the maximum discharge), recession lamb (the ending period of peak flow, and returns to groundwater-derived baseflow), and level of baseflow.

3.3 Results

3.3.1 Comparison of four parameter estimation methods

The soil parameters obtained from four combinations are shown in Table 3.4. The first combination “Initial PTFs” derived soil parameters from FAO database, thus, 8 different parameter sets were obtained for individual catchment. The second combination “Initial Huagrauma” was obtained from the in-situ experiment data at Huagrauma (Buytaert et al., 2005). The Van Genuchten parameters were numerically fitted using the water retention data.

The Van Genuchten parameter n measures the uniformity of pore sizes in the soil. The value ranges between 1.336 and 1.400 using the first method, which is slightly lower than the value of 1.560 obtained from the in-situ experiment. The Van Genuchten parameter α indicates the soil structure. The experiment estimation gives much lower value 0.557 than the PTFs estimation, which ranges from 1.473 to 2.545. There is significantly gap in the water retention properties between the PTFs estimation and the experiment values. The values of θsat are between 0.422 to 0.565, which is a value that is lower compared to the experiment data 0.900.

The third combination “Modified Huagrauma” was similar to the “Initial Huagrauma”, but reduces the wilting point to a lower level (i.e. from 0.500 to 0.431 in PIU_01) according to the lower boundary of the experimental data of páramo covered Andosol (Crespo et al., 2011). This modification allows more water to be extracted from the soil column.

The fourth combination “modified PTFs” is similar to the first one, but replaces the Van Genuchten parameters to the values of the second combination. The increasing value of θcrit has reduced the soil moisture extraction by the vegetation (following e.q. 2.12) as the moisture availability factor (β) decreased.

Table 3.4 Soil parameters used in JULES

parameter estimation method	Catchment	n	α	θsat	θcrit	θwilt	hcon	hcap	K
Initial PTFs	PIU	1.359	2.288	0.463	0.333	0.217	0.219	1189944	0.0034
	CHA	1.350	2.545	0.492	0.321	0.173	0.199	1110088	0.0057
	HUA	1.386	2.364	0.422	0.280	0.167	0.264	1259371	0.0066
	LLO	1.400	1.980	0.467	0.271	0.104	0.225	1146028	0.0097
	JTU	1.319	1.715	0.565	0.387	0.161	0.149	938752.8	0.0052
	TAM	1.350	1.479	0.464	0.335	0.176	0.223	1169057	0.0044
	PAU	1.336	2.049	0.542	0.354	0.156	0.163	996455	0.0056
	TIQ	1.384	1.473	0.479	0.342	0.189	0.207	1144154	0.0022
Initial Huagrauma		1.560	0.557	0.900	0.751	0.500	0.037	221412	0.0034
Modified Huagrauma		1.560	0.557	0.900	0.716	0.431	0.037	221412	0.0034
Modified PTFs	PIU	1.560	0.557	0.463	0.371	0.217	0.219	1189944	0.0034
	CHA	1.560	0.557	0.492	0.373	0.173	0.199	1110088	0.0057
	HUA	1.560	0.557	0.422	0.327	0.167	0.264	1259371	0.0066
	LLO	1.560	0.557	0.467	0.332	0.104	0.225	1146028	0.0097
	JTU	1.560	0.557	0.565	0.415	0.161	0.149	938752.8	0.0052
	TAM	1.560	0.557	0.464	0.356	0.176	0.223	1169057	0.0044
	PAU	1.560	0.557	0.542	0.398	0.156	0.163	996455	0.0056
	TIQ	1.560	0.557	0.479	0.371	0.189	0.207	1144154	0.0022

3.3.2 River flow under four sets of soil parameter

Table 3.5 and Table 3.6 summarize the evaluation of the JULES model driven by using the four soil parameter sets, with the hydrological indices (see Section 2.2.7).

In PIU_01 (Figure 3.3a), the JULES run driven by the parameter values estimated using the "initial PTFs", underestimates the runoff by 35.1% (RR:0.445 vs 0.686) but has a baseflow ratio similar to the observations (BFI: 0.417 vs 0.425). The model performance improves most under the "initial Huagrauma" setup (NSE:0.680), which gives a better runoff estimation (RR:0.654). However, the hydrograph shows that baseflow has mostly increased (BFI:0.647), which leads to a higher regulation capacity (as expressed in the slope of the flow duration curve R2FDC), than that of the observed flow (R2FDC: -0.61 vs -1.29). The "modified Huagrauma" setup drops the wilting point to a lower value (θwilt: 0.500->0.431) compared to "initial Huagrauma", which increased the water availability for vegetation extraction. This lowers the flow (RR: 0.654 -> 0.559), particularly the subsurface flow (BFI: 0.654 -> 0.610). The "modified PTFs" setup increases the value of θcrit from "initial PTFs", which reduces the water extraction of vegetation. Runoff is considerably higher (RR: 0.445 -> 0.566) with the subsurface flow increased as well (BFI: 0.417 -> 0.611).

In the adjacent catchment, PIU_02 (Figure 3.3b), the parameters estimated with the "initial PTFs" yield a lower runoff than the observations (RR: 0.550 vs 0.639), whereas the slope of the FDC is closer to the observed value of (R2FDC: -1.34 vs -1.37). A higher runoff is simulated under the "initial Huagrauma" setup (RR: 0.690), which has a lower wilting point compared to the "modified Huagrauma" setup (RR:0.623). The "modified PTFs" gives a more precise prediction for both runoff (RR: 0.637 vs 0.639) and baseflow (BFI: 0.588 vs 0.598), which also shows the highest NSE value (0.774) out of the four combinations.

In PIU_04 (Figure 3.3c), the use of the “initial PTFs” has underestimated flow (RR: 0.197 vs 0.389), which is characterised by low baseflow (BFI: 0.575 vs 0.851). The issue is again overcome by using “modified PTFs”. The runoff ratio is considerably closer to the observed flow (RR: 0.469 vs 0.389) and the catchments’ regulation capacity is also well presented (BFI: 0.857, R2FDC: -1.13). The experimentally-based setup, “initial Huagrauma” and “modified Huagrauma” overpredict the flow in this catchment.

In PIU_07 (Figure 3.3d), the initial PTFs parameters simulated the flow best of all the four soil types with the highest NSE value. The flow is considerably lower than the observation (RR: 0.123 vs 0.269). The simulated flow is much higher under the other three sets of parameters (RR > 0.437).

In JTU_03 (Figure 3.4a), the “initial PTFs” setup simulates lower flows than the observed value (RR: 0.255 vs 0.368). The “modified PTFs” manage to model the flow accurately with the RR (0.332 vs 0.368), BFI (0.881 vs 0.742), flow duration curve (R2FDC: -0.42 vs -0.58) closed to its observation. The experimental soil parameters both overestimate the flow (RR > 0.535).

A low flow (RR: 0.071) was observed in JTU_02 (Figure 3.4b). The “initial PTFs” setup gives the closest estimation of flow out of the four set of parameters. However, Model performance is lower (NSE < -0.20) since flows are overestimated under all parameter sets (RR >0.129). The observed flow is more variable (Qvar: 5.77) than all of the simulated values (Qvar <2.71) due to the absence of baseflow.

Similar simulations are found in the restored páramo catchment LLO_02 (Figure 3.4c) and its adjacent grazed páramo catchment LLO_01 (Figure 3.4d). The “initial PTFs” setup simulates the flow that matches the observations best, but is still considerably higher than its observed values (RR: 0.457 vs 0.138 in LLO_02; 0.414 vs 0.121 in LLO_01). The large gap of flow between the simulations and observations leads to a very low model performance for both catchments (NSE < -23.77).

Table 3.5 Hydrological summary indices as calculated from the observed flow time series and the 4 parameter estimation methods for JULES. OBS: Observation, PTF: initial PTFs, EXP: initial experiment data, MOD: modified experiment data, PTFm: modified PTFs; RR: Rainfall-runoff ratio, BFI: Baseflow index, Qvar: Coefficient of variation in daily flows, Qskew: Skewness in daily flows, R2FDC: the slope of the flow duration curve, NSE: Nash–Sutcliffe model efficiency.

Site	Land cover	Soil set	RR	BFI	Qvar	Qskew	R2FDC	NSE
PIU_01	Natural páramo	OBS	0.686	0.425	1.09	2.19	-1.29	n/a
		PTF	0.445	0.417	1.32	3.00	-1.46	0.626
		EXP	0.654	0.654	0.77	2.81	-0.63	0.680
		MOD	0.559	0.610	0.87	2.80	-0.75	0.655
		PTFm	0.566	0.611	0.91	2.80	-0.84	0.670
PIU_02	Grazed páramo	OBS	0.639	0.598	1.15	2.46	-1.37	n/a
		PTF	0.550	0.441	1.32	2.88	-1.35	0.727
		EXP	0.690	0.617	0.89	2.71	-0.67	0.721
		MOD	0.623	0.587	0.96	2.72	-0.78	0.737
		PTFm	0.637	0.589	1.01	2.65	-0.95	0.774
PIU_04	Puna forest	OBS	0.389	0.851	0.95	2.73	-0.85	n/a
		PTF	0.197	0.575	1.54	3.25	-2.47	0.184
		EXP	0.585	0.898	0.49	1.37	-0.69	0.437
		MOD	0.440	0.871	0.58	1.46	-0.85	0.587
		PTFm	0.469	0.857	0.82	1.61	-1.13	0.711
PIU_07	Cultivated puna	OBS	0.269	0.703	1.57	4.36	-1.18	n/a
		PTF	0.123	0.501	2.06	4.15	-0.96	0.366
		EXP	0.537	0.906	0.43	1.66	-0.60	-0.027
		MOD	0.437	0.893	0.46	2.29	-0.56	0.245
		PTFm	0.446	0.882	0.71	1.32	-1.24	0.316
JTU_03	Natural páramo	OBS	0.368	0.742	0.90	4.53	-0.58	n/a
		PTF	0.255	0.245	1.87	3.01	-1.86	-0.217
		EXP	0.601	0.923	0.23	1.70	-0.17	-0.198
		MOD	0.535	0.649	0.87	2.97	-0.42	-0.301
		PTFm	0.332	0.881	0.48	1.51	-0.42	0.211
JTU_02	Grazed páramo	OBS	0.071	0.577	1.44	5.77	-1.03	n/a
		PTF	0.129	0.652	0.97	2.71	-1.08	-0.201
		EXP	0.627	0.930	0.23	1.56	-0.23	-30.57
		MOD	0.471	0.912	0.28	1.71	-0.30	-15.79
		PTFm	0.287	0.880	0.50	1.02	-0.74	-5.047

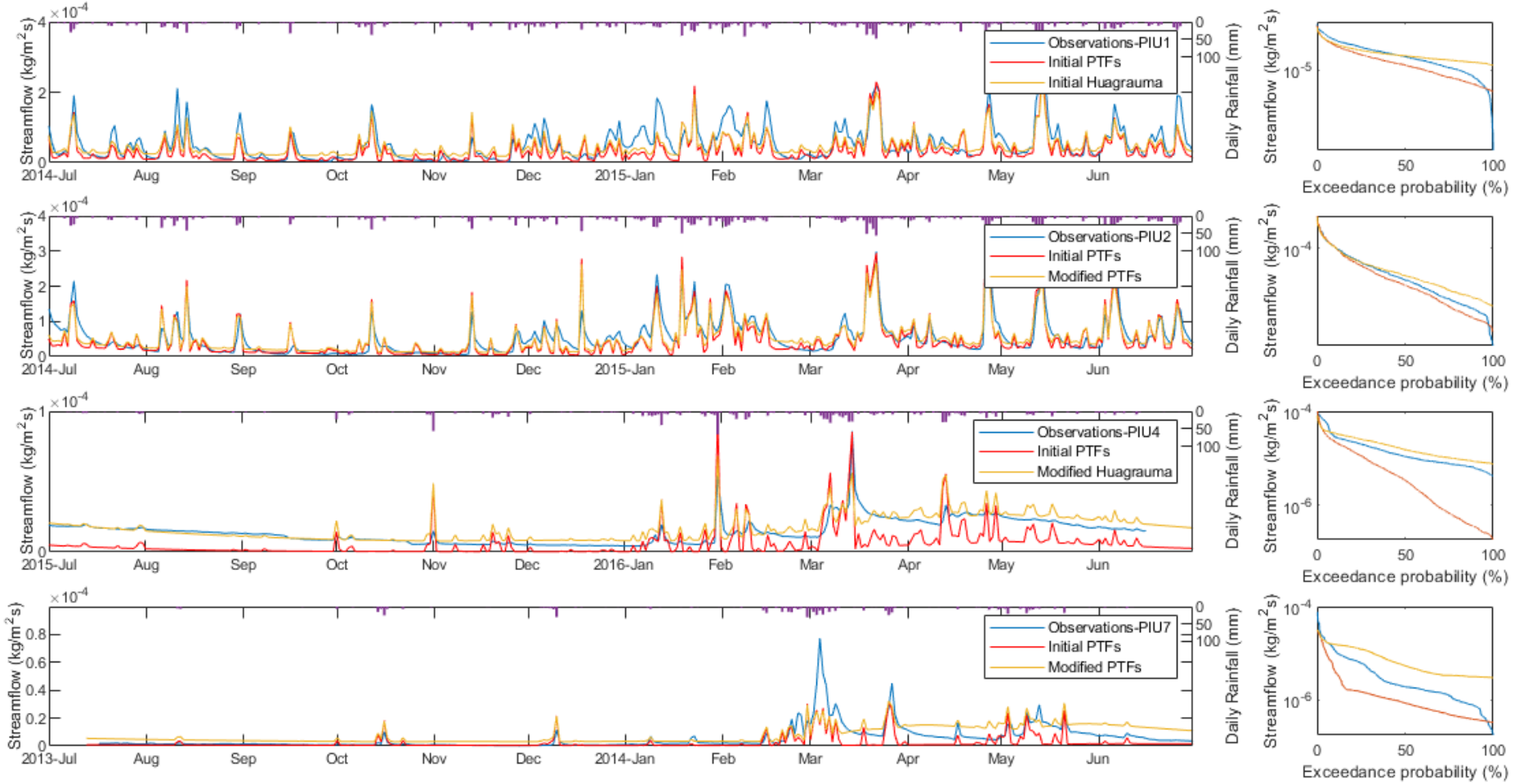

Figure 3.3 Modelling, observations, and flow duration curve in a. PIU1 b. PIU2 c. PIU4 d. PIU7

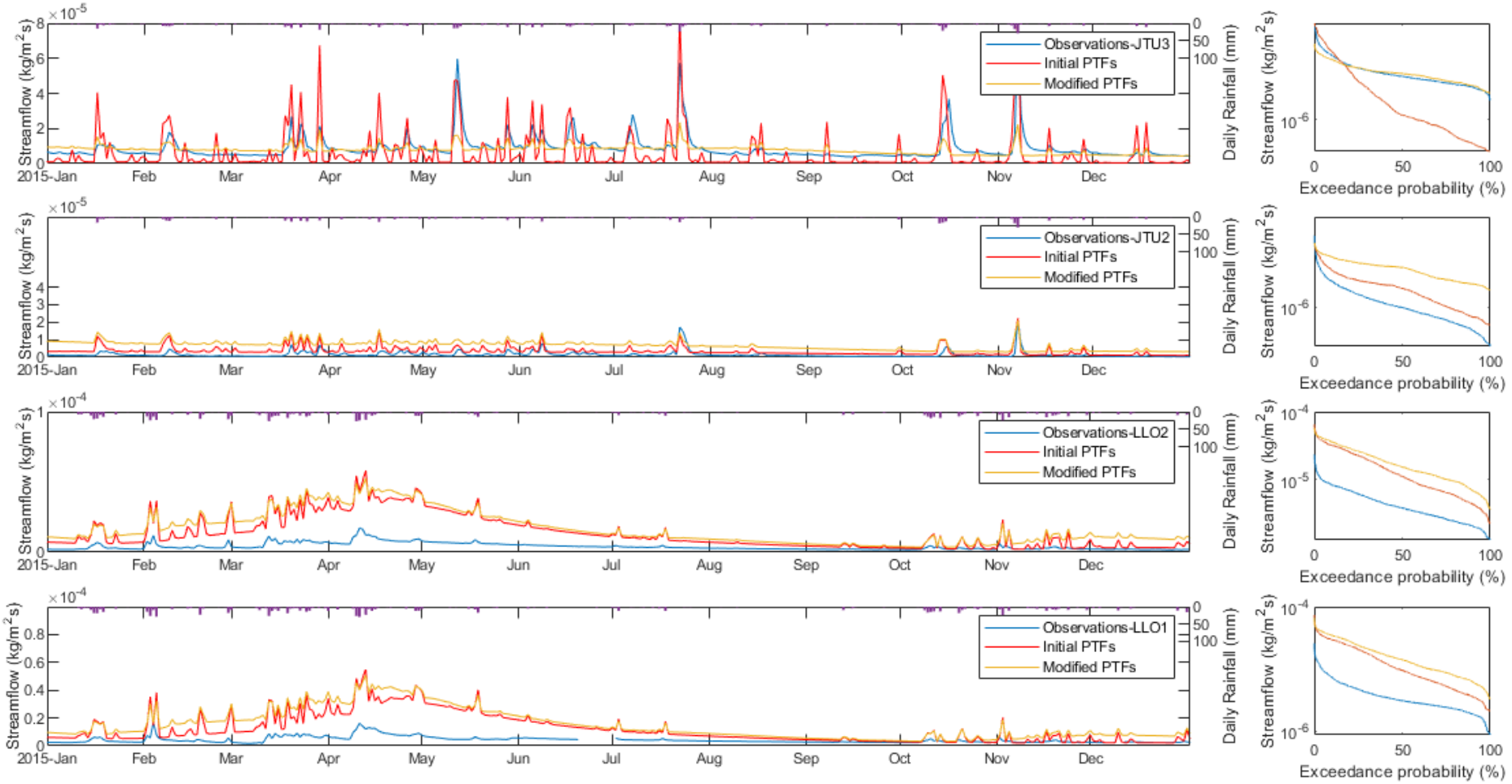

Figure 3.4 Modelling, observations, and flow duration curve in a. JTU3 b. JTU2 c. LLO2 d. LLO1

The flow in the conserved jalca catchment CHA_02 (Figure 3.5a) can be predicted best by using “initial Huagrauma” setup (RR: 0.576 vs 0.805). Most of the peak flows are still lower than the observation but their shape and recession and flow duration curve (R2FDC: -0.45 vs 0.53) is captured adequately. The average runoff is lower when using the other 3 soil parameter sets due to lower simulation of subsurface flow. In its adjacent afforested catchment CHA_01 (Figure 3.5b), the modelling results with “modified PTFs” show the best model performance (NSE: 0.346).

In the conserved puna catchment HUA_01 (Figure 3.5c) and its neighbour grazed catchment HUA_02 (Figure 3.5d), the modified PTFs parameter gives an accurate estimation of the average runoff (HUA1 RR: 0.648, HUA2 RR: 0.618). The magnitude of peak flow could be captured, but the recession processes are faster than the observation. Most of the difference may be caused by the faster recession in the model and the higher baseflow than the observed flow in dry seasons, which leads to a steeper slope in the FDC (R2FDC: -1.28 vs -3.23 in HUA_01; -1.26 vs -2.93 in HUA_02).

Table 3.6 Hydrological summary indices as calculated from the observed flow time series and the 4 parameter estimation methods for JULES. OBS: Observation, PTF: initial PTFs, EXP: initial experiment data, MOD: modified experiment data, PTFm: modified PTFs; RR: Rainfall-runoff ratio, BFI: Baseflow index, Qvar: Coefficient of variation in daily flows, Qskew: Skewness in daily flows, R2FDC: the slope of the flow duration curve, NSE: Nash–Sutcliffe model efficiency.

Site	Land cover	Soil set	RR	BFI	Qvar	Qskew	R2FDC	NSE
LLO_02	Restored páramo	OBS	0.138	0.880	0.60	1.72	-0.69	n/a
		PTF	0.457	0.830	0.74	1.05	-1.17	-26.55
		EXP	0.724	0.917	0.31	1.07	-0.40	-55.26
		MOD	0.596	0.903	0.35	1.04	-0.52	-34.13
		PTFm	0.562	0.886	0.58	0.83	-0.81	-38.36
LLO_01	Grazed páramo	OBS	0.121	0.862	0.68	2.47	-0.53	n/a
		PTF	0.414	0.823	0.78	1.18	-1.19	-23.77
		EXP	0.703	0.914	0.32	1.19	-0.42	-53.68
		MOD	0.564	0.900	0.37	1.16	-0.50	-31.91
		PTFm	0.527	0.880	0.64	0.96	-0.92	-35.45
CHA_02	Natural jalca	OBS	0.805	0.550	1.26	4.73	-0.53	n/a
		PTF	0.184	0.148	1.79	3.65	-5.91	0.073
		EXP	0.576	0.709	0.65	3.36	-0.45	0.448
		MOD	0.517	0.531	1.04	3.30	-0.94	0.550
		PTFm	0.301	0.560	1.01	3.47	-0.82	0.171
CHA_01	Afforested jalca	OBS	0.302	0.441	1.98	3.97	-1.40	n/a
		PTF	0.080	0.199	2.15	4.16	-9.60	0.251
		EXP	0.493	0.864	0.36	3.50	-0.21	0.263
		MOD	0.087	0.508	1.28	3.87	-0.77	0.132
		PTFm	0.268	0.798	0.57	3.32	-0.51	0.346
HUA_01	Natural puna	OBS	0.638	0.674	1.30	1.64	-3.23	n/a
		PTF	0.508	0.526	1.06	2.67	-1.35	0.540
		EXP	0.675	0.685	0.67	2.40	-0.67	0.520
		MOD	0.650	0.536	1.08	2.56	-1.06	0.484
		PTFm	0.631	0.692	0.95	2.03	-1.28	0.648
HUA_02	Grazed puna	OBS	0.579	0.712	1.29	1.53	-2.93	n/a
		PTF	0.491	0.529	1.04	2.43	-1.40	0.483
		EXP	0.655	0.686	0.65	2.28	-0.65	0.453
		MOD	0.594	0.661	0.81	2.33	-0.69	0.458
		PTFm	0.616	0.695	0.92	1.82	-1.26	0.618

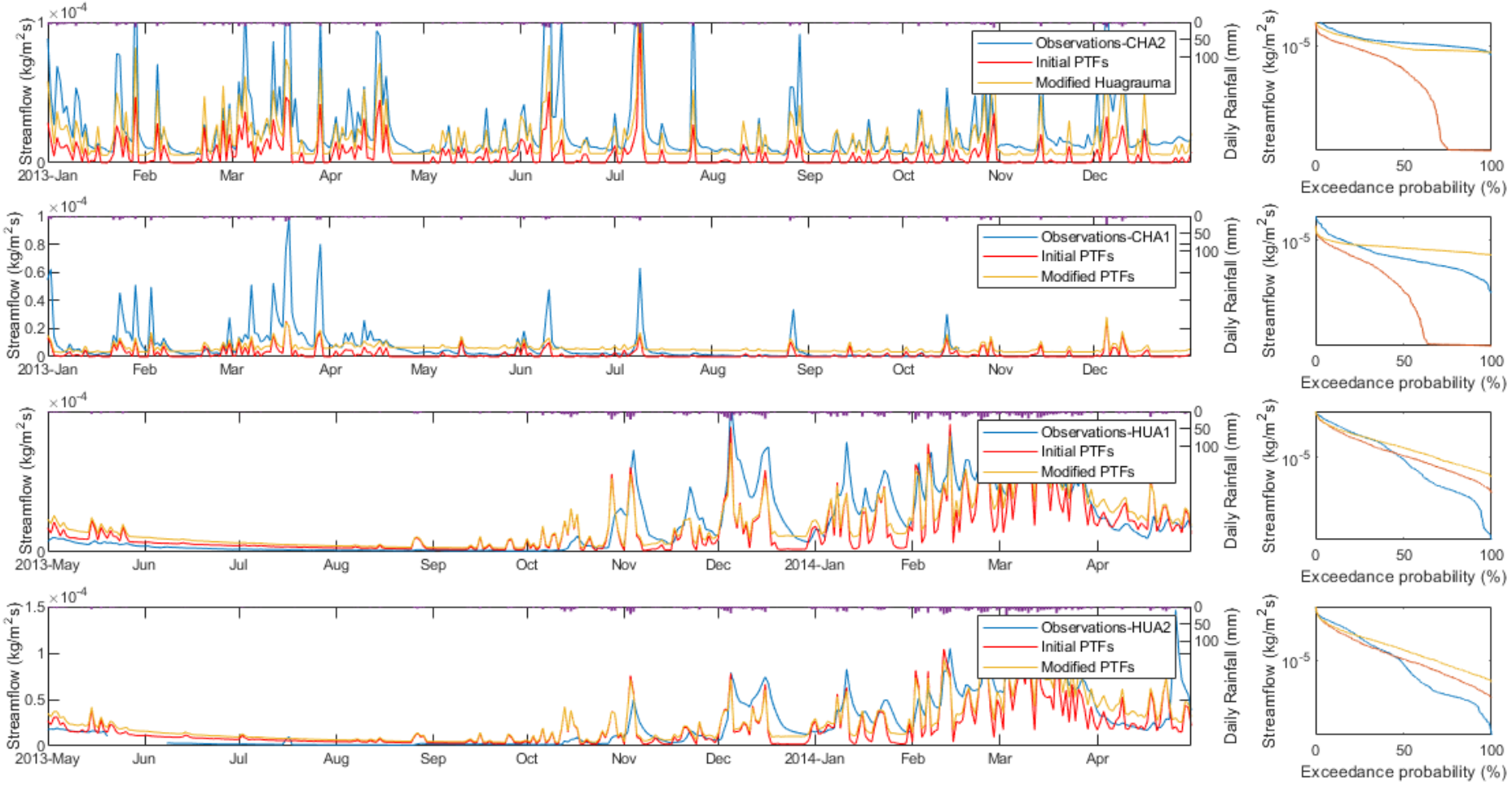

Figure 3.5 Modelling, observations, and flow duration curve in a. CHA2 b. CHA1 c. HUA1 d. HUA2

3.4 Discussion

The four sets of soil parameters result in substantial differences to the modelling results. The “initial PTFs” setup generated the lowest flow out of the four set of parameters, which could be attributed to its lowest subsurface flow generation. The “Initial Huagrauma” setup used higher values of saturated, critical, and wilting point obtained from the experimental data. This setup generated the highest flow in all 12 catchments because it reduced the vegetation extraction effectively. The “Modified Huagrauma” setup reduces the wilting point to a lower level than “initial Huagrauma”, which allows more water to be extracted from the soil column. This modification reduces the runoff compared to the “initial Huagrauma” setup. The “Modified PTFs” scenario increases the value of critical point from the “initial PTFs” setup, which reduces the soil moisture extraction effectively.

The total flow is the most important factor to affect the model performance. Using the “initial PTFs” setup results in the closest estimation for the catchments with lower flow (RR< 0.27: PIU_07, LLO_02, LLO_01, JTU_02), since the other three setups considerably overestimates the total flow. However, for these catchments, the low level of water yield in observation could be attributed to the unobserved subsurface and groundwater preferential flow from deep soil layers (Buytaert et al., 2006; Ochoa-Tocachi et al., 2016). This uncertainty in observation should be taken into consideration as the model performance is still lower than other catchments.

The “initial Huagrauma” setup generates the highest modelled flow, which made it suitable to be used in high flow catchments (PIU_01 and CHA_02). However, the “modified PTFs” setup simulated the best performance for the six catchments, including PIU_02, PIU_04, CHA_01, JTU_03, HUA_01, and HUA_02. The low variation in flow and the flattest R2FDC shows that this setup is more suitable to simulate baseflow-dominated flow (high regulation capacity) in these study regions.

3.5 Conclusions

Soil hydraulic models determine the water movement in the physically-based hydrological model by using physically meaningful soil parameters. However, the soil parameters are commonly derived from a large scale soil textual database, which is highly simplified and tends to lead to a coarser representation of surface hydrological processes. In the study sites, which were mainly covered by Andosols, the commonly used pedotransfer functions underestimate the values of saturated water content (i.e. 0.900 -> 0.463 in PIU_01), and residual water content (i.e. 0.500 -> 0.217 in PIU_01) compared to the values investigated from the local experiment data. This can be attributed to the insufficient of pedotransfer functions for high-Andean soils.

This chapter explores whether the soil parameterisation can be improved by using experimentally obtained soil data. To this purpose, streamflow for the 12 tropical Andean catchments has been simulated using a JULES setup that combines large-scale meteorological data with citizen science-collected local precipitation data. I find that the soil water retention properties (saturated, critical, and wilting point) affect the flow generation effectively with their impacts on soil moisture extraction. The high-water retention property of high-Andean soils can be presented better by modifying the water retention curve with experimental data from the Histic Andosol in South Ecuador. The experiment-based parameter values reduce the soil moisture extraction compared to the PTFs generated data. It may not be the best fit for most of catchments since it is not the exact local for individual sites. However, it shows better performance than the “initial PTFs” setup with its higher baseflow simulation, which is more suitable to be used in these baseflow-dominated catchments.

The “modified PTFs” shows best overall performance. This parameter set is based on the local data, which allows difference in soils to be represented for each catchment.

The simulated results showed that the modification on water retention curve can considerably increase the ability to simulate baseflow. I therefore recommend this setup to be used if local experimental data is not available.

The modelling results show that the modified soil water retention properties can make a significant contribution to improving the land cover parameterizations of JULES for dominant land-use types of the region. These generated parameter “libraries” in the paired catchment could be used to assess the potential impact of land use change on hydrology in the following studies.

4 Assessing the hydrological impacts of land use and land cover changes in tropical Andean catchments

4.1 Introduction

The Andean páramo consitute the headwaters of the major largest rivers of the Amazon basin (Célleri et al., 2009), The water supply is highly reliable because of its large water surplus, extreme water regulating capacity, and sustained base flow (Buytaert et al., 2006), which covers the water needs for major downstream Andean populations, smallholder irrigated agriculture, industrial consumption, and hydroelectricity production (Buytaert et al., 2014). Despite its importance of water supply, these mountain areas are particularly vulnerable and prone to human impact. Drastic changes in the water cycle have been produced by human activities (cultivation, afforestation and grazing) as a result of the rapid economic growth during the past half-century (Buytaert et al., 2006; Harden, 2006). The hydrological responses could be affected in the forms of changing vegetation cover, soil, and landscape. An increasing hydraulic conductivity was found when Andosols were cultivated (Buytaert et al., 2006). Increasing transpiration, interception, and evaporation is found when grasslands or shrublands are afforested, which leads to 40% decrease in runoff (Farley, Jobbágy & Jackson, 2005). This emphasises the need to identify quantitatively the hydrological impacts of specific land use changes.

The potential impacts have been assessed by a pair-wised catchment comparison, which used a 'trading space for time' approach to compare paired-catchments under similar physical, climatic conditions and different land management types (Ochoa-Tocachi, Buytaert & De Bièvre, 2016; Singh et al., 2011). This monitoring setup allows observing the continuous hydrological responses under the controlled/affected

catchments, which reduces the time required for long-term record to evaluate the land use impact. The iMHEA participatory hydrological monitoring network has been monitoring 28 small and homogenous headwater catchments, which cover a variety of both pristine and human-altered land cover types and are representative for the major biomes of the tropical Andes, i.e., páramo, puna, and jalca (Célleri et al., 2009; Ochoa-Tocachi et al., 2018). This setup allows faster analysis, which is often required in view of the urgency of policy decisions. However, the difference in catchment characteristics and meteorological drivers between the paired catchments can still contribute to hydrological change. In order to account explicitly for differences in catchment characteristics and meteorological input between the paired catchments, the hydrological change under LUCC has been assessed by using the land-surface model JULES. This approach allows scenario analysis by using physically meaningful parameters that distinguish the contribution of LUCC.

In the standard JULES setup, five plant functional types (PFTs), i.e. broadleaf trees, needle-leaf trees, C3 and C4 grasses, and shrubs, are used to represent the global vegetative land cover. In order to improve the estimation on gross and net primary productivity (GPP and NPP, respectively), new vegetation parameter sets of nine PFTs, i.e. tropical and temperate broadleaf evergreen trees, broadleaf deciduous trees, needle-leaf evergreen and deciduous trees, C3 and C4 grasses, and evergreen and deciduous shrubs, were developed (Harper et al., 2016). For the crops, 4 globally common crop types, wheat, soybean, maize, and rice, were included in the JULES-crop model (Osborne et al., 2015). In previous studies, this has led to improvements in the simulation on leaf area index, gross primary production and canopy height.

These parameters are not representative for the complex local vegetation. However, new vegetation parameters are not available for the study region due to the insufficient data availability. Therefore, as an alternative, I evaluate the hydrological

sensitivity of vegetation parameters by changing three parameters: canopy height, leaf area index, root depth, which are related to plant structure (Harper et al., 2016). The hydrological impacts of LUCC impacts are modelled using the soil parameter "libraries" modelled in the previous chapter, which were shown to lead to considerably improvements in the hydrological simulation.

First, I evaluate whether the land cover parameterizations of JULES are capable of simulating adequately the hydrological responses of the soil and land-cover types that are represented in the iMHEA dataset (Chapter 3). Subsequently, the ability of JULES to represent land-use change is then evaluate by extrapolating the parameter values which represents the affected catchment to their referenced paired catchment.

4.2 Methods

4.2.1 Hydrological sensitivity of vegetation parameters

Vegetation transpiration rates are influenced by changes in rooting characteristics, leaf area, stomatal response, surface albedo (Farley, Jobbágy & Jackson, 2005). Therefore, hydrological sensitivity of three vegetation parameters (canopy height, leaf area index, root depth) related to plant structure (Harper et al., 2016) is investigated. The experimental catchment PIU_02 (85% C4 and 15% BS) is selected to represent C4 grasses (C4), and PIU_04 (80% BF and 20% C4) is selected to represented Broadleaf forest (BF) since these two catchments are covered with the higher percentage of these respective vegetation types.

The canopy height indirectly affects the hydrological cycle, as it mainly affects the nitrogen exchange in JULES (Clark, D. B. et al., 2011; Harper et al., 2016). The canopy height is simulated within range of ±10% in the sensitivity analysis. The leaf area per unit ground area (LAI) controls canopy water interception, radiation extinction, water and carbon gas exchange. The canopy water (C_m) is calculated using a linear equation:

$$C_m = A_m + B_m * LAI \quad (4.1)$$

In which A_m is the interception by leafless vegetation and B_m is the rate of change of the water holding capacity with LAI (Best et al., 2011). LAI is changed within range of ±0.5 in the sensitivity analysis. Root depth affects the soil moisture extraction (Best et al., 2011), which I changed within a range of ±0.5 m, because it is limited by the depth of soil layer which is set at 3 m.

The 'modified PTFs' soil parameter set is used as this set yielded the highest modelling performance in both sites (see Chapter 3). The model is simulated from 2013/7/6 to 2017/1/1 in PIU_02, and from 2013/7/12 to 2016/8/9 in PIU_04 using all the available precipitation data (Ochoa-Tocachi et al., 2018).

4.2.2 Parameterisation of vegetation in JULES

I evaluate the changes of hydrological flux in the major processes, including subsurface flow from drainage, saturated excess surface flow, evaporation from soil and canopy, transpiration from plants, under different land cover scenarios in site PIU_01. The setup of wheat is selected to represented 'crop' since the predominant crop types in the region, potato and tubers, are not covered in JULES-crop (Osborne et al., 2015). In order to evaluate the interaction between land cover and soil properties, the modelling results are compared under two types of soil water retention setup (initial PTFs and initial Huagrauma), respectively. Initial Huagrauma has a higher water retention, which allows more water to be stored and evaporated from the soil column. The model is simulated from 2013/7/6 to 2017/1/1 in PIU_01 using all the available precipitation data (Ochoa-Tocachi et al., 2018).

4.2.3 Comparison between pair-wise catchment observations and JULES modelling

The hydrological monitoring data in paired catchments under similar physical, climatic conditions and different watershed interventions allows LUCC impacts to be assessed by a pair-wise catchment comparison (Ochoa-Tocachi et al., 2016). However, the difference in catchment characteristics and meteorological drivers between the paired catchments could still contribute to hydrological changes. The difference of the physical properties between the paired catchments are summarised in Table 4.1. The table shows that the difference in catchment size can be as high as 6.95 times in the case of PIU_01 and its paired catchment, PIU_02. In addition, the difference in altitude may affected meteorological variables, which need to be adjusted for altitude. For example, the altitude gap between PIU_04 and PIU_07 could lead to 4.4°C difference in average temperature, which affects evaporation. The difference in precipitation is another consideration since it can be as high as 683.5 mm/year in paired catchments (between PAU_01 and PAU_04).

In this chapter, I assess the hydrological changes under LUCC using JULES v5.3. The model allows scenario analysis with using physically meaningful parameters, which distinguished the contribution of LUCC. The land surface has been parameterised in JULES vn5.3 for the catchments monitoring by the iMHEA network (Ochoa-Tocachi et al., 2018). The hydrological response under LUCC is assessed by substituting land cover fraction (Table 4.2), and the soil parameters (Table 4.3) from the natural catchment setup to the value modified in the affected catchment (Figure 4.1). Meanwhile, the meteorological condition and catchment setup remains unchanged. The potential changes of grazing are modelled in three páramo covered watersheds (PIU_01, LLO_02, JTU_03), and three puna watersheds (PIU_04, HUA_01,

HMT02). The effects of cultivation are explored for both a páramo watershed (PAU_01), and a puna watershed (TIQ_02). The effects of pine afforestation are modelled for 3 biomes, i.e. páramo (PAU_02), humid puna (TAM_02), and jalca (CHA_02).

The hydrological indicators (RR, BFI, Qvar, Qskew, and R2FDC) are used to identify the impact under LUCC with using JULES model and paired catchments comparison. The adequacy of the LUCC simulation to prediction of hydrological phenomenon was systematically compared and evaluated addressing on the effect of grazing, cultivation and afforestation accordingly.

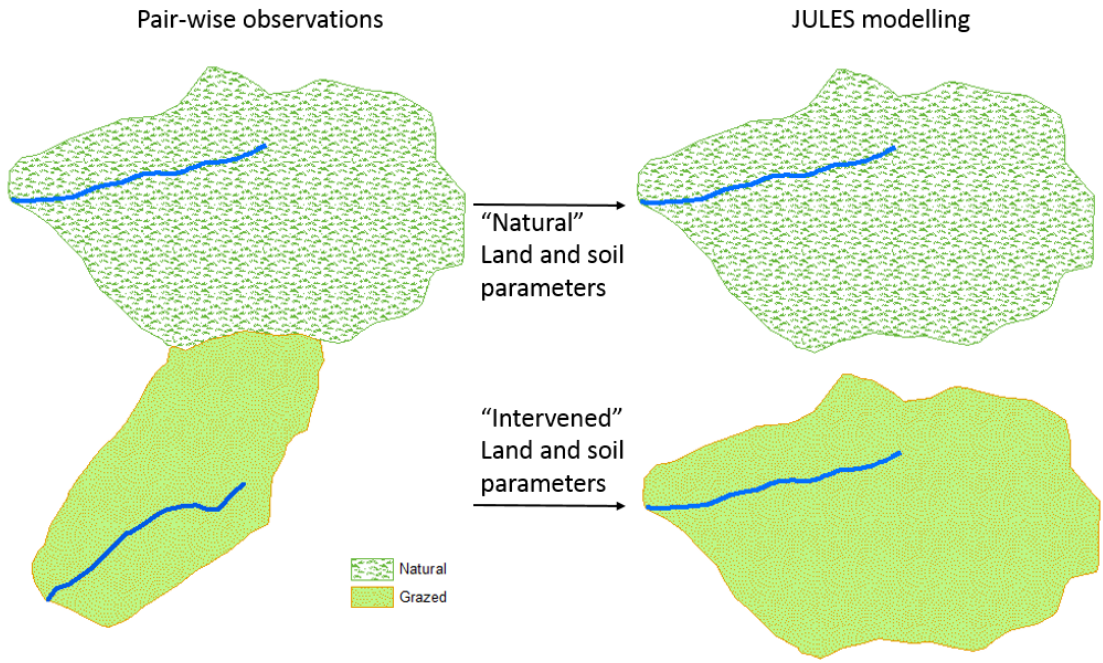

Figure 4.1 Conceptual representation of using modified parameters in 'natural' and 'intervened' catchments for JULES modelling

Table 4.1 Comparison of the properties in the paired catchments used in the JULES model

Code of catchment		Annual rainfall [mm]		Area [km^2]		Altitude [m]		Temperature [°C]	
Natural	Affected	Natural	Affected	Natural	Affected	Natural	Affected	Natural	Affected
PIU_01	PIU_02	2240.2	2588.5	6.60	0.95	3193	3245	9.6	9.3
LLO_02	LLO_01	996.7	989.0	2.21	1.79	4088	3825	4.1	5.7
JTU_03	JTU_02	861.6	755.1	2.25	2.42	4144	4085	7.0	7.2
HUA_01	HUA_02	1325.9	1270.4	4.22	2.38	4306	4356	4.3	4.3
HMT_02	HMT_01	529.9	564.4	1.69	2.09	3914	4002	5.4	4.8
PIU_04	PIU_07	1306.0	650.3	2.32	7.80	2727	3120	12.9	8.5
PAU_01	PAU_04	1366.7	683.2	2.63	1.55	3675	3562	5.3	6.2
TIQ_02	TIQ_01	725.2	847.9	1.73	0.69	4182	4140	3.9	4.6
PAU_02	PAU_03	1088.4	952.1	1.00	0.59	2976	3255	8.2	6.5
TAM_02	TAM_01	1330.4	1061.6	1.67	0.82	3708	3851	12.5	11.5
CHA_02	CHA_01	939.7	677.7	1.63	0.95	2934	3030	10.9	10.4

Table 4.2 Land cover type representing the study catchments under natural and intervened conditions and the JULES land cover setup. BF: Broadleaf Forest, NF: Needleleaf Forest, CR: crop, C4: C4 grasses, SH: Shrub, BS: Bare soil.

Catchment	Natural		Intervened	
	Land cover	JULES setup	Land cover	JULES setup
PIU_01	Natural páramo	15% BF, 85% C4	Grazed páramo	15% BS, 85% C4
LLO_02	Restored páramo	10% BF, 90% C4	Grazed páramo	10% SH, 90% C4
JTU_03	Natural páramo	80% C4, 20% SH	Grazed páramo	100% C4
PIU_04	Puna forest	80% BF, 20% C4	Cultivated puna	35% CR, 45% C4, 20% SH
HUA_01	Natural puna	75% C4, 25% BS	Grazed puna	70% C4, 30% BS
HMT_02	Grazed dry puna	85% C4, 5% SH, 10% BS	Grazed dry puna	75% C4, 10% SH, 15% BS
PAU_01	Natural páramo	100% C4	Cultivated páramo	70% C4, 30%CR
TIQ_02	Natural humid puna	95% C4, 5% BS	Grazed humid puna	35% C4, 35% CR, 30% BS
PAU_02	Natural páramo	80% C4, 20% BF	Afforested páramo	80% C4, 20% NF
TAM_02	Natural humid puna	60% C4, 40% BF	Afforested humid puna	80% C4, 20% NF
CHA_02	Natural jalca	10% BF, 90% C4	Afforested jalca	80% NF, 20% C4

Table 4.3 Soil parameters representing the study catchments under natural and intervened conditions

Catchment	Condition	1/(n-1)	1/a	θsat	θcrit	θwilt	hcon	hcap	K
PIU_01	Natural	1.786	1.795	0.900	0.758	0.520	0.037	221412	0.0034
	Grazed	1.786	1.795	0.900	0.732	0.450	0.037	221412	0.0034
LLO_02	Natural	2.501	0.505	0.467	0.271	0.104	0.225	1146028	0.0097
	Grazed	2.501	0.505	0.467	0.271	0.104	0.225	1146028	0.0097
JTU_03	Natural	1.786	1.795	0.565	0.415	0.161	0.149	938752.8	0.0052
	Grazed	3.133	0.583	0.565	0.387	0.161	0.149	938752.8	0.0052
PIU_04	Natural	1.786	1.795	0.900	0.714	0.400	0.037	221412	0.0034
	Grazed	2.787	0.437	0.463	0.333	0.217	0.219	1189944	0.0034
HUA_01	Natural	1.786	1.795	0.422	0.327	0.167	0.264	1259371	0.0066
	Grazed	1.786	1.795	0.900	0.717	0.410	0.037	221412	0.0034
HMT_02	Grazed	2.590	0.423	0.422	0.280	0.167	0.264	1259371	0.0066
	Grazed	2.590	0.423	0.422	0.280	0.167	0.264	1259371	0.0066
PAU_01	Natural	1.786	1.795	0.900	0.751	0.500	0.037	221412	0.0034
	Cultivated	1.786	1.795	0.463	0.371	0.217	0.219	1189944	0.0034
TIQ_02	Natural	2.603	0.679	0.479	0.342	0.189	0.207	1144154	0.0022
	Cultivated	2.603	0.679	0.479	0.342	0.189	0.207	1144154	0.0022
PAU_02	Natural	1.786	1.795	0.463	0.371	0.217	0.219	1189944	0.0034
	Afforested	2.787	0.437	0.463	0.333	0.217	0.219	1189944	0.0034
TAM_02	Natural	1.786	1.795	0.900	0.788	0.600	0.037	221412	0.0034
	Afforested	1.786	1.795	0.900	0.729	0.440	0.037	221412	0.0034
CHA_02	Natural	1.786	1.795	0.900	0.803	0.640	0.037	221412	0.0034
	Afforested	1.786	1.795	0.492	0.373	0.173	0.199	1110088	0.0057

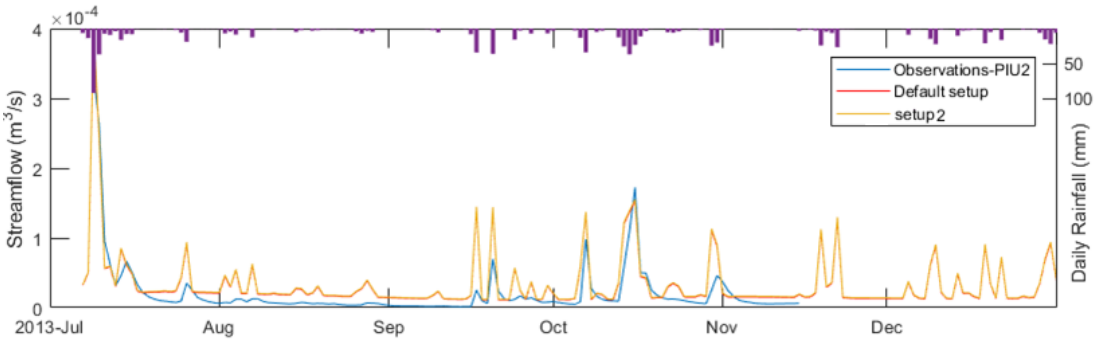

Figure 4.2 Modelling flows with different vegetation setup

4.3 Results and discussion

4.3.1 Sensitivity of vegetation parameters

The hydrological sensitivity of three vegetation parameters (canopy height, leaf area index, root depth) is simulated in site PIU_02 for C4 grasses (Table 4.4), and in site PIU_04 for broadleaf forest (Table 4.5). The increase in canopy height merely increases the total runoff, mainly in subsurface flow. In contrast, a larger leaf area index reduces the runoff with increasing transpiration from vegetation. The transpiration also increases as the root depth is increased. For C4 grasses, the largest increase in runoff occurs when the leaf area index was decreased from 4.0 to 3.5, but this represents merely 0.62% of the total runoff. A similar effect is observed for broadleaf forest, as 1.4 % of the total flow only increases with 1.4% if the LAI is decreasedfrom 5.0 to 4.0. These results show that changes in vegetation parameters have only a minor effect on the generation of flow, which can barely be observed in the simulated hydrograph (Figure 4.2).

Table 4.4 The hydrological effects using different C4 vegetation parameter setup in PIU_02

	Canopy height [m]	Leaf area index	Root depth [m]	Runoff [mm/year]
Standard C4	1.26	4.0	0.5	1457.0
Set 1	1.40	4.0	0.5	1458.9
Set 2	1.13	4.0	0.5	1455.0
Set 3	1.26	4.5	0.5	1448.5
Set 4	1.26	3.5	0.5	1466.0
Set 5	1.26	4.0	1.0	1442.2

Table 4.5 The hydrological effects using different BF vegetation parameter setup in PIU_04

	Canopy height [m]	Leaf area index	Root depth [m]	Runoff [mm/year]
Standard BF	19.01	5.0	3.0	640.7
Set 1	20.91	5.0	3.0	642.4
Set 2	17.11	5.0	3.0	639.3
Set 3	19.01	5.5	3.0	633.0
Set 4	19.01	4.5	3.0	649.4
Set 5	19.01	5.0	2.5	641.3

4.3.2 Parameterisation of vegetation in JULES

The hydrological fluxes modelled with using “initial PTFs” are shown in Table 4.6 with the percentage shown in Figure 4.3. The transpiration is highest when covered by broadleaf forest, which also generates the lowest subsurface flow and total flow. Shrub has the lowest transpiration, which leads to the highest subsurface flow. It also has the highest evaporation out of the 5 PFTs. The highest flow is modelled under bare soil, which is 335.6 mm/year higher than broadleaf forest coverage. Unrealistically low transpiration is modelled under crop (wheat) setup. The result is compared with the simulation using the soil setup used in previous JULES-crop study (Williams et al., 2017). The VG parameter in the study is higher than the values of both “initial PTFs” and “initial Huagrauma”, which requires further investigation.

The modelling results are compared with the “initial Huagrauma” experiment data and shown in Table 4.7 with the percentage shown in Figure 4.4. The “initial Huagrauma” experiment has higher saturated water retention than the “initial PTFs” setup (θsat: 0.900 vs 0.463), which allows more water to be stored in the soil column. Hence, this reduces surface flow.

The highest flow using “initial Huagrauma” is 1513.7 mm/year when covered by needle-leaf forest. The results show that the modelled flow is considerably affected under different land cover types.

Table 4.6 Hydrological flux under different land cover types [mm/year] (in PIU_1, initial PTFs)

	Evapotranspiration [mm/year]			Flow [mm/year]	
Land Cover	Transpiration	Evaporation	Total	Subsurface	Total
PIU1 (15% BF+85% C4)	680.7	469.2	1149.9	285.7	1095.4
Broadleaf forest (BF)	725.8	541.1	1266.9	189.8	988.0
Needle-leaf forest (NF)	482.6	603.6	1086.2	366.7	1163.9
C3 grasses	653.6	505.6	1159.2	275.7	1081.5
C4 grasses	664.7	457.6	1122.3	311.0	1121.9
Shrubs (SH)	381.3	703.0	1084.3	350.8	1159.3
Crop (wheat)	9.5	979.4	988.9	425.3	1251.8
Crop*	417.2	770.6	1187.8	4.3	1049.3
Bare soil (BS)	0.0	913.0	913.0	349.9	1323.6

*The simulation under the soil setup used in previous JULES-crop study (Williams et al., 2017)

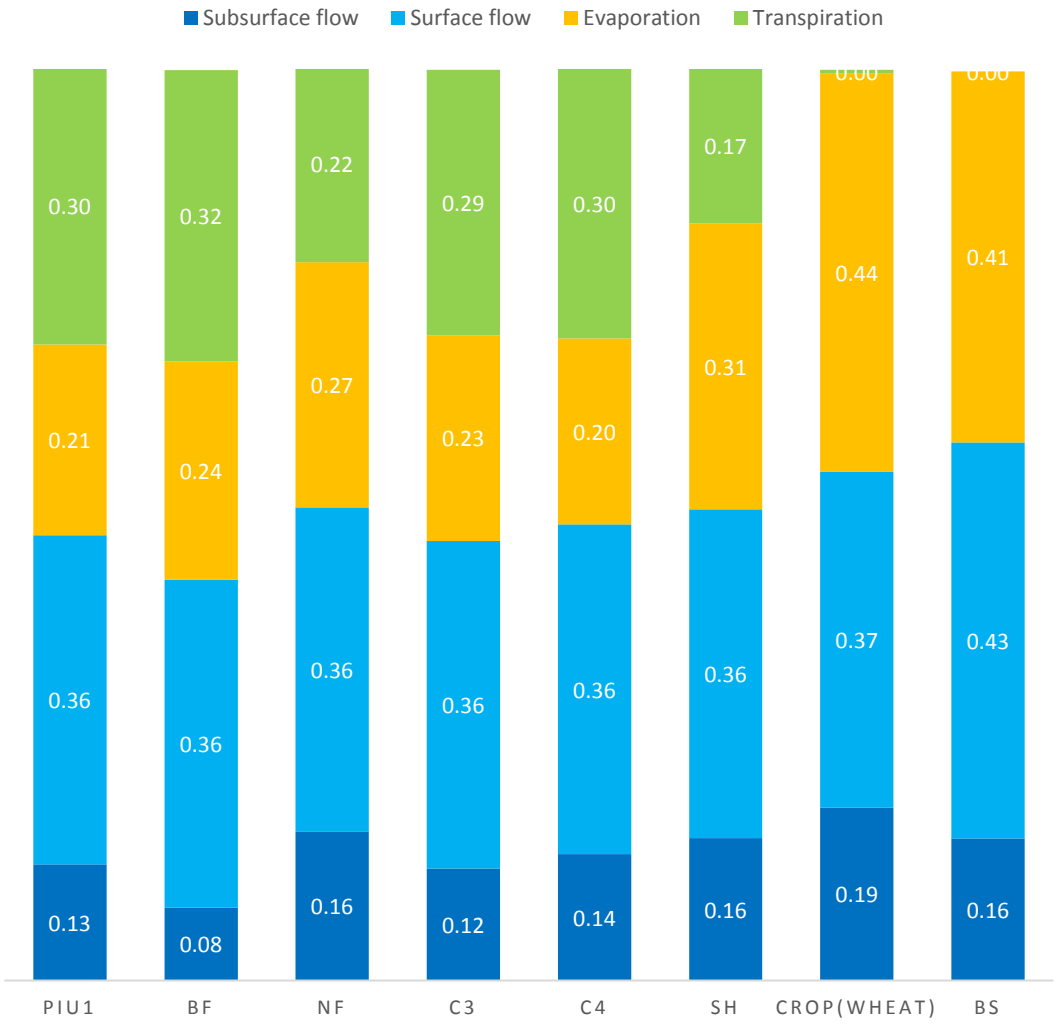

Figure 4.3 The percentage of hydrological flux under different land cover (initial PTFs)

Table 4.7 Hydrological flux under different land cover types [mm/year] (in PIU_1, initial Huagrauma)

	Evapotranspiration			Flow	
	Transpiration	Evaporation	Total	Subsurface	Total
PIU1 (15% BF+85% C4)	270.4	499.3	769.7	779.0	1466.5
Broadleaf forest (BF)	252.4	554.5	806.9	773.8	1435.9
Needle-leaf forest (NF)	131.1	591.5	722.6	848.8	1513.7
C3 grasses	210.5	587.5	798.0	739.0	1433.0
C4 grasses	272.4	490.0	762.4	780.7	1472.7
Shrubs (SH)	87.1	729.9	817.0	722.0	1409.6
Crop (wheat)	0.0	945.4	945.4	576.1	1257.1
Bare soil (BS)	0.0	875.7	875.7	509.6	1319.6

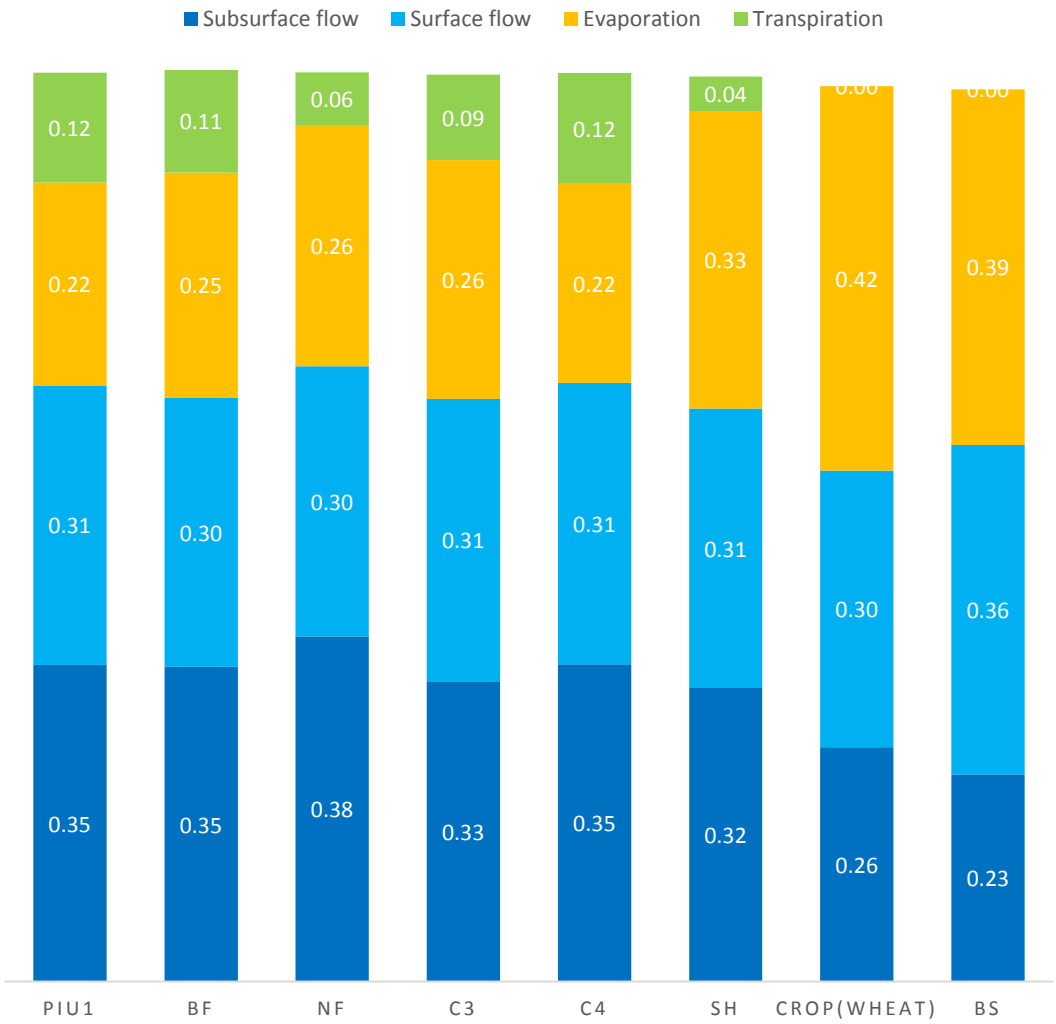

Figure 4.4 The percentage of hydrological flux under different land cover (initial Huagrauma)

4.3.3 The effects of grazing in páramo

The hydrological indicators are used to identify the impact under LUCC by using the JULES model setup and a paired catchments comparison (Table 4.8). In PIU_01, the resulting simulated discharge time series is shown in Figure 4.5, which shows that the flow has been reduced by 14.5% (RR: 0.69 to 0.59) under the potential grazing activities. The water regulation capacity reduces correspondingly, as shown by the lower BFI, and a steeper R2FDC in the model simulation under LUCC. Comparing the observed discharge of the paired catchments also shows that water yield of the grazed catchment PIU_01 is 6.8% lower than the natural catchment (RR: 0.73 vs 0.68). The flow in the grazed catchment PIU_02 is higher than the simulated value, which could be attribute to the difference in precipitation (PIU_01: 2240.2 mm/year vs PIU_02:2588.5 mm/year), which has considerable impact ona the total flow.

In LLO_02, the change in land cover (10% of forest -> 10% of shrub) has slightly increased the water yield (RR: 0.38 -> 0.39) with little effects on the other flow indicators. Since there is no difference in the intrinsic soil properties, these results imply that soil properties are more important than the vegetation parameters in determining the rainfall-runoff ratio. As shown in Figure 4.6, the flows observed in the pair of catchments were lower both than the simulated flow. The main reason is that some intense rainfall events exist in the rainfall record, which do not show an according peak in the flow observations. However, in the observed discharges, a minor change between the conserved and grazed catchment can also be observed (RR: 0.14 vs 0.12).

On the other hand, a much more substantial difference is present in JTU_03, in which the modelled flow shows a reduction in the grazed catchment (RR: 0.37 -> 0.26), which is also present in the observed discharge (0.36 vs 0.07; see also Figure 4.7). In

the model, the grazing activities in JTU_03 reduced the soil water retention, which leads to a baseflow reduction (BFI: 0.57 ->0.25), a more unstable flow (Qvar: 1.09 ->1.87), and a lower water regulation (R2FDC: -0.66 -> -1.81).

Table 4.8 Hydrological indices of catchment in natural state and under potential LUCC impacts, obtained from both the observed discharge time series, and the time series simulated by JULES. RR: Rainfall-runoff ratio, BFI: Baseflow index, Qvar: Coefficient of variation in daily flows, Qskew: Skewness in daily flows, R2FDC: the slope of the flow duration curve

		Observed discharge					JULES modelling				
Catchment	Land cover	RR	BFI	Qvar	Qskew	R2FDC	RR	BFI	Qvar	Qskew	R2FDC
PIU_01	Natural	0.73	0.42	1.09	2.19	-1.29	0.69	0.66	0.77	2.86	-0.57
	Grazed	0.68	0.59	1.15	2.46	-1.36	0.59	0.61	0.88	2.84	-0.73
LLO_02	Natural	0.14	0.85	0.60	1.72	-0.69	0.46	0.83	0.74	1.05	-1.17
	Grazed	0.12	0.84	0.68	2.47	-0.52	0.39	0.85	0.71	0.98	-1.17
JTU_03	Natural	0.36	0.86	0.90	4.53	-0.54	0.37	0.88	0.48	1.50	-0.42
	Grazed	0.07	0.63	1.44	5.77	-1.02	0.23	0.35	1.62	2.98	-1.11
PIU_04	Natural	0.39	0.85	0.95	2.73	-0.85	0.39	0.86	0.61	1.39	-0.90
	Grazed	0.26	0.70	1.57	4.36	-1.12	0.31	0.75	1.07	2.01	-1.66
HUA_01	Natural	0.70	0.67	1.30	1.65	-3.23	0.63	0.69	0.95	1.91	-1.36
	Grazed	0.54	0.71	1.29	1.52	-2.93	0.63	0.52	1.10	2.40	-1.22
HMT_02	Natural	0.21	0.59	2.63	4.88	-2.04	0.27	0.38	2.31	4.63	-0.56
	Grazed	0.23	0.57	2.87	5.51	-2.99	0.27	0.38	2.30	4.62	-0.51
PAU_01	Natural	0.68	0.70	0.87	3.33	-0.74	0.71	0.70	0.61	2.73	-0.49
	Cultivated	0.58	0.48	1.34	3.46	-1.11	0.62	0.66	0.71	2.85	-0.63
TIQ_02	Natural	0.33	0.72	2.20	6.47	-0.53	0.33	0.37	2.23	4.40	-0.99
	Cultivated	0.25	0.65	2.15	3.97	-2.04	0.32	0.33	2.35	4.27	-1.60
PAU_02	Natural	0.40	0.83	0.73	2.08	-0.68	0.49	0.90	0.38	0.92	-0.40
	Afforested	0.23	0.72	0.97	3.37	-0.90	0.34	0.81	0.55	1.41	-0.62
TAM_02	Natural	0.53	0.95	0.67	1.94	-0.59	0.52	0.85	0.80	0.79	-1.61
	Afforested	0.19	0.96	0.96	1.93	-0.86	0.41	0.81	0.97	1.01	-1.93
CHA_02	Natural	0.76	0.55	1.26	4.73	-0.53	0.60	0.58	0.92	3.21	-0.75
	Afforested	0.29	0.44	1.98	3.97	-1.42	0.40	0.49	1.15	3.36	-0.98

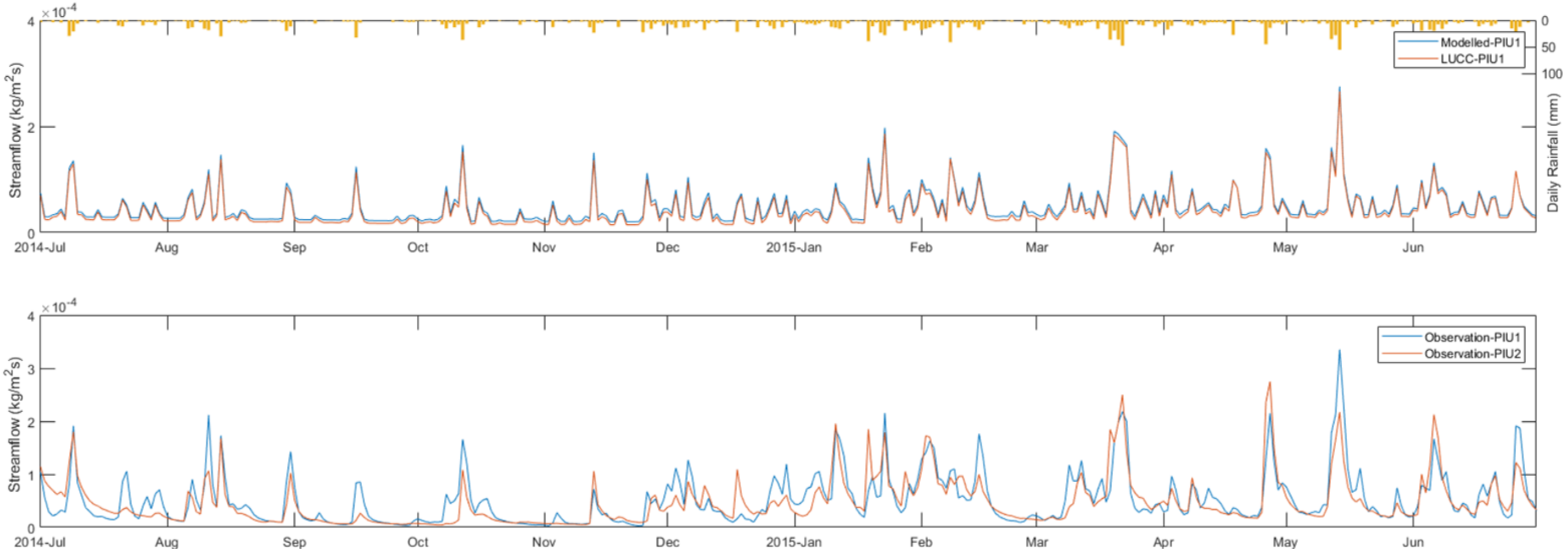

Figure 4.5 (a) Comparison of flow under natural páramo watershed (PIU1) using JULES modified on the observed data ("Modelled") and modified on the grazed catchment (PIU2) with changed parameters ("LUCC"); (b) pair-wise observations for the natural (PIU1) and grazed (PIU2) catchments.

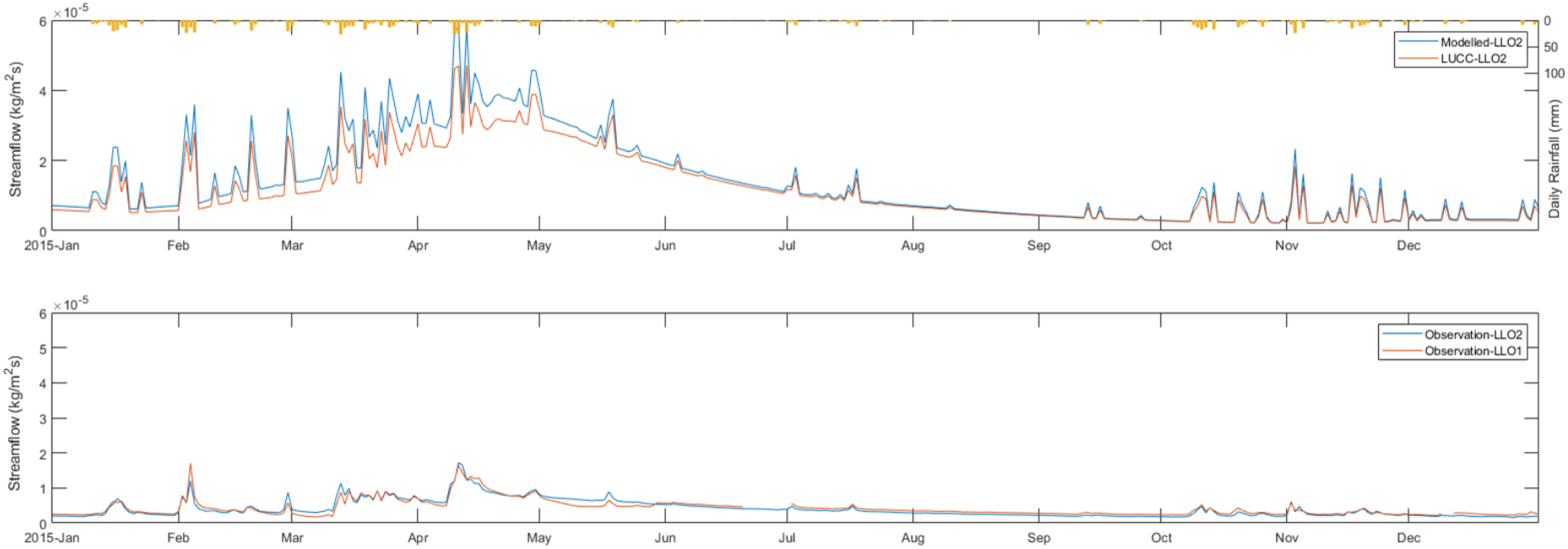

Figure 4.6 (a) Comparison of flow under natural páramo watershed (LLO2) using JULES modified on the observed data ("Modelled") and modified on the grazed catchment (LLO1) with changed parameters ("LUCC"); (b) pair-wise observations for the natural (LLO2) and grazed (LLO1) catchments.

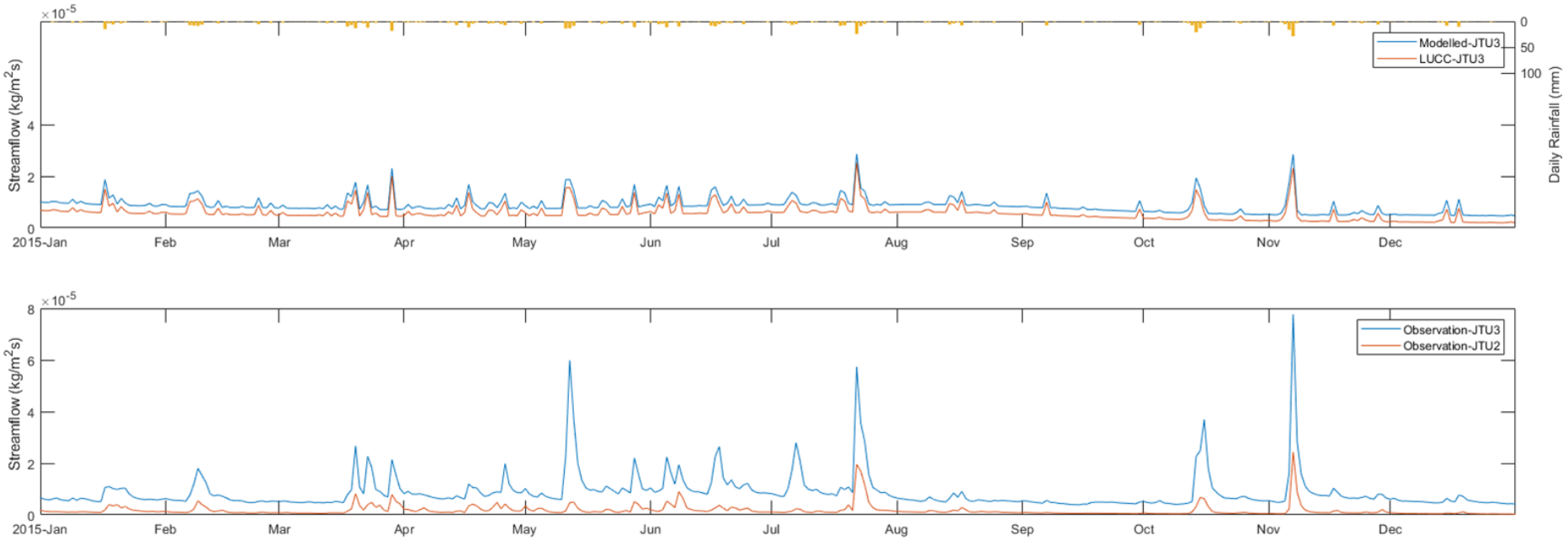

Figure 4.7 (a) Comparison of flow under natural páramo watershed (JTU3) using JULES modified on the observed data ("Modelled") and modified on the grazed catchment (JTU2) with changed parameters ("LUCC"); (b) pair-wise observations for the natural (JTU3) and grazed (JTU2) catchments.

4.3.4 The effects of grazing in puna

PIU_04 is a catchment partially covered by páramo forest (0.80 BF, 0.20 C4). The land cover is different to its neighbouring watershed PIU_07 (0.35CR, 0.45 C4, 0.20 SH), in which grazing, and cultivation activities had taken place. Figure 4.8 clearly shows a lower flow (RR: 0.26 vs 0.39) and increasing level of peak flows (Qskew: 4.36 vs 2.73) in the overgrazed puna watershed, compared to the adjacent natural catchment. This change in land use is present in the modified soil parameters, which show a lower water retention is modified in the grazed catchment. This directly results in a reduced flow simulated by the model (RR: 0.39 -> 0.31), and similarly, a reduction in BFI and R2FDC. A lower flow is observed in the grazed catchment PIU_07 compared to its simulated value. This could be attribute to the lower precipitation (PIU_04: 1306.0 mm/year vs PIU_07: 650.3 mm/year) in PIU_07, which further decreases the flow in addition to the effects of grazing. The observed and modelled effects of low-density grazing in a humid puna watershed (HUA_01) are as shown in Figure 4.9. Reduced flow (RR: 0.70 vs 0.54) has been monitored in the grazed catchment (HUA_02) compared to the natural catchment. To simulate the grazing activities, the soil water retention parameters were changed in the model by means of a minor change of LUCC (5 % of grass -> bare soil). The modelled change in average flow is not significant. However, the hydrograph shows more flashy response under LUCC.

Figure 4.10 shows the altered flow under high density grazing in dry puna (HMT_02). In the grazed catchment (HMT_01), a higher peak flow is observed (Qskew: 5.51 vs 4.88) accompanied by an increased water yield (RR: 0.21 vs 0.23). The changes are not considerably detected by the model since minor differences were made in both of soil water retention and LUCC.

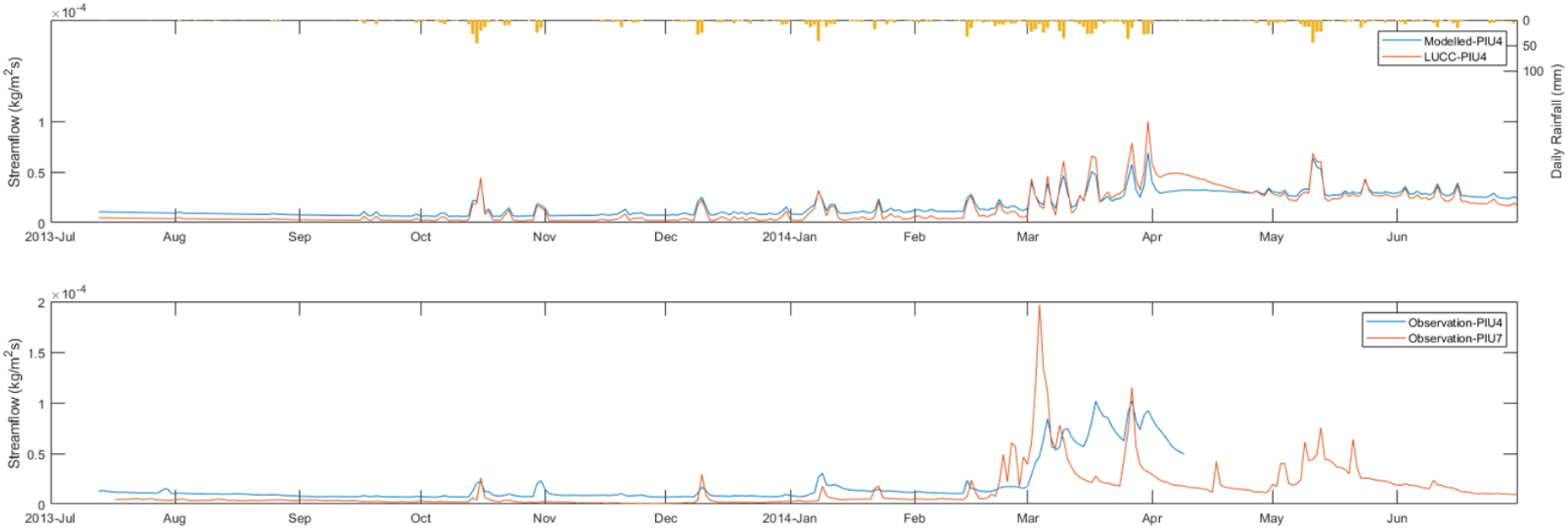

Figure 4.8 (a) Comparison of flow under natural páramo watershed (PIU4) using JULES modified on the observed data ("Modelled") and modified on the grazed catchment (PIU7) with changed parameters ("LUCC"); (b) pair-wise observations for the natural (PIU4) and grazed (PIU7) catchments.

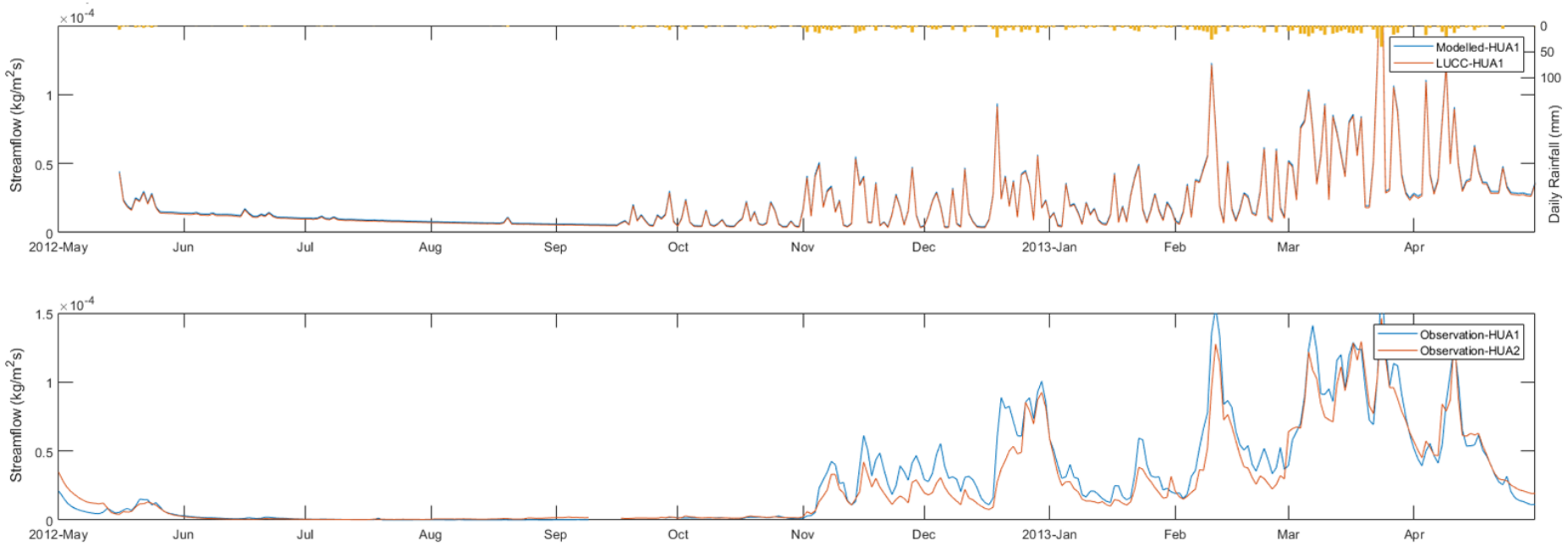

Figure 4.9 (a) Comparison of flow under natural páramo watershed (HUA1) using JULES modified on the observed data ("Modelled") and modified on the grazed catchment (HUA2) with changed parameters ("LUCC"); (b) pair-wise observations for the natural (HUA1) and grazed (HUA2) catchments.

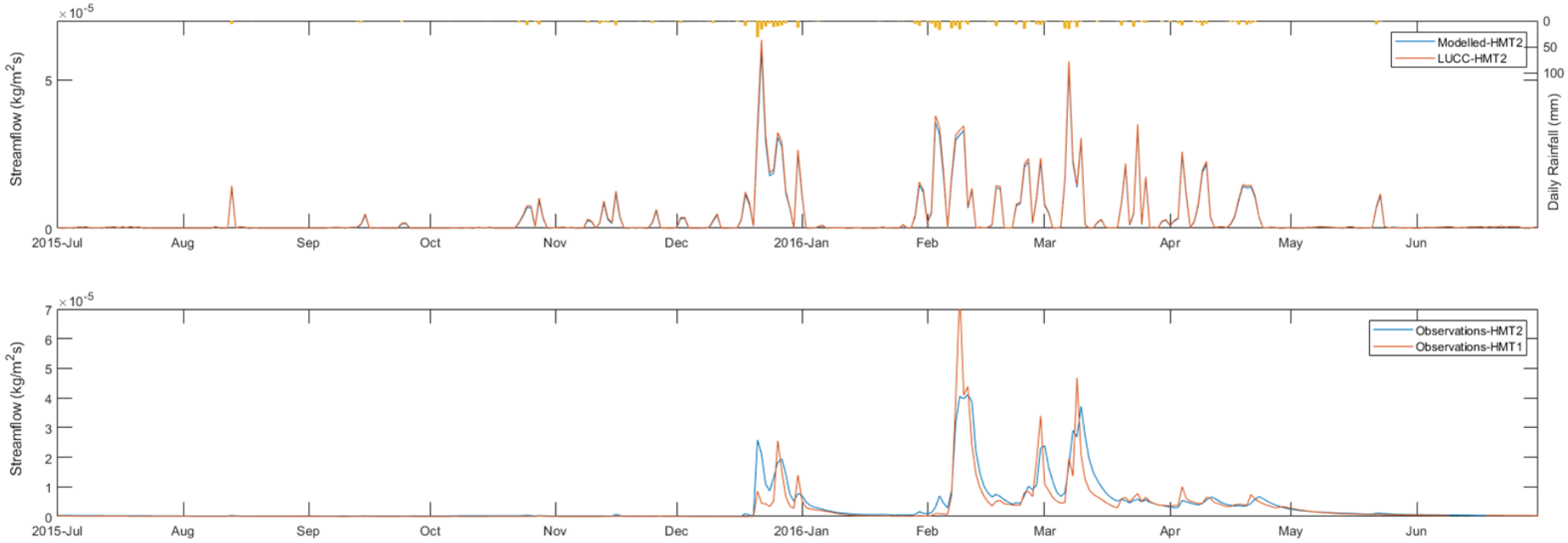

Figure 4.10 (a) Comparison of flow under natural páramo watershed (HMT2) using JULES modified on the observed data ("Modelled") and modified on the grazed catchment (HMT1) with changed parameters ("LUCC"); (b) pair-wise observations for the natural (HMT2) and grazed (HMT1) catchments.

4.3.5 The effects of cultivation

The effects of cultivation are explored for both a páramo watershed (PAU_01), and a puna watershed (TIQ_02). A lower (RR: 0.58 vs 0.68) and more unstable flow (Qvar: 1.34 vs 0.87) with reduced base flow (BFI: 0.48 vs 0.70) has been monitored in the cultivated páramo watershed (PAU_04), compared to their natural counterparts (Figure 4.11). To model this change, 30 % of land cover was converted to "cultivated" in JULES, which reduced the flow by 12.6 % (RR: 0.71 ->0.62). These changes could also be attributed to the changing soil water retention modified between the natural and cultivated watershed.

Figure 4.12 displays the effect under cultivated puna (TIQ_01). The ability of water regulation is decreased (R2FDC: -2.04 vs -0.53) with reduced water yield (RR: 0.25 vs 0.33). In the model, 35% of the catchment area is represented as cultivated, and 30 % by barren area. According this simulation a lower water yield (RR: 0.33 -> 0.30) is generated with a lower baseflow (BFI: 0.37 -> 0.33), which reduces the catchment's ability of water regulation (R2FDC: -0.99 -> -1.60).

In comparison with the observed data and modelling results among páramo watershed (PAU_01) and cultivated puna (TIQ_01), it is found that water yield and water regulation could be threatened by cultivation. The minor change on the R2FDC (the slope of the flow duration curve) from -0.49 to -0.63 in PAU_01, whilst from -0.99 to -1.60 in TIQ_01 is clearly consistent with this observation.

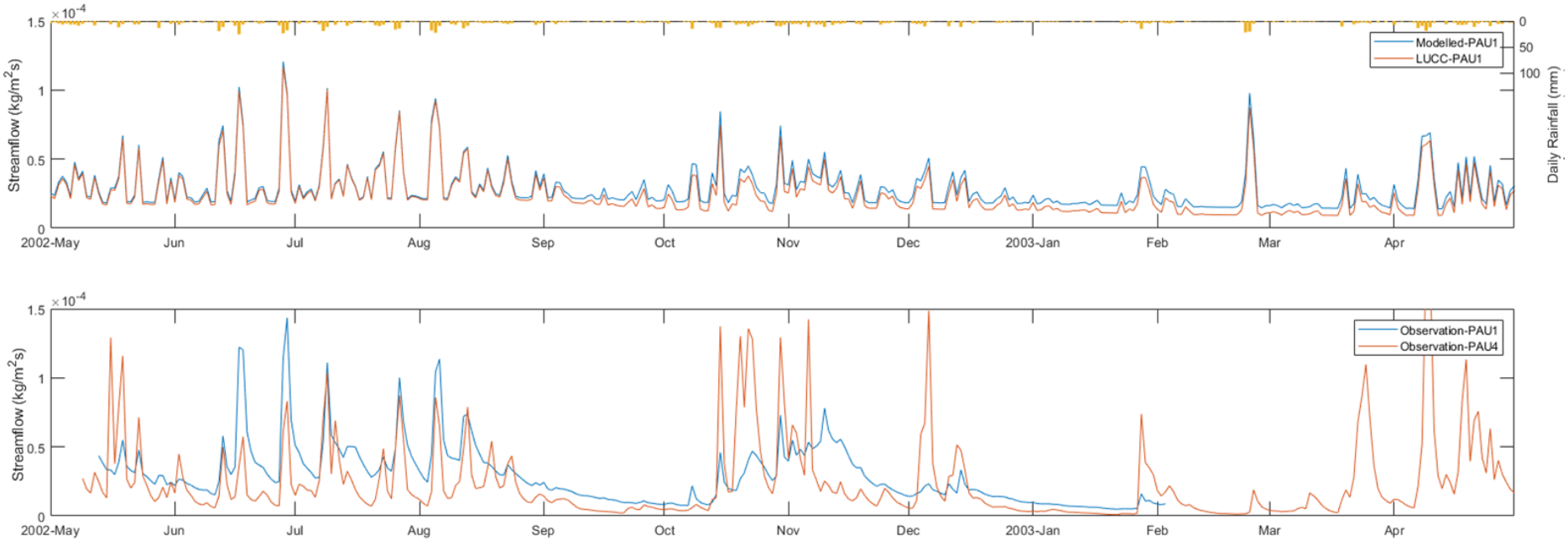

Figure 4.11 (a) Comparison of flow under natural páramo watershed (PAU1) using JULES modified on the observed data ("Modelled") and modified on the cultivated catchment (PAU4) with changed parameters ("LUCC"); (b) pair-wise observations for the natural (PAU1) and cultivated (PAU4) catchments.

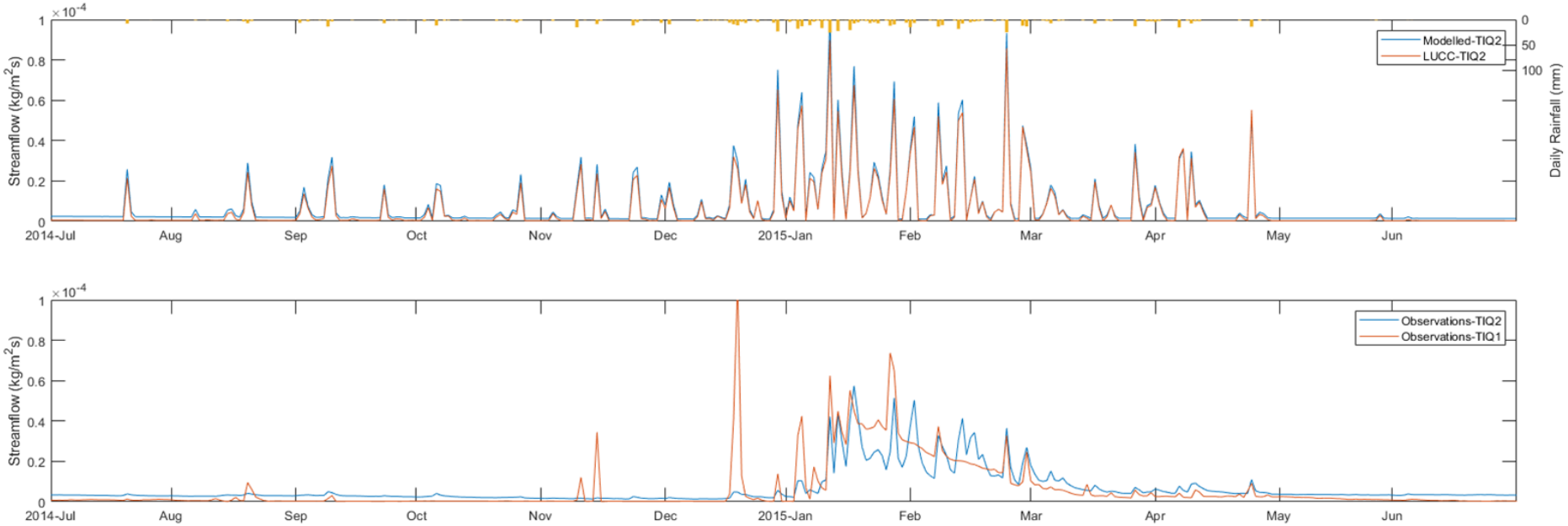

Figure 4.12 (a) Comparison of flow under natural puna watershed (TIQ2) using JULES modified on the observed data ("Modelled") and modified on the cultivated catchment (TIQ1) with changed parameters ("LUCC"); (b) pair-wise observations for the natural (TIQ2) and cultivated (TIQ1) catchments.

4.3.6 The effects of afforestation

The effects of pine afforestation are modelled for 3 biomes, i.e. páramo (PAU_02), humid puna (TAM_02), and jalca (CHA_02). In the páramo watershed, the observed and simulated hydrological responses show similar trends (Figure 4.13). The impact of LUCC leads to an evenly decreased runoff (RR: 0.42 vs 0.23 by observation; 0.49 -> 0.34 by model). The water regulation also decreased (R2FDC: -0.68 vs -0.90 by observation; -0.40 -> 0.62 by model) with a reduced ratio of baseflow (BFI: 0.83 vs 0.72 by observation; 0.90 -> 0.81 by model) and a higher variation in flow (Qvar: 0.73 vs 0.97 by observation; 0.38 -> 0.55 by model). The JULES modelling demonstrates a very good fit with the observations of the paired catchments.

In the humid puna watershed (TAM_02), only a few months of data is available from Apr-2012 to Aug-2012 as shown in Figure 4.14. Lower water yield has been monitored in the pine afforested catchment (RR: 0.53 vs 0.19) with no peak flow generated during this period, due to the absence of rainfall events. The JULES model was implemented from Apr-2012 to Apr-2013. The results show a significantly increased flow in the wet season (Dec-2012 to Apr-2013). The model also points out a decrease in flow (RR: 0.52 -> 0.41), as well as a less stable (Qvar: 0.80 ->0.97), and less regulated response (R2FDC: -1.61 -> -1.93) under LUCC. Within the pair-wise catchment comparison, afforestation reduces the flow by 64.2% (RR: 0.53 -> 0.19). However, the difference in precipitation (TAM_02: 1330.4 mm/year vs TAM_01: 1061.6 mm/year) is likely to be a contributing factor to the lower runoff observed in TAM_01. Figure 4.15 shows the simulation of the impact of pine afforestation monitored in the jalca watershed (CHA_02). The JULES modelling results show a decrease in flow (RR: 0.60 -> 0.40) if 80 % of land cover been afforested. The regulation ability (R2FDC: -0.75 -> -0.98) of flow decreases with more variable peak flow (Qvar:

0.92 -> 1.15). The reduction is more significant in the observed flows of the paired catchments (RR: 0.76 vs 0.29), in which the flow of the afforested catchment is more fluctuated (Qvar: 1.26 vs 1.98) and unregulated (R2FDC: -0.53 vs -1.42).

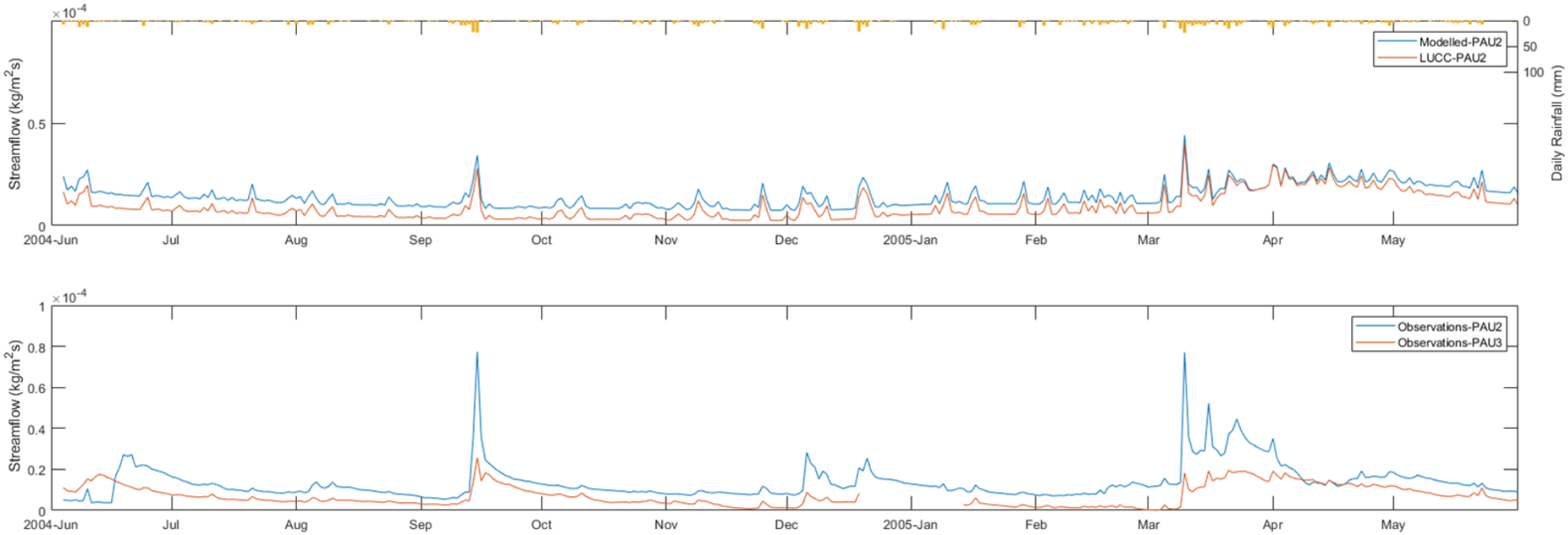

Figure 4.13 (a) Comparison of flow under natural páramo watershed (PAU2) using JULES modified on the observed data ("Modelled") and modified on the afforested catchment (PAU3) with changed parameters ("LUCC"); (b) pair-wise observations for the natural (PAU2) and afforested (PAU3) catchments.

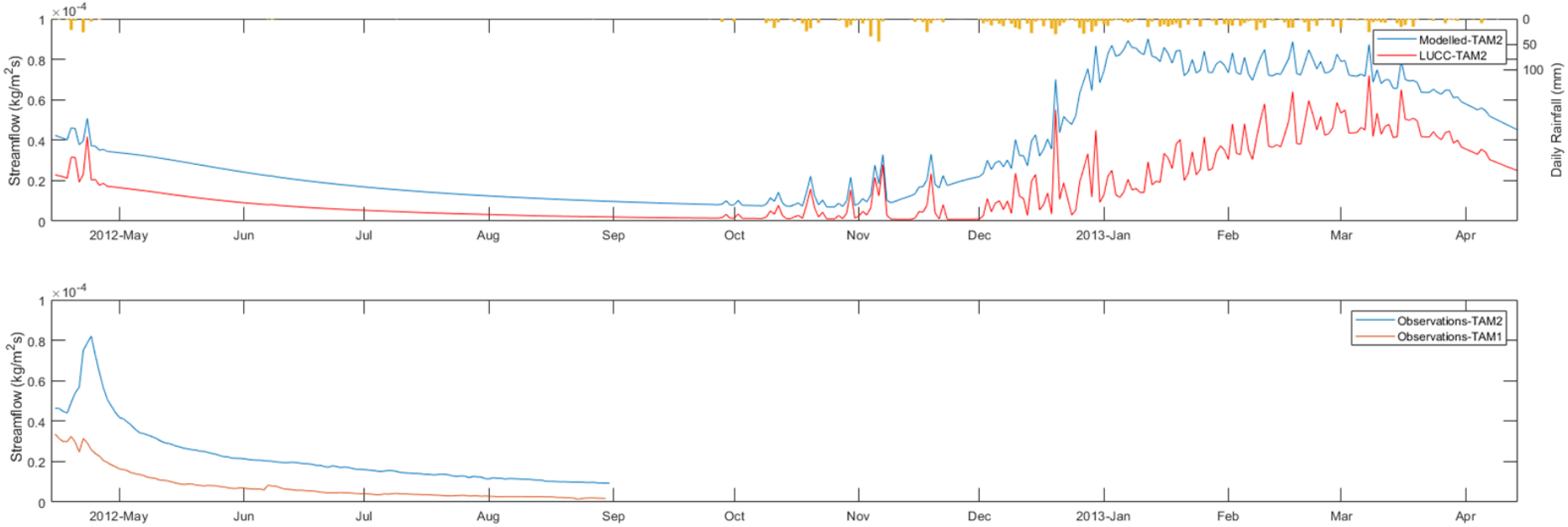

Figure 4.14 (a) Comparison of flow under natural puna watershed (TAM2) using JULES modified on the observed data ("Modelled") and modified on the afforested catchment (TAM1) with changed parameters ("LUCC"); (b) pair-wise observations for the natural (TAM2) and afforested (TAM1) catchments.

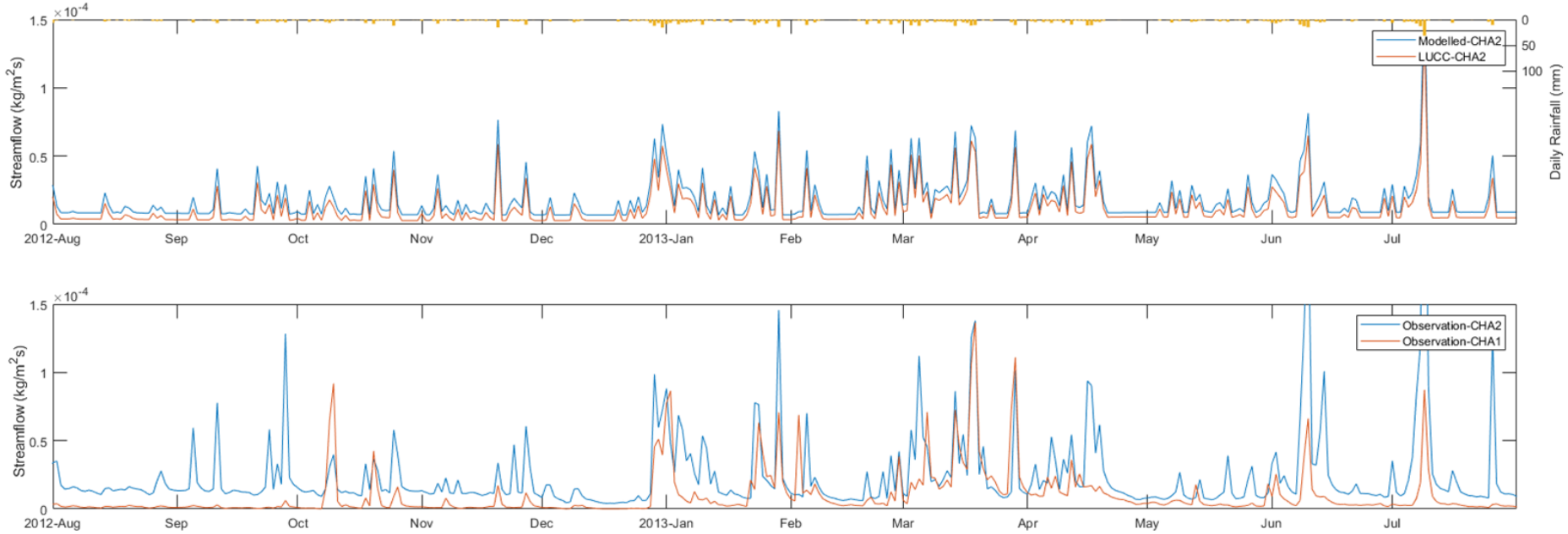

Figure 4.15 (a) Comparison of flow under natural jalca watershed (CHA2) using JULES modified on the observed data ("Modelled") and modified on the afforested catchment (CHA1) with changed parameters ("LUCC"); (b) pair-wise observations for the natural (CHA2) and afforested (CHA1) catchments.

4.4 Conclusions

Land use and land cover change (LUCC) is a major driver of change in the hydrological cycle. However, the impacts are hard to quantify and predict due to the complexity of catchment characteristics and the external meteorological drivers. Pair-wised catchment comparison serves as an effective approach to compare the hydrological responses under the controlled/affected catchments. However, the hydrological effects of difference in catchment characteristics and meteorological drivers between the paired catchments cannot be assessed directly in this way. Therefore, I evaluated the potential of a physics-based hydrological model (JULES) to simulate the impacts under a variety of scenarios of grazing, cultivation, and pine afforestation, by altering the soil and land cover parameters in JULES in a physically sensible way.

In this chapter, I find that modification of a single vegetation parameter (canopy height, leaf area index, root depth) has a minor effect (< 1.4% of total flow) on the hydrological response. However, the land cover change has significant impact on the evapotranspiration and generation of flow. The result also implies that the effect of soil properties is more pronounced given the low percentage of land cover change between the paired catchments. Also, given the insufficient data available for calibration of vegetation parameters, I drove the model with soil parameters modified in the paired catchment identifying LUCC. A reduction of flow can be found in all types of human intervention, as well as increasing peak flow, and the loss of water regulation capacity. The simulated LUCC impacts are consistent with the assessment under pair-wised catchment comparison, which is to be expected because the parameters strongly depend on the local observation. The difference in precipitation could be an important driver that contributes to the flow change (e.g. PIU_01/PIU_02;

PIU_04/PIU_07; TAM_02/TAM_01). I conclude that using a hydrological model helps filtering out the impacts of catchment characteristics and micro-meteorological conditions, and makes it therefore possible to analyse more specifically the contribution of LUCC to the flow generation.

5 Modelling regional LUCC dynamics in the tropical Andes

5.1 Introduction

Land use and land cover change (LUCC) is a dynamic process governed by the interaction between biophysical factors and socioeconomic activities (Moulds, Buytaert & Mijic, 2015). In its turn, it is an important driving factor of degrading biodiversity and threatening of sustainable ecosystem services (Foley et al., 2005; Turner, Billie L., Lambin & Reenberg, 2007). In terms of water resources management, sediments, hydrochemistry and hydro-ecology could all be affected directly by the changing land use (McIntyre et al., 2014). These effects may disrupt the surface energy and water balance; thus, affect the climate on both local and regional scale (Boysen et al., 2014; Pitman et al., 2009). Therefore, a sound understanding and prediction of land use change is important factor to be considered in hydrological science (McIntyre et al., 2014).

Although land use management becomes increasingly important for solving water resources issues, the impact of land use change on the hydrology is still hard to identify because of the highly heterogeneous conditions of catchments (McIntyre et al., 2014). Land use change models are common measures to understand and quantify the driving factor of land use and land cover change (Veldkamp & Lambin, 2001). They allow past and future change under different scenarios to be simulated at various spatial scales (Mas et al., 2014). The simulated results can be applied to support the decision making process of land use planning and environmental management on both local and regional scale (Moulds, Buytaert & Mijic, 2015; Veldkamp & Lambin, 2001). In addition, the impact of change on biodiversity, water resources, and climate variability could be investigated accordingly.

The hydrology of tropical Andes is significantly affected by human activities such as intensive cattle grazing, cultivation, and pine planting (Buytaert et al., 2006) accompanied by the rapid economic growth during the past half-century, which as a consequence has decreased the water storage capacity of Andean catchments (Harden, 2006). In this chapter, I investigate the LUCC processes in the Andean region of Perú and Ecuador by using an open-source land use change model, i.e. the lulcc R software package (Moulds, Buytaert & Mijic, 2015). This package is a spatially explicit land-use change model, which aims to quantify key processes affecting LUCC, and to simulate the potential future changes. It has been demonstrated to generate adequate annual land cover map for India between 1960 and 2010 (Moulds, Buytaert & Mijic, 2018). I apply the lulcc R model to my study region to analyse the LUCC dynamics between 2001 and 2016, and to simulate the potential land use change in 2030, which is the time horizon most relevant for policy making in the region. The model is also used so simulate the historic period that is not covered by available land cover maps, to make it possible to input a continuous time series of land use change data in the large scale hydrological modelling software JULES, to assess the potential changing hydrology under LUCC dynamics.

5.2 Methods

5.2.1 The lulcc R model

A variety of land-use change models have been developed for different purposes. Of these, spatially explicit models are operated over a spatial grid to predict the location of land-use/land cover changes (Mas et al., 2014). The models can be classified by their use of an inductive or deductive approach. In inductive spatially explicit modelling, the suitability to change is predicted for each grid by using a function of spatially explicit predictor variables (Moulds, Buytaert & Mijic, 2015). In a deductive spatially explicit model, the location of change is predicted by analysing the drivers of change. These two approaches can be combined to provide a better representing on the land use change in a complex system. The output of such models is a set of land use maps simulated by the model, which ideally describe the change over time for the target region comprehensively.

In this research, I analyse the land cover dynamics by applying the lulcc R package developed by Moulds, Buytaert & Mijic (2015) to the tropical Andes. Traditionally, land-use/land cover change models are developed as software package or extension to geographic systems such as ArcGIS (Moulds, Buytaert & Mijic, 2015). It is uncommon for the source code of model implementations to be made available (Rosa, Ahmed & Ewers, 2014). The lulcc R package is an object-oriented framework for land use change modelling written in the R programming language. It is taken as an alternative to the major closed-source, specialised software packages. The lulcc R package provides a framework for users to perform the whole modelling process within the same environment. This allows for a very efficient workflow implementation, which reduces the likelihood of user errors. It has the added advantage to ensure the reproducibility of simulated scientific results.

5.2.2 Assessing historical land cover changes

Figure 5.1 shows the data processing workflow of the lulcc R package. The historical land use map of my study region (Ecuador and Perú) was obtained from the MODIS Land Cover Type (MCD12Q1) Version 6 data (Friedl & Sulla-Menashe, 2015). The satellite-based map is used as a reference and referred to as the "observed" map. The original classification of 17 land use classes from the Annual International Geosphere-Biosphere Programme (IGBP) were reclassified into 6 major land use types in the study region as Figure 5.2. The region is mainly covered by forest, followed by C3/C4 grasses in the highlands, and bare soil occurrences in coast and urban area. I classified three minor land cover classes (ice, water, urban) as 'others' since these areas are barely changed during the modelling period.

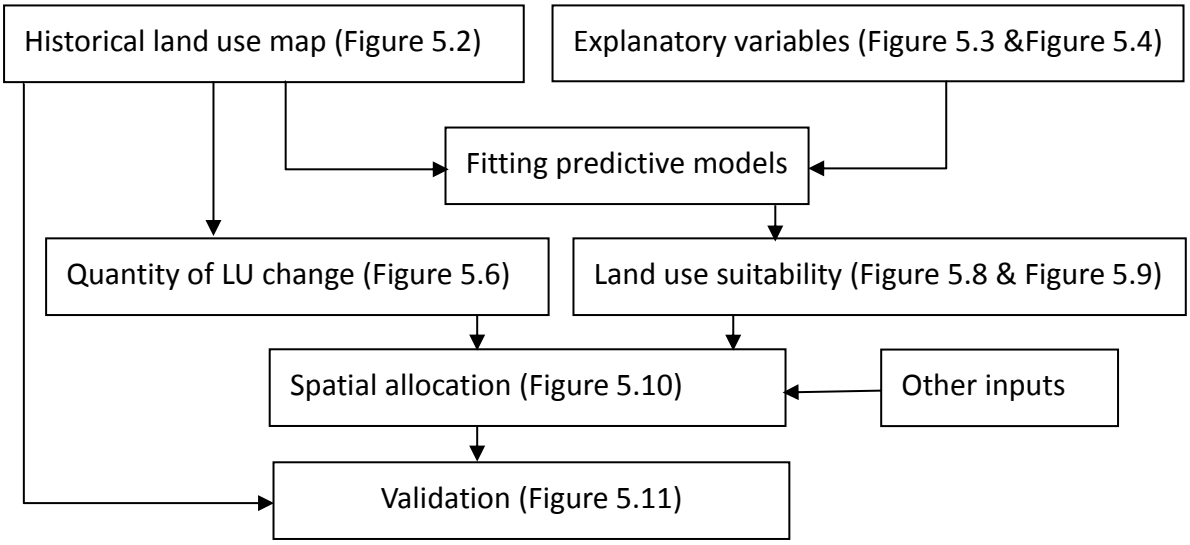

Figure 5.1 The workflow of the lulcc R package

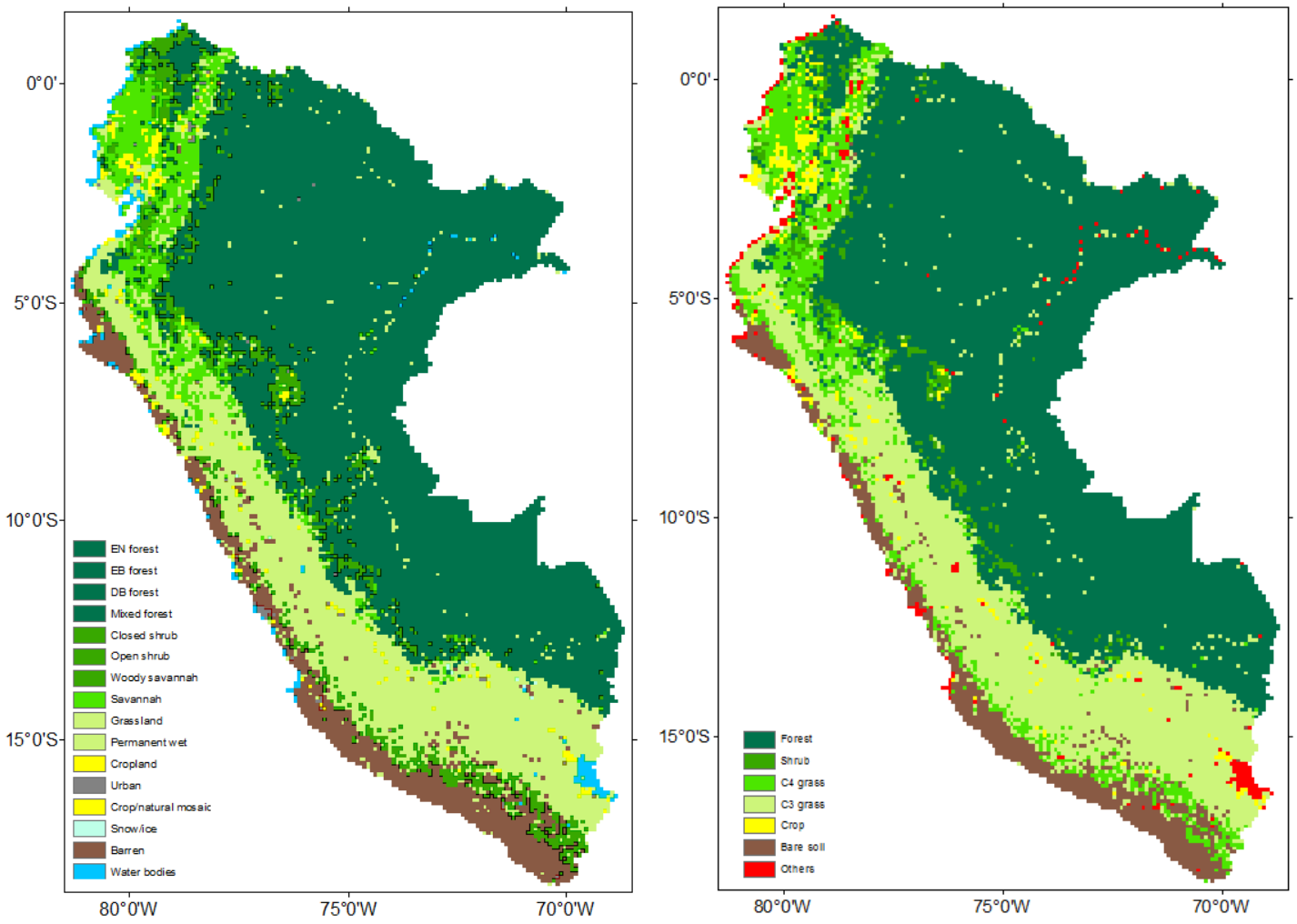

Figure 5.2 Land cover classification (right) in 2001 from IGBP map (left)

5.2.3 Predicting future land cover changes

Binary logistic regression was applied in the predictive model to predict the presence or absences of each land use type by using two topography, and three socioeconomic explanatory variables(Table 5.1). The topographical variables (elevation, slope; Figure 5.3) are important drivers for vegetation types, given that the Andean ecosystem is strongly altitude dependent (Célleri et al., 2009). In the Amazon, nearly 95% of all deforestation occurred within 5.5 km of roads or 1 km of rivers (Barber et al., 2014). Therefore, socioeconomic variables (Figure 5.4) are selected to determinate accessibility to human activities (distance to river, distance to road), and their development pressure under population growth (population density).

An alternative predictive model, recursive partitioning and regression trees, provided by the rpart package (Therneau & Atkinson, 2019), was used for comparison. The predictive models were evaluated by using he receiver operator characteristic (ROC) of the ROCR package (Sing et al., 2005). The ROC is a curve of the true positive rate against the false positive rate, which is plotted using multiple thresholds to classify true values as 1, and false value as 0 (Pontius & Parmentier, 2014). The area under the curve (AUC) was summarised, where 1 indicates a perfect fit and 0.5 indicates a purely random model.

Table 5.1 Explanatory variables for lulcc R

Variable	Spatial resolution [°]	Source
Elevation	0.083	HydroSHEDS (Lehner, Verdin & Jarvis, 2008)
Mean slope	0.083	FAO (Fischer, van Velthuizen & Nachtergaele, 2000)
Road network	0.0083	(DIVA-GIS, 2019)
River network	0.0083	(DIVA-GIS, 2019)
Population density	0.0083	(DIVA-GIS, 2019)

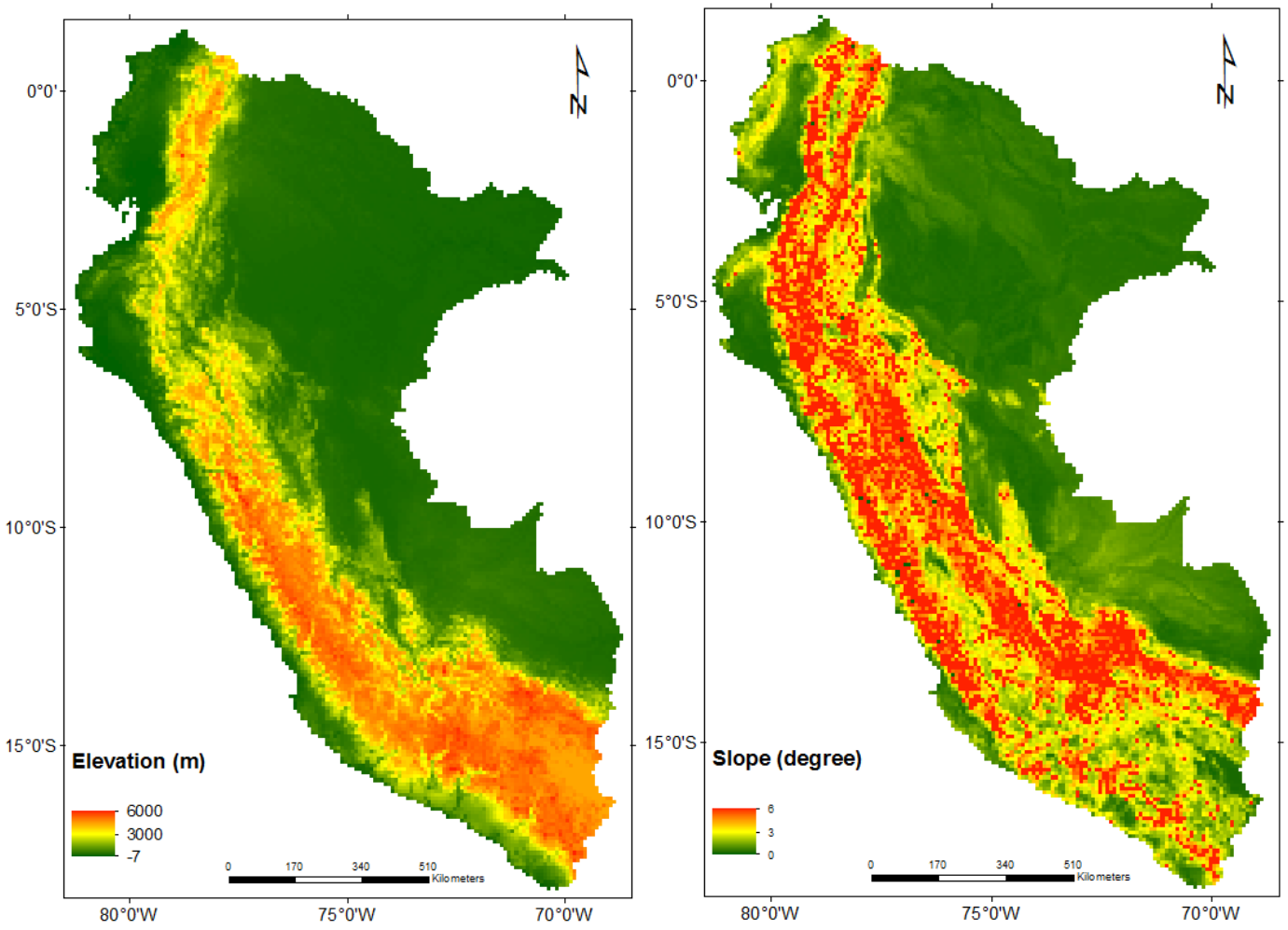

Figure 5.3 Explanatory variables for lulcc R (topography)

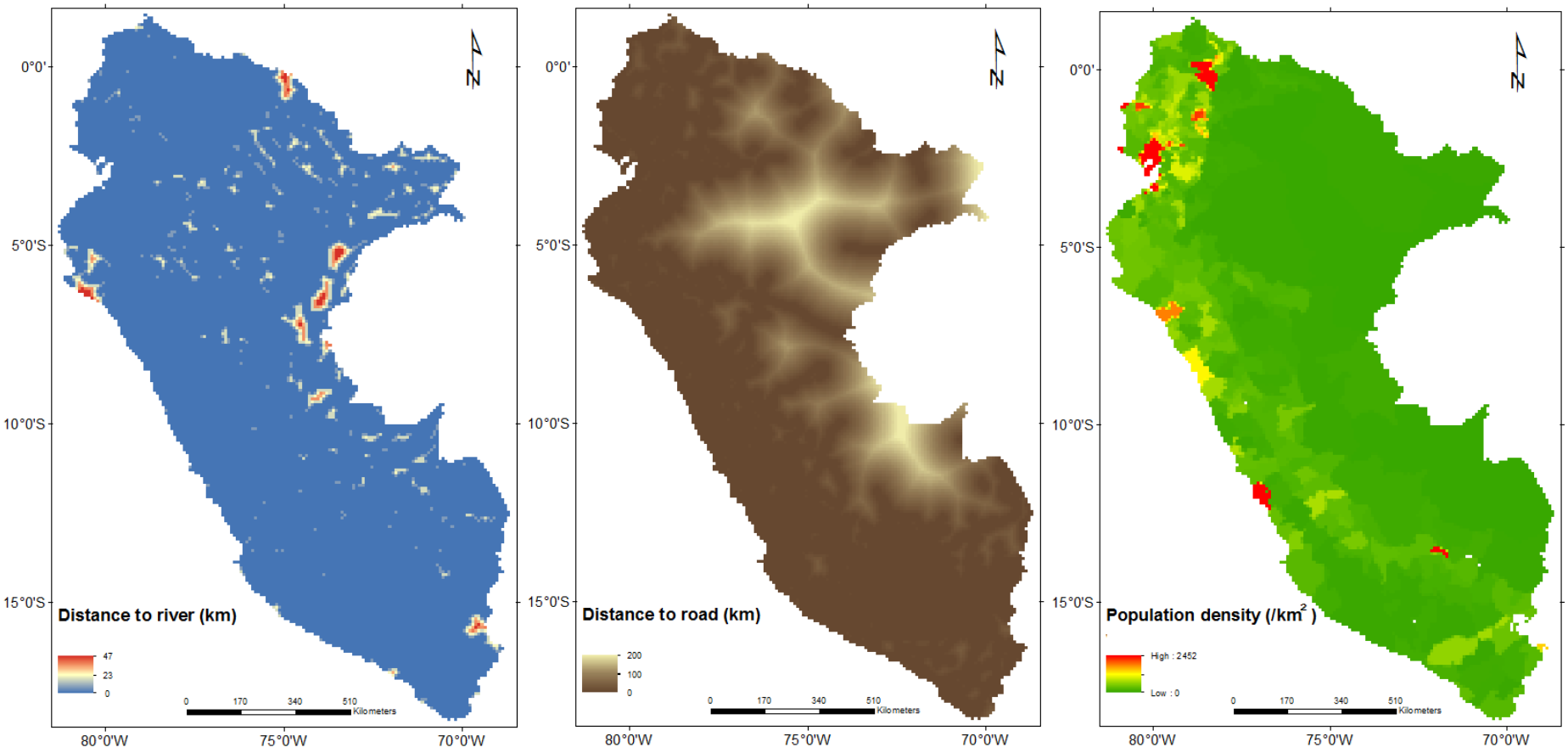

Figure 5.4 Explanatory variables for lulcc R (socioeconomic)

The land cover changes during 2001 to 2030 were allocated by using two allocation algorithms, the CLUE-S algorithm (Verburg et al., 2002), and a stochastic ordered algorithm (Fuchs et al., 2012). The CLUE-S algorithm allocates each cell to the land use type with the highest suitability determined by the predictive model. The number of pixels allocated to each land use type was calculated subsequently. If the number of allocated pixels of a land use type is smaller or greater then the demand, the suitabily of each pixel of a certain land use type will be increased or decreased. The model uses an iterative procedure until the allocation of all land use types meet their demand. The ordered allocation algorithm uses a hierarchical way to allocate land use according to the perceived socialeconomic value of each land use. For land use types with decreasing demand, the pixels belonging to certain land use type with lower suitability will be changed to other land use type with increasing demand.

I further validated the simulated land cover map in 5 selected river basins for which observed streamflow data exist (Table 5.2; Figure 5.5). The basins are deemed representative for the regional biogeographical variability of the study region.

Table 5.2 The selected catchments for LUCC validation. BF: Forest, C3: C3 grasses, C4: C4 grasses, SH: Shrub, BS: Bare soil.

Basin	Elevation (m)	Area (km^2)	Major land cover (% in 2016)
BELLAVISTA	110	100677	92.4 BF; 3.9 C3
SAN REGIS	93	363848	67.0 BF; 16.3 C3; 8.4 SH; 6.8 C4
EL TIGRE	44	4792.6	45.6 SH; 31.6 C4; 15.8 BF
CONTA	324	3161	77.5 C3; 15.0 C4; 7.5 BS; 7.0 C3
EGEMSA KM 105	2,302	9712.1	87.7 C3; 5.3 BF

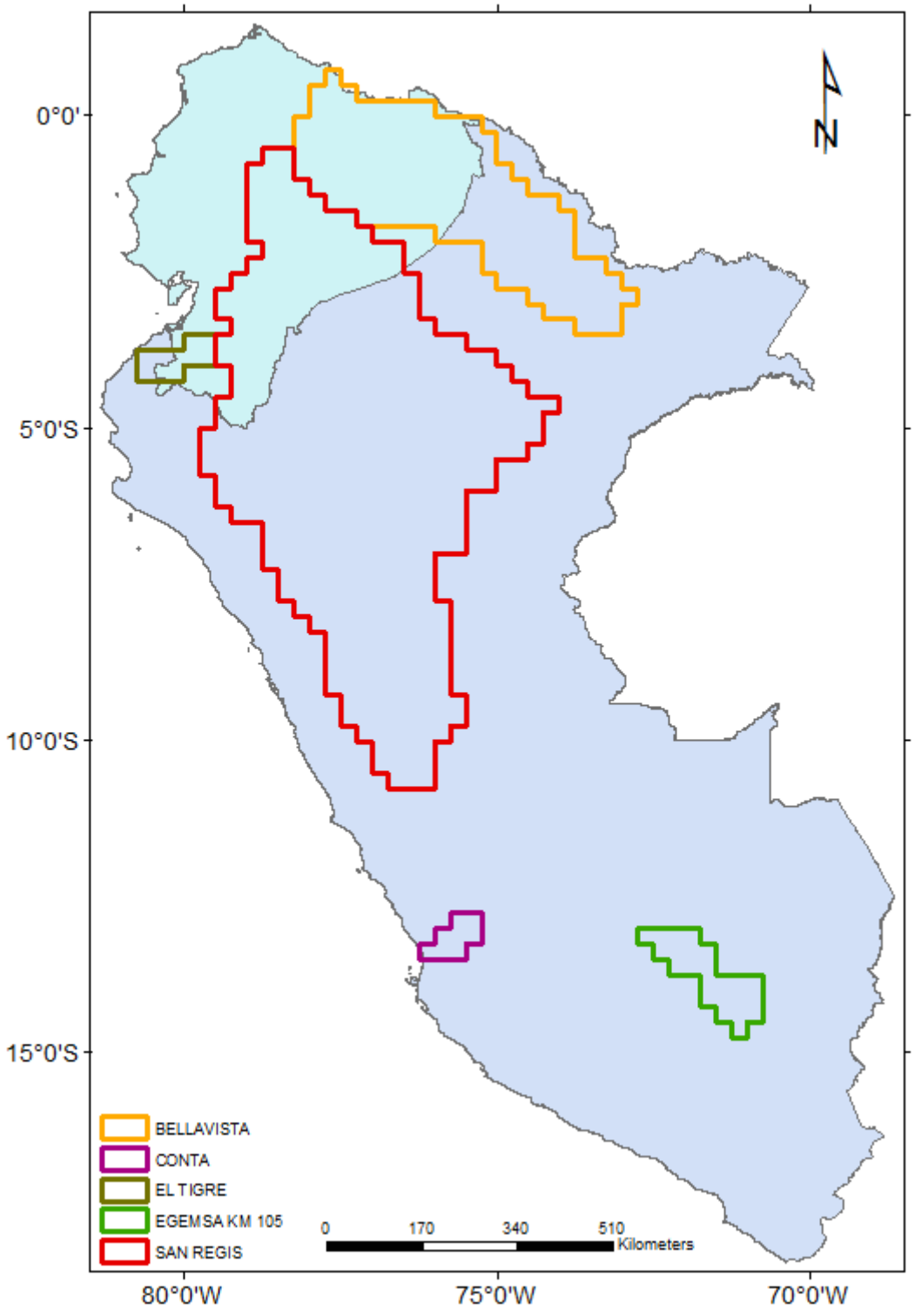

Figure 5.5 The boundary of lulcc R setup and the select catchments for validation

5.3 Results and discussion

5.3.1 Allocating the land cover changes

Figure 5.6 shows the land cover changes during 2001 to 2016 identified by using MODIS Land Cover Type (MCD12Q1) Version 6 data (Friedl & Sulla-Menashe, 2015). The model covers an area of 1.57 million km^2 in the Andean region of Perú and Ecuador. Overall, 8.2% of land cover has been changed between this period, including a continuous trend of deforestation which has decreased the forest area by 28186 km^2. Table 5.3 shows that these deforested areas have been mainly transformed to shrub and C3/C4 grasses.

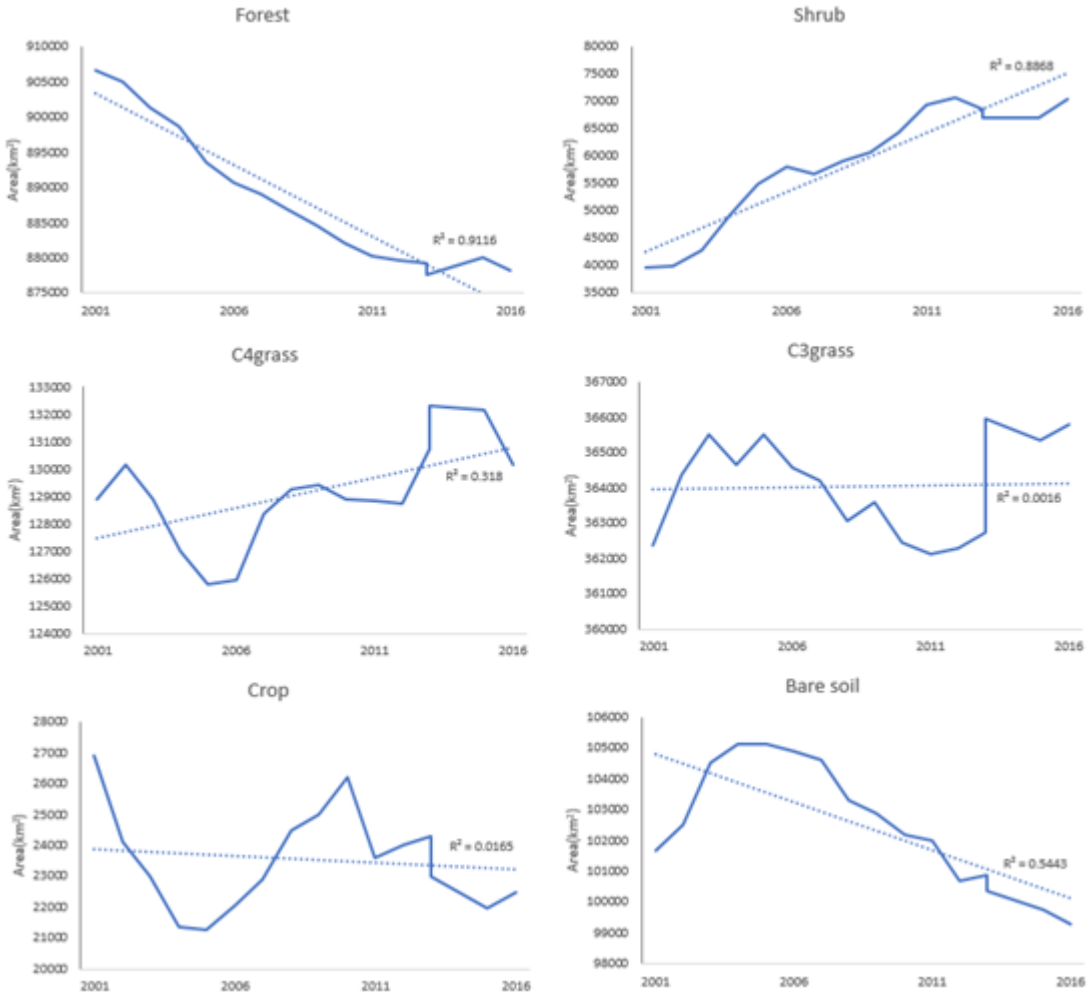

Figure 5.6 The land cover changes from 2001 to 2016 and a linear regression fit

Table 5.3 Cross-tabulated change between 2001 and 2016 (in pixels)

2001\2016	Forest	Shrub	C4grass	C3grass	Crop	Bare soil	Others
Forest	9952	341	45	67	3	0	1
Shrub	41	329	58	27	1	0	0
C4grass	30	79	1107	189	32	42	1
C3grass	54	39	180	3831	38	16	2
Crop	4	21	54	46	184	0	0
Bare soil	0	0	50	35	0	1081	1
Others	0	0	0	4	0	1	270

In Figure 5.7, the AUC suggests reasonable prediction using both glm/rpart model. A suitability map for each land cover was fit using binary logistic regression model as Figure 5.8.

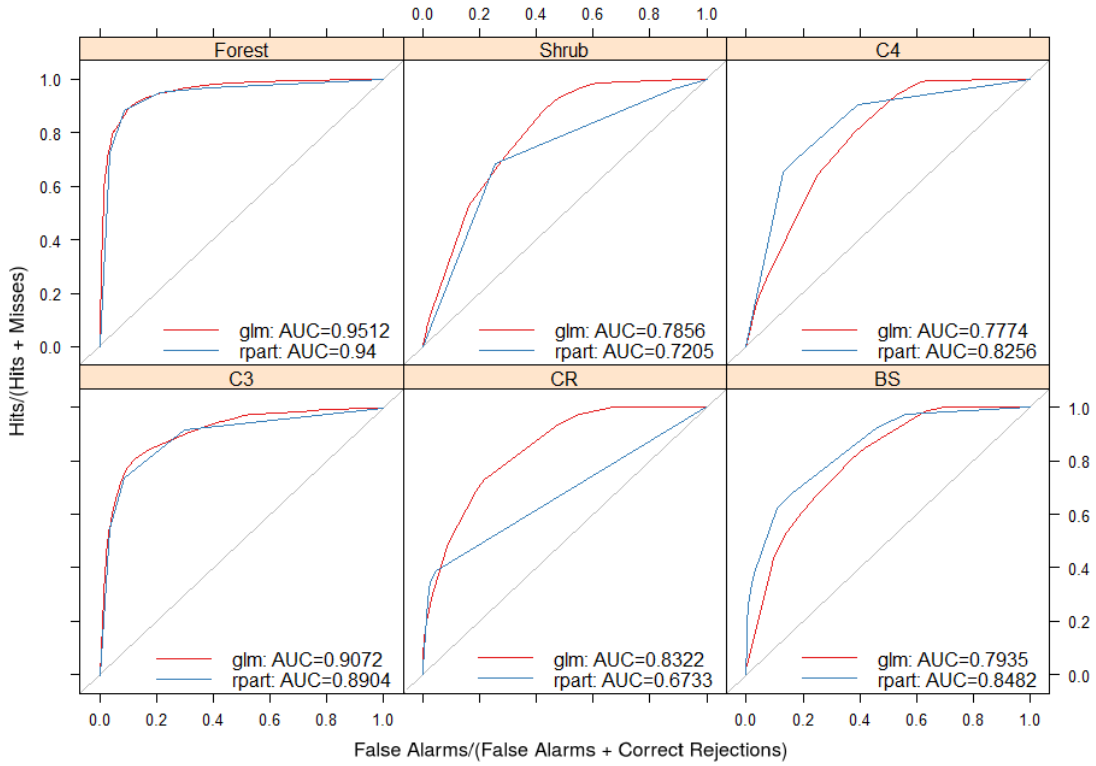

Figure 5.7 ROC curves showing the ability to simulate the observed pattern of land use in 2001

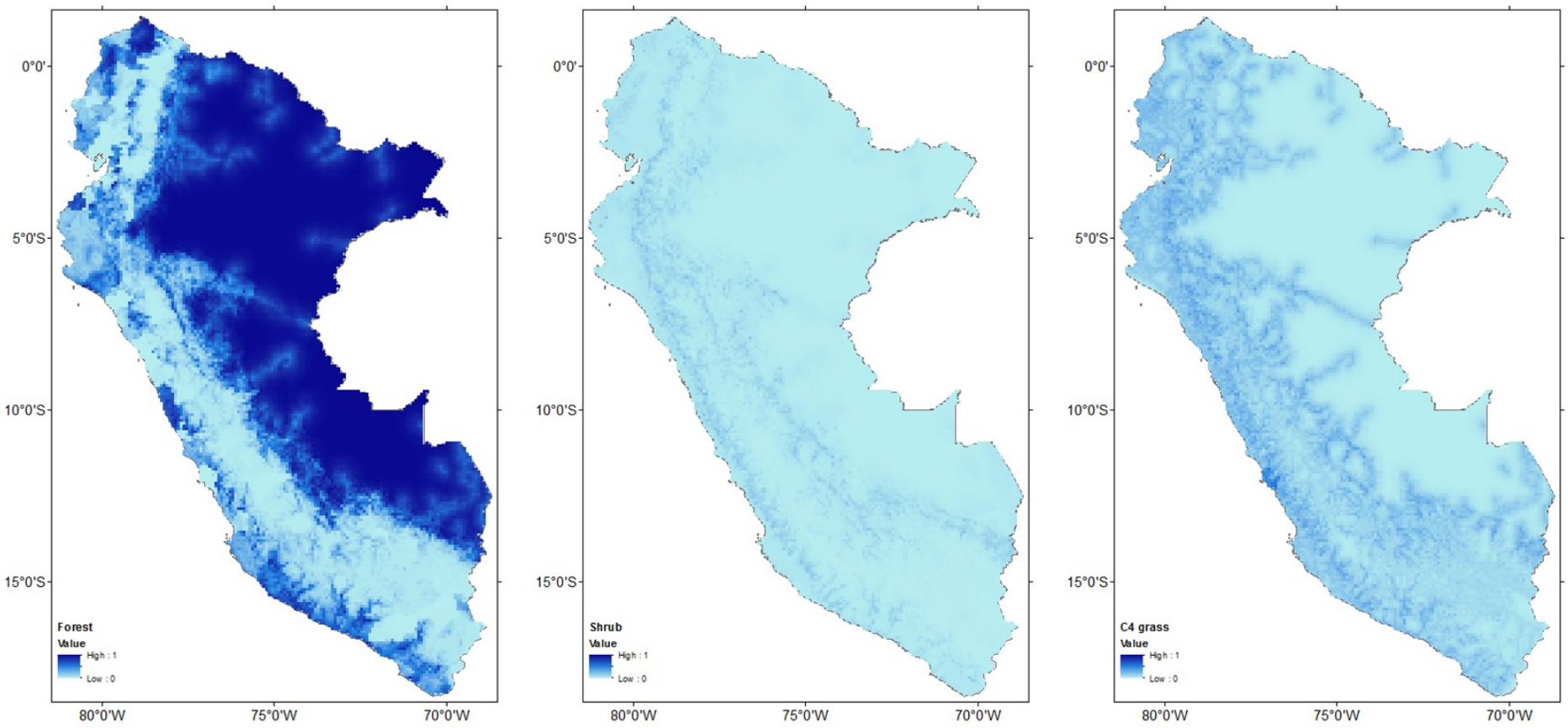

Figure 5.8 Suitability map for each land cover (Forest, Shrub, C4 grass) according to binary logistic regression model

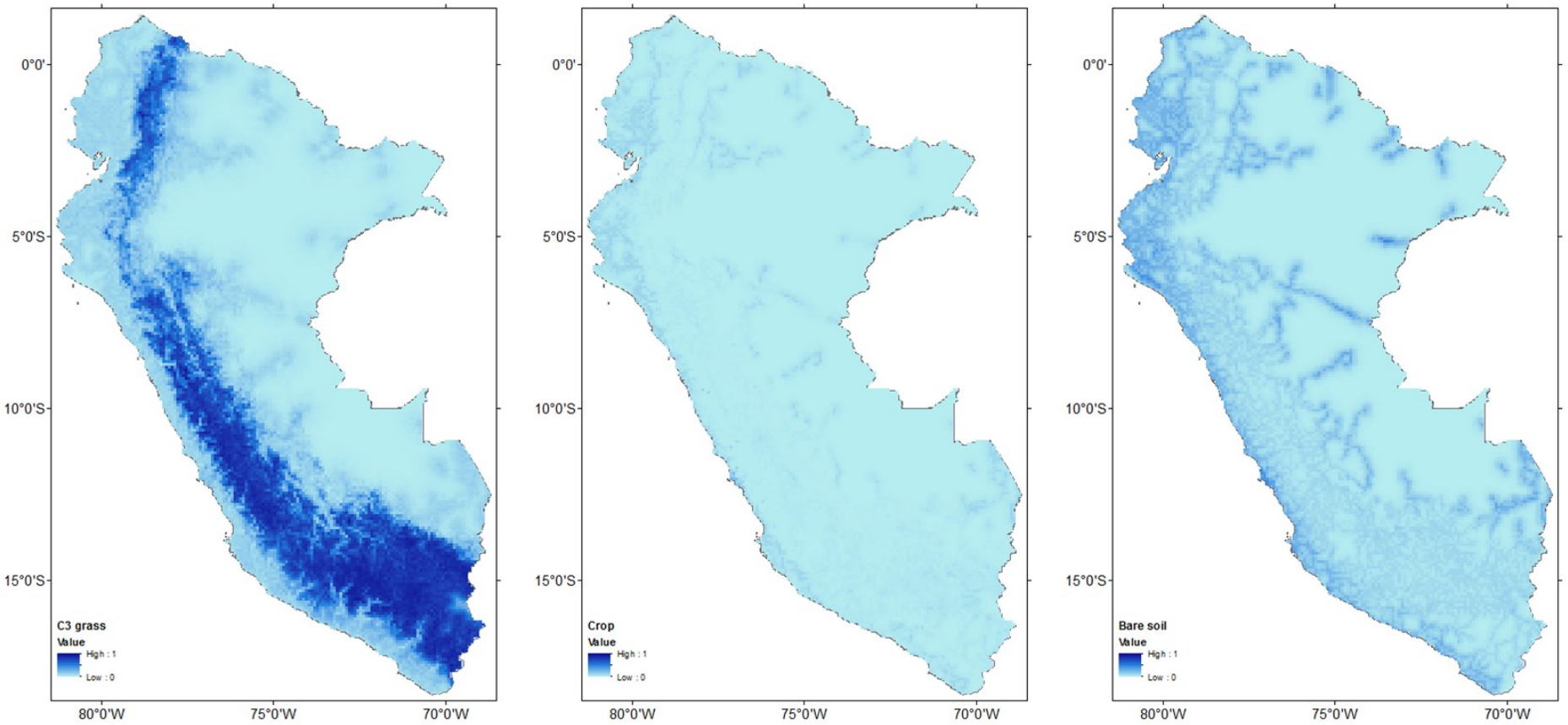

Figure 5.9 Suitability map for each land cover (C3 grass, crop, bare soil) according to binary logistic regression model

The allocation results were compared and validated with the historical land cover map of 2016 (Figure 5.10). The modelled results predicted more afforestation in the lowland area, which shows a higher suitability for forest. In Figure 5.11, the land use changes were classified as afforestation and deforestation. The modelling results and observation all show that deforestation mainly occurs over the Andes mountains.

With using the ordered algorithm, Table 5.4 shows the number of correctly allocated changes of the model. For the finest resolution, 87.6% of unchanged land cover was simulated correctly, whereas only 15.9% of changes were detected. The model performance increased with coarser resolution (Figure 5.12). 62.7% of changes were simulated under the resolution used in the JULES model (0.25 degree). However, 40.6% of changes was simulated as wrong categories. Table 5.5 shows the allocation analysis using the CLUE-S algorithm. CLUE-S has slightly better performance simulating the persistence of land cover. However, a higher percentage of the changes were allocated to wrong categories. The model performance increases with decreasing resolution (Figure 5.13). The ordered algorithm allocated the land cover with 88.2% accuracy under the finest resolution. The number is 89.1% for the CLUE-S algorithm.

The potential land cover for the year 2030 was allocated using both the ordered model (Figure 5.14) and the CLUE-S model (Figure 5.15), in which the demand of land cover was extrapolated linearly from the historical data. Both algorithms show that future deforestation is most likely to occur close to the area that was already deforested in 2016.

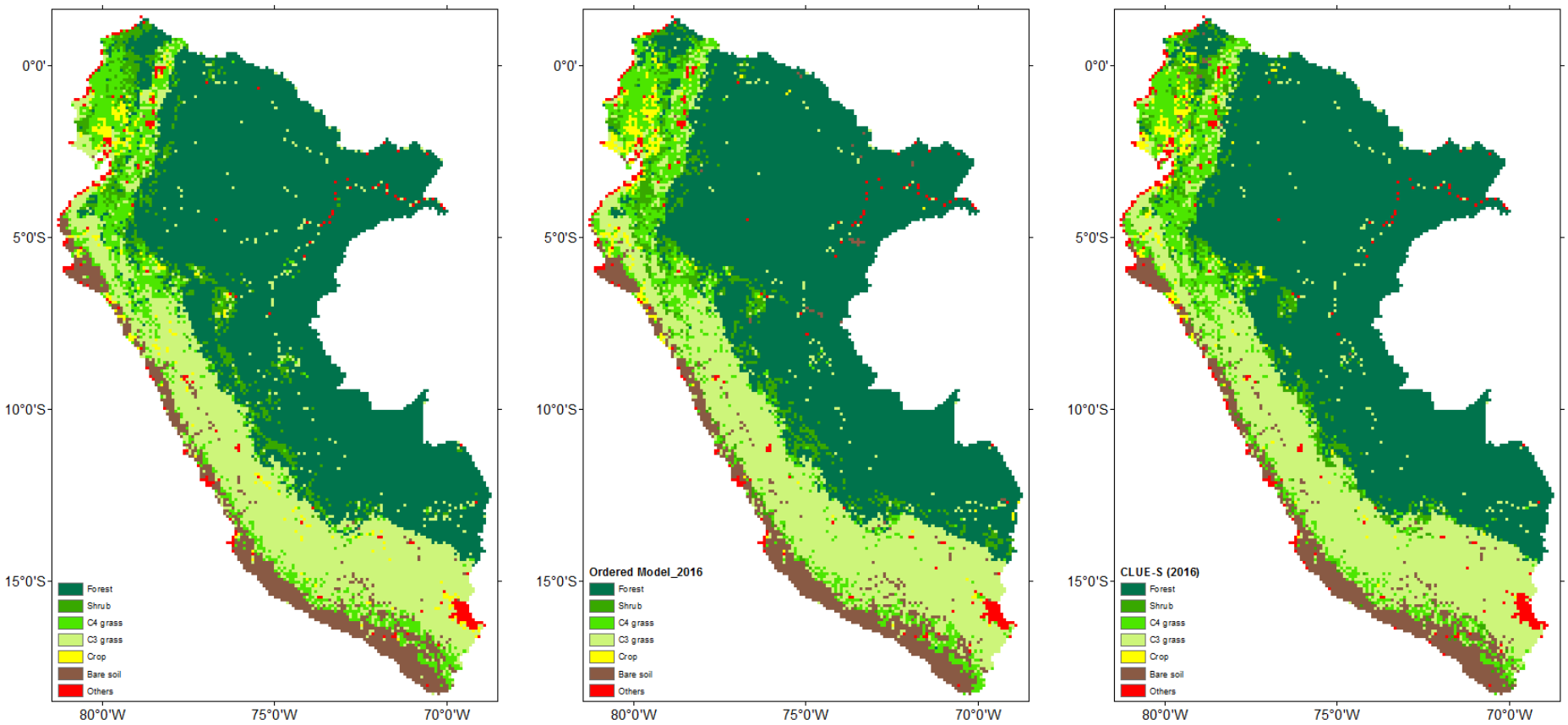

Figure 5.10 The land cover in 2016 a) the reference land cover map b) allocated by the ordered model c) allocated by the CLUE-S model

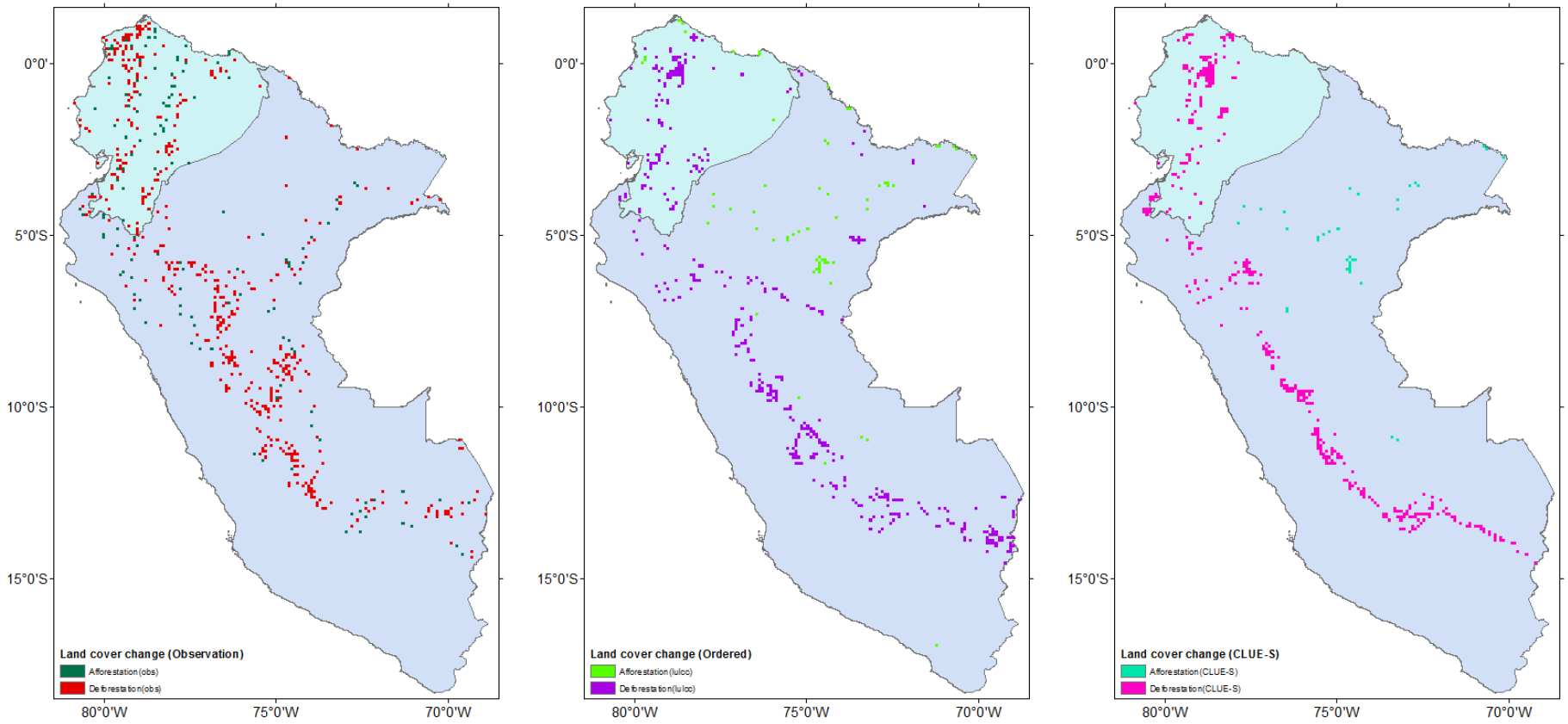

Figure 5.11 The afforestation/deforestation from 2001 to 2016 identified by a) the referenced land cover map b) the ordered model allocation c) the CLUE-S model allocation

Table 5.4 Indicators of agreement and disagreement at multiple resolutions using the ordered model. (1) Change simulated as persistence (misses) (2) Change simulated correctly (hits) (3) Change simulated as change to wrong category (wrong hits) (4) Persistence simulated as change (false alarms) (5) Persistence simulated correctly (correct rejections). Pixel = level of aggregation in multiple of pixels (i.e. decreasing resolution) compared to the original map. Resolution is expressed in degrees lat/lon.

Pixel (resolution)	(1)	(2)	(3)	(4)	(5)
1 (0.083)	0.069	0.006	0.007	0.042	0.876
4 (0.167)	0.034	0.010	0.019	0.030	0.906
9 (0.25)	0.019	0.013	0.019	0.024	0.925
16 (0.333)	0.012	0.013	0.021	0.018	0.934
25 (0.417)	0.009	0.014	0.019	0.013	0.945
36 (0.50)	0.008	0.014	0.021	0.011	0.947

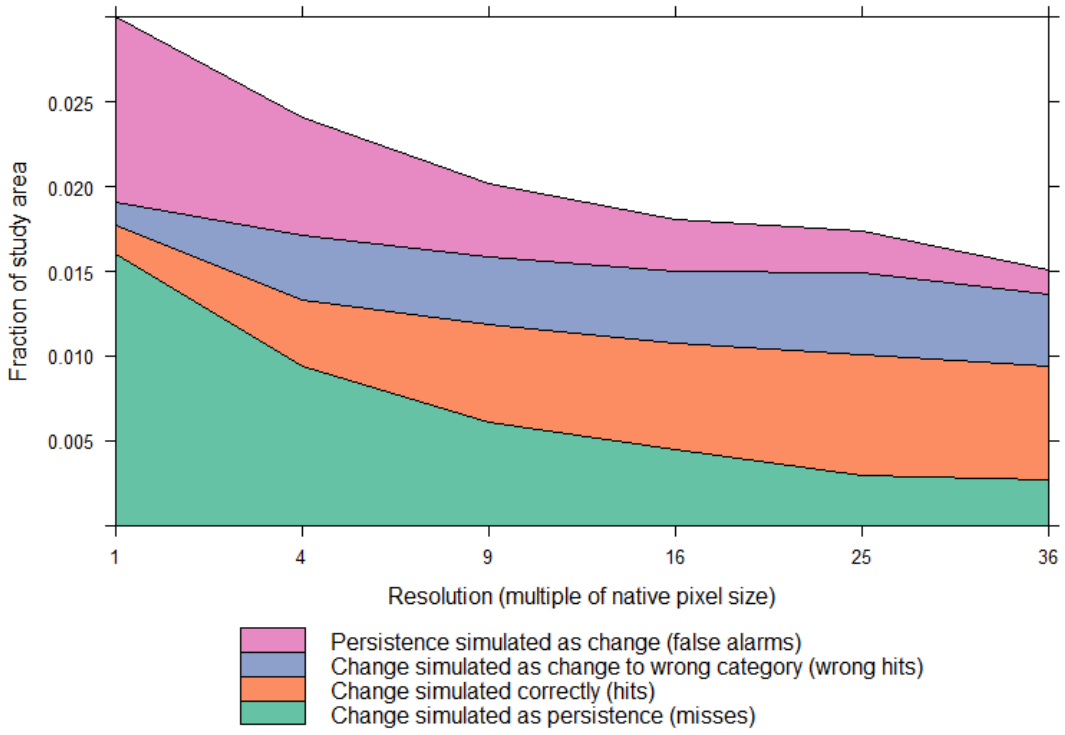

Figure 5.12 The number of correctly allocated changes as fraction of the total study area (ordered model)

Table 5.5 Indicators of agreement and disagreement at multiple resolutions using the CLUE-S model. (1) Change simulated as persistence (misses) (2) Change simulated correctly (hits) (3) Change simulated as change to wrong category (wrong hits) (4) Persistence simulated as change (false alarms) (5) Persistence simulated correctly (correct rejections). Pixel = level of aggregation in multiple of pixels (i.e. decreasing resolution) compared to the original map. Resolution is expressed in degrees lat/lon.

Pixel (resolution)	(1)	(2)	(3)	(4)	(5)
1 (0.083)	0.073	0.004	0.005	0.030	0.887
4 (0.167)	0.037	0.008	0.018	0.022	0.914
9 (0.25)	0.022	0.011	0.017	0.018	0.932
16 (0.333)	0.014	0.012	0.020	0.013	0.940
25 (0.417)	0.011	0.014	0.017	0.011	0.945
36 (0.50)	0.008	0.014	0.018	0.007	0.953

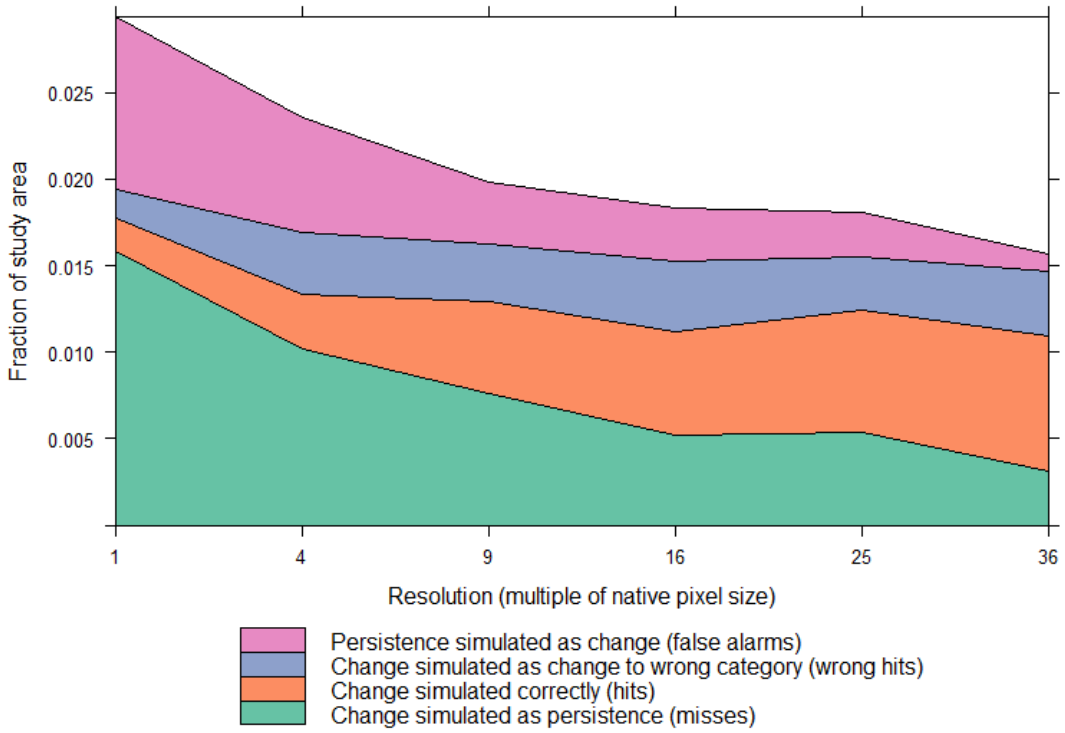

Figure 5.13 The number of correctly allocated changes as fraction of the study area (CLUE-S model)

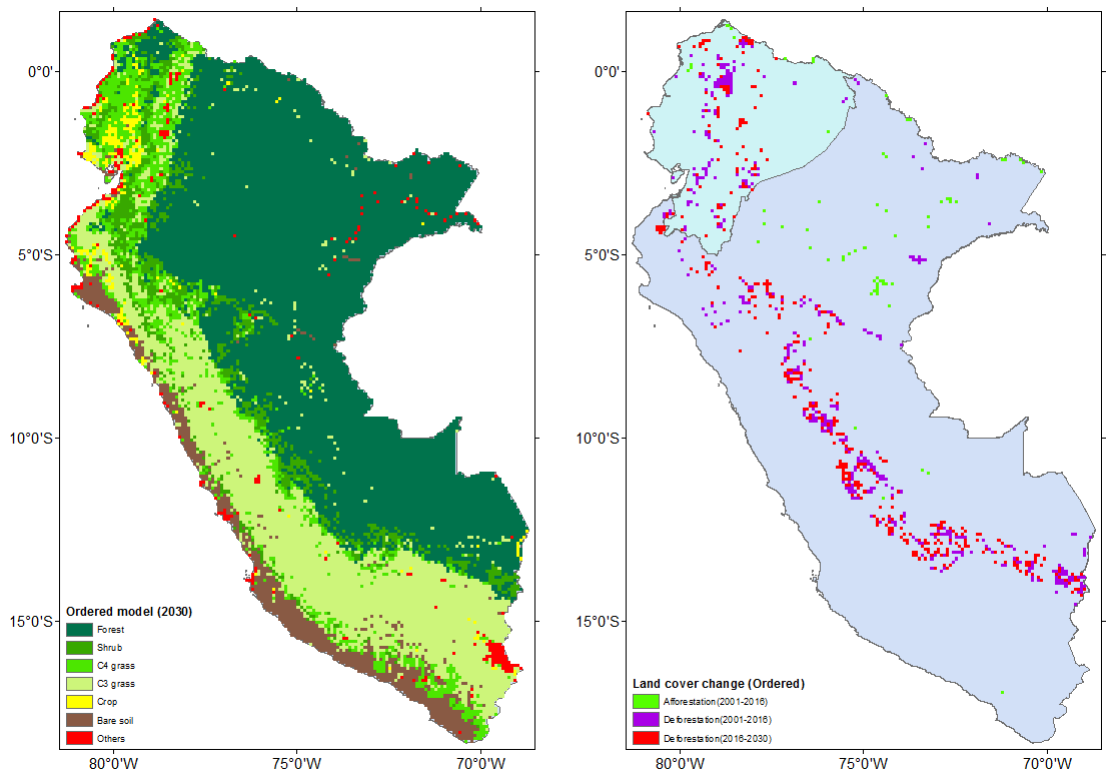

Figure 5.14 Simulation of land cover allocation and changes with the ordered model for 2030

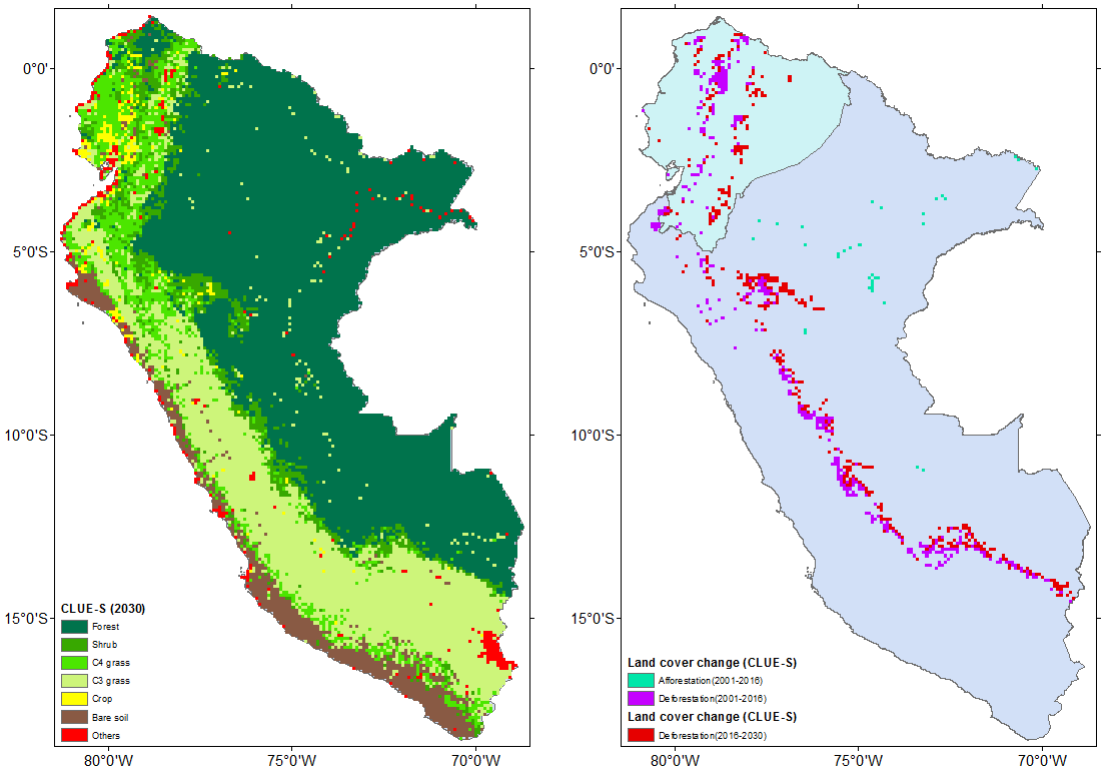

Figure 5.15 Simulation of the land cover allocation and changes with the CLUE-S model for 2030

5.3.2 Land cover changes in basins

In this section, I review and discuss the obtained results for each of the modelled basins in sequence.

Conta is a C3 grass covered catchment located in southern Perú. In this basin, no significant change was detected from observation from 2001 to 2016, and as a result, neither in the model results from 2016 to 2030 (Table 5.6).

EGEMSA KM 105 (Table 5.7) is also located in southern Perú, and mainly covered by C3 grasses. The major part of land cover was modelled correctly with only 6 forest pixels that were simulated as wrong category.

EL TIGRE is located in northern Perú at the boundary of forest and shrub. Table 5.8 shows that the land cover allocated in 2016 is closest to the observed allocation. The observations, the ordered algorithm, and the CLUE-S algorithm, all show that part of forest has been transformed into shrub from 2001 to 2016. The lulcc R model suggests that the trend of deforestation will continue between 2016 and 2030.

Table 5.6 The pixels of land cover allocated in CONTA

	Observation		Ordered model		CLUE-S model	
	2001	2016	2016	2030	2016	2030
Shrub	0	0	3	3	0	0
C4grass	6	6	3	3	6	6
C3grass	30	31	30	30	30	30
Bare soil	4	3	4	4	4	4

Table 5.7 The pixels of land cover allocated in EGEMSA KM 105

	Observation		Ordered model		CLUE-S model	
	2001	2016	2016	2030	2016	2030
Forest	5	6	0	0	0	0
Shrub	3	2	3	3	7	7
C4grass	1	1	5	5	1	1
C3grass	101	100	102	103	103	104
Crop	1	1	1	1	0	0
Bare soil	1	2	1		1	0
Others	2	2	2	2	2	2

Table 5.8 The pixels of land cover allocated in EL TIGRE

	Observation		Ordered model		CLUE-S model	
	2001	2016	2016	2030	2016	2030
Forest	13	9	9	4	5	1
Shrub	17	26	27	36	23	27
C4grass	20	18	14	10	22	22
C3grass	7	4	7	7	7	7

Table 5.9 The pixels of land cover allocated in BELLAVISTA

	Observation		Ordered model		CLUE-S model	
	2001	2016	2016	2030	2016	2030
Forest	1076	1074	1073	1068	1073	1052
Shrub	21	27	18	21	27	47
C4grass	19	13	26	27	14	14
C3grass	41	45	38	39	42	43
Crop	3	0	3	3	4	4
Bare soil	0	0	2	2	0	0
Others	2	3	2	2	2	2

The modelling results were further validated in two large forest catchments, BELLAVISTA in Ecuador, and SAN REGIS in northern Perú. In BELLAVISTA, minor changes of forest were detected from the observation between 2001 and 2016 (Table 5.9). The lulcc R model also suggests that the region will not be significantly deforested in 2030 with ordered algorithm. However, the CLUE-S algorithm simulated decreasing forest area in 2030.

In SAN REGIS, a clear trend of deforestation can be observed both in the land use map and in the simulation (Table 5.10). Respectively, 4.5%/3.4%/3.5% of deforestation is found with the observations/ ordered algorithm/ CLUE-S algorithm from 2001 to 2016. The lulcc R predicts that respectively 3.6% and 5.6% of forest area will be lost from 2016 to 2030, using the ordered algorithm and the CLUE-S algorithm

Table 5.10 The pixels of land cover allocated in SAN REGIS

	Observation		Ordered model		CLUE-S model	
	2001	2016	2016	2030	2016	2030
Forest	2607	2489	2522	2400	2516	2349
Shrub	198	313	276	372	271	437
C4grass	264	251	296	314	283	283
C3grass	591	607	584	595	591	593
Crop	27	29	9	9	27	27
Bare soil	6	4	6	3	5	4
Others	23	23	23	23	23	23

5.4 Conclusions

I explored the use of the open source land use change model, lulcc R, to allocate historic and predict future land cover change in Ecuador and Perú. The model was set and validated with the current available land use map from 2001 to 2016. Deforestation is identified as the major change in the tropical Andes, with the forest having a high potential to be transferred to shrub. The modelling results of lulcc R indicate that most of the changes could be detected under the resolution (0.25 degree) projected to be used in the JULES model. However, some forest area was simulated as C3/C4 grasses rather than shrub as indicated by the observed land cover maps. The simulated land cover changes were further assessed at a basin scale. The major type of land cover is correctly allocated in the selected basins. In the basins mainly covered by C3 grasses, there is a low potential to be changed to forest or other land cover types. For the forest dominated catchments, continuous deforestation is detected, and the historic change could be estimated reasonably well. The model has detected continuous land cover change of over the past observations and based on these trends makes predictions on the location of future changes. These predications can be embedded in the hydrological model in cases where an up-to-date land cover map is not available, as well as to make predictions about future change.

6 Hydrological assessment of land-use impacts on the basin scale using JULES

6.1 Introduction

Land use and land cover change (LUCC) is a major driver of changes in the hydrological cycle. Hydrological processes, including transpiration (Zhang, Walker & Dawes, 1999), infiltration, interception (Le Maitre, Scott & Colvin, 1999), and an overall change in streamflow are observed when the land cover is changed. Deforestation is the major type of LUCC worldwide (Borrelli et al., 2017; Turner, B. L., Meyer & Skole, 1994). The Andean region is one of the hotspots of deforestation. Therefore, the impacts on hydrological responses need to be studied because of its important role in regional water supply and vulnerability to human activities (Buytaert et al., 2006).

In this chapter, the LUCC impacts are investigated systematically by using the JULES model. The geographical focus is on the Andes of Ecuador and Perú, which covers an area of 1.57 million km^2. In this area, forest area has decreased by 28186 km^2 (1.80% of total area) between 2001 and 2016,which was identified by using MODIS Land Cover Type (MCD12Q1) Version 6 data (Friedl & Sulla-Menashe, 2015).

The hydrological fluxes are simulated using the JULES model, which is a model that is increasingly used for hydrological assessment (Le Vine et al., 2016; Zulkafli et al., 2013). It has the advantage that it represents the physical processes using physically meaningful parameters, which can be adjusted to assess the impacts of LUCC. It is not commonly used in tropical regions due to the data requirement to represent detailed hydrological processes (Buytaert, Célleri & Timbe, 2009; Célleri & Feyen, 2009). A relevant study was carried out in Peruvian Andes–Amazon (Zulkafli et al., 2013), which suggested reasonable river flow simulation in four selected humid tropical mountain

basins using the JULES model. However, the study also highlightedremining discrepancies between the simulated and observed flow. In particular, the study identified an insufficient baseflow estimation, an underestimated evapotranspiration rate, and an absence of dry-season flow (MacKellar et al., 2013), which are issues still needed to be addressed.

The main purpose of this research is twofold. The first aim is to improve the current regional hydrological modelling setup of JULES by using the citizen science generated soil and land cover information that were introduced earlier in this thesis. The simulated flow is evaluated by monitoring data in 17 selected basins distributed over the Andes. Subsequently, the regional JULES model is used to assess the impacts of LUCC on the regional hydrology. The potential hydrological impacts as a result of deforestation are evaluated.

6.2 Methods

6.2.1 The regional JULES setup

The JULES model has been initialised at a resolution of 0.25° over a geographical region that covers the area of Ecuador and Perú (1.57 million km^2). The required time series of meteorological data, downward short-wave and long-wave radiation, temperature, specific humidity, wind speed, and surface pressure, were extracted from a globally available reanalysis dataset, i.e. the NCEP-DOE Reanalysis II data (Kanamitsu et al., 2002) from 2001 to 2016. The data were disaggregated to 0.25° from its original scale of 2.0° on the T62 Gaussian grid. The dataset comes at a 6-hourly temporal resolution and covers the time period of 1979/01 up-to-date. Precipitation data was obtained from a remote sensing product TRMM_3B42.7 (Huffman et al., 2007), which provides a higher spatial resolution (0.25° scales),temporal resolution (3-hourly), and better hydrological simulation (Zulkafli et al., 2013) than the NCEP-DOE Reanalysis II data.

The land cover was obtained from the Terra and Aqua combined Moderate Resolution Imaging Spectroradiometer (MODIS) Land Cover Type (MCD12Q1) Version 6 data (Friedl & Sulla-Menashe, 2015). The 17 IGBP land cover classes were reclassified to the 10 land-use type used in JULES according to Table 6.1 (Houldcroft et al., 2009). This linear mapping algorithm has been developed to represent for the variation in land cover, (Dunderdale, Muller & Cox, 2000).

Model performance was evaluated using two soil parameter sets. The first one is the most commonly used ‘pedotransfer function’ approach, which derives the soil parameters using the global soil textural fractions (percentage of sand, silt and clay), and chemical properties (pH, DBD, SOC, CEC) from the Harmonized World Soil Database version 1.21 (Fao/Iiasa/Isric/Isscas/Jrc, 2012). The second parameters set

uses modified soil parameters, in which the Van Genuchten parameters (n, α) are obtained from the experimental data obtained from Buytaert et al. (2005). This setup gives a higher estimation of the critical point, which reduces transpiration and consequently generates more subsurface runoff, which improves the hydrological simulation at the catchment scale (see Chapter 3). For the modified soil parameters, only Leptosols, Cambisols, Andosols, and Phaeozems were modified as these soil types were examined with iMHEA observation (Chapter 3) and the changing water retention properties shown improving performance for these soil types.

Table 6.1 Mapping of IGBP into fractions of JULES surface types (%).

IGBP description	BF	NF	C3	C4	SH	Crop	Urban	Water	Bare Soil	Ice
EN forest	0.0	69.4	22.2	0.0	0.0	0.0	0.0	0.0	8.4	0.0
EB forest	85.9	0.0	0.9	7.0	0.0	0.0	0.0	0.0	6.2	0.0
DN forest	0.0	65.3	25.6	0.0	0.0	0.0	0.0	0.0	9.1	0.0
DB forest	62.3	0.0	7.0	8.9	3.7	0.0	0.0	0.0	18.1	0.0
Mixed forest	35.5	35.5	20.8	0.0	0.0	0.0	0.0	0.0	8.2	0.0
Closed shrub	0.0	0.0	25.0	0.0	60.0	0.0	0.0	0.0	15.0	0.0
Open shrub	0.9	0.0	3.1	14.7	34.1	0.0	0.0	0.0	47.2	0.0
Woody savannah	50.0	0.0	15.0	0.0	25.0	0.0	0.0	0.0	10.0	0.0
Savannah	20.0	0.0	0.0	75.0	0.0	0.0	0.0	0.0	5.0	0.0
Grassland	0.0	0.0	65.9	15.7	4.9	0.0	0.0	0.0	13.5	0.0
Permanent wet	2.2	0.0	80.8	0.0	1.4	0.0	0.0	15.0	0.6	0.0
Cropland	0.0	0.0	0.0	0.0	0.0	79.6	0.0	0.0	20.4	0.0
Urban	0.0	0.0	0.0	0.0	0.0	0.0	100.0	0.0	0.0	0.0
Crop	2.5	2.5	27.5	7.5	5.0	45.0	0.0	0.0	10.0	0.0
Snow/ice	0.0	0.0	0.0	0.0	0.0	0.0	0.0	0.0	0.0	100.0
Barren	0.0	0.0	0.0	0.0	0.0	0.0	0.0	0.0	100.0	0.0
Water bodies	0.0	0.0	0.0	0.0	0.0	0.0	0.0	100.0	0.0	0.0

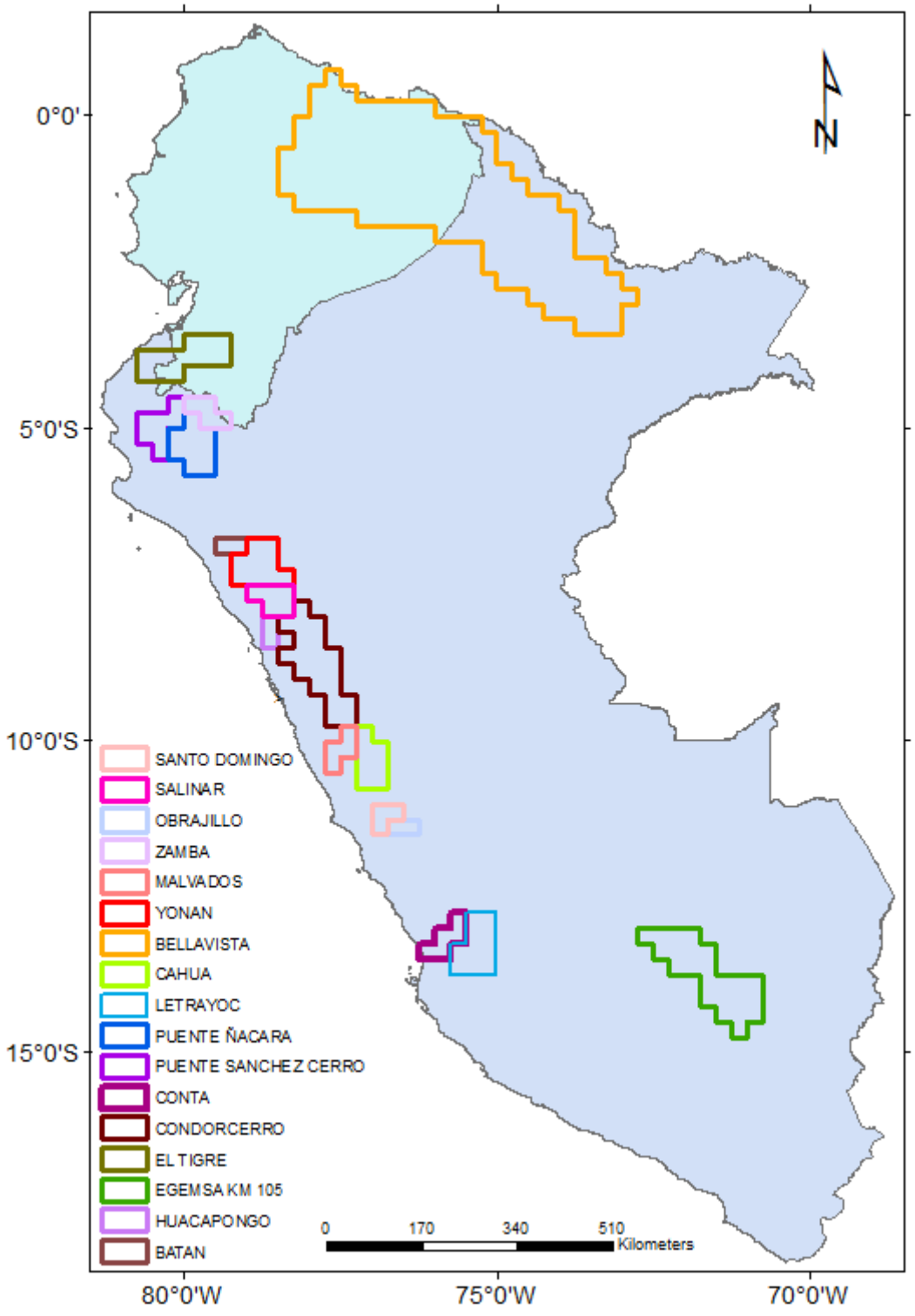

Figure 6.1 The boundary of JULES setup and the 17 catchments selected for validation

6.2.2 Assessing the basin hydrology

In this chapter, the JULES model was extended beyond the represented land covers in the iMHEA sites to broader basin scale in Andes of Ecuador and Perú. The modelling flow was evaluated with the observation in 17 selected basins (Figure 6.1) delineated using the HydroBASINS data (Lehner, Verdin & Jarvis, 2008; Lehner & Grill, 2013). Observed streamflow are available from the Sistema Nacional de Información de Recursos Hídricos (Autoridad Nacional del Agua, 2019) in Perú, and are described in Table 6.2.

As JULES does not have an integrated routing function, the simulated subsurface and surface flow was routed using a simple delay function:

$$\mathrm{Q}_{sim,t} = \sum_{i=1}^{n} \left(Q_{surface,t-t_{i1}} + Q_{subsurface,t-t_{i2}} \right) ; t_{i1} = \frac{d_i}{C_1} ; t_{i2} = \frac{d_i}{C_2}$$

in which the flood wave velocity C1 was set to 1.0 m/s (fast response catchment) and 0.25 m/s (slow response catchment) for surface flow, and a fixed value of 0.25 m/s for subsurface flow, according to the Monte Carlo optimisation implemented previously for the Peruvian Andes–Amazon (Zulkafli et al., 2013). For each pixel, d_i marks the distance to the outlet of basin. The lag time t_i is calculated accordingly. The modelling performance was assessed with hydrological indices RR for the water yield, BFI for the baseflow, and Nash–Sutcliffe model efficiency (NSE) for the overall performance (as described in section 2.2.7).

Table 6.2 Overview of the hydrometric stations used for validation.

Station	River	Coordinates		Elevation	Area (km^2)	Period of available data	Dominate soil	Land cover
BELLAVISTA		-73.085	-3.488	110	100676.5	1998-2013	Gleysols, Cambisols	BF
EL TIGRE	Tumbes	-80.457	-3.769	44	4792.6	1963-2019	Leptosols	BF, C4
ZAMBA	CANAL QUIROZ	-79.900	-4.667	585	2171.6	2011-2019	Cambisols	C4
SALINAR	Chicama	-78.967	-7.667	350	3800	1950-2016	Leptosols, Cambisols	C3, C4
PUENTE ÑACARA	Piura	-80.170	-5.110	119	4733.7	2014-2019	Cambisols, Arenosols	C3, C4
PUENTE SANCHEZ CERRO	Piura	-80.617	-5.183	23	7571	1925-2018	Cambisols, Arenosols	C3, C4
BATAN	Zaña	-79.289	-6.803	246	738.5	2016-2019	Leptosols	C3, C4, BF
YONAN	Jequetepeque	-79.100	-7.250	428	3509.3	2001-2019	Leptosols, Regosols	C3, C4
HUACAPONGO	VIRU	-78.667	-8.383	280	958.2	2014-2017	Leptosols, Regosols	C3, CR
CONDORCERRO	Santa	-78.250	-8.650	450	10540	1977-2019	Leptosols, Regosols	C3
MALVADOS		-77.628	-10.336	1071*	1545.3	2000-2017	Leptosols	C3
CAHUA	Pativilca	-77.224	-10.547	3518*	3134.1	2000-2019	Leptosols	C3
SANTO DOMINGO	Chancay - Huaral	-77.028	-11.370	620	1870.5	1921-2017	Leptosols, Regosols	C3, BS
OBRAJILLO	Chillón	-76.622	-11.453	2,706	452.4	1968-2019	Leptosols, Regosols	C3
CONTA	SAN JUAN	-75.975	-13.439	324	3161	2011-2019	Leptosols, Regosols	C3
LETRAYOC	Pisco	-75.720	-13.640	756	3120.1	2011-2019	Leptosols, Regosols	C3
EGEMSA KM 105	Vilcanota	-72.533	-13.183	2,302	9712.1	1985-2019	Regosols	C3

6.2.3 Assessing LUCC impacts on regional hydrology

The impacts of LUCC on the catchment hydrological response were assessed using the JULES model. First, the flow was modelled under the land cover map in 2016 to represent for the current state of hydrology. A comparative simulation was setup subjected to a land cover map in 2001. The comparison indicated the change in flow under LUCC between the 2001 and the 2016 land use scenario. Subsequently, scenario analysis was carried out between land use scenarios for resp. 2016 and 2030 to predict the potential change of river flow. For this, the land cover maps simulated by lulcc R (CLUE-S) were used. The modelling results were further compared in SAN REGIS basin to assess the basin hydrology subjected to deforestation.

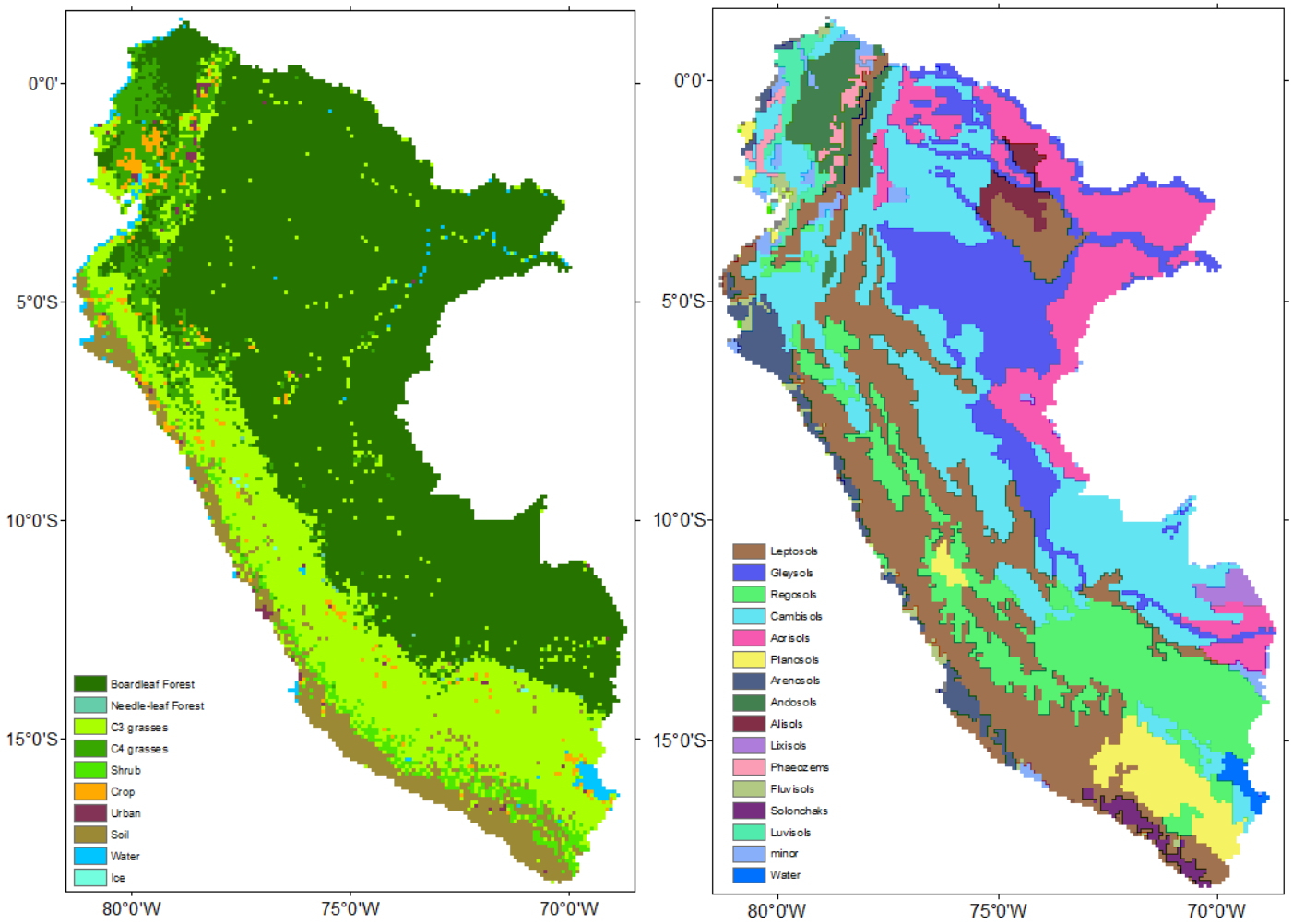

Figure 6.2 The a) land cover and b) dominant soils in the study area

Table 6.3 The distribution of dominant soil types

Soil type	Percentage
Leptosols	22.91%
Cambisols	22.52%
Regosols	13.28%
Gleysols	12.59%
Acrisols	11.60%
Planosols	4.20%
Andosols	3.46%
Arenosols	2.86%
Luvisols	1.38%
Alisols	1.19%
Fluvisols	1.19%
Solonchaks	0.84%
Phaeozems	0.69%
Lixisols	0.59%
Minor class	0.69%

6.3 Results and discussion

6.3.1 The effects of modifying soil parameters

The region is mainly covered by forest, following by C3/C4 grasses, and bare soil along the coast and urban areas (Figure 6.2a). Soils were classified as shown in Figure 6.2b. Table 6.3 shows that Leptosols, Cambisols, Regosols, Gleysols are the dominated soil types in this region.

First, I evaluated the impact of changing the soil parameters from the regional Van Genuchten parameters to the use of the locally modified soil parameters (Figure 6.3; see Chapter 3). Figure 6.4 shows that the use of locally modified soil parameter values increases the flow up to 305.8 mm/year compared to the default PTFs parameters.

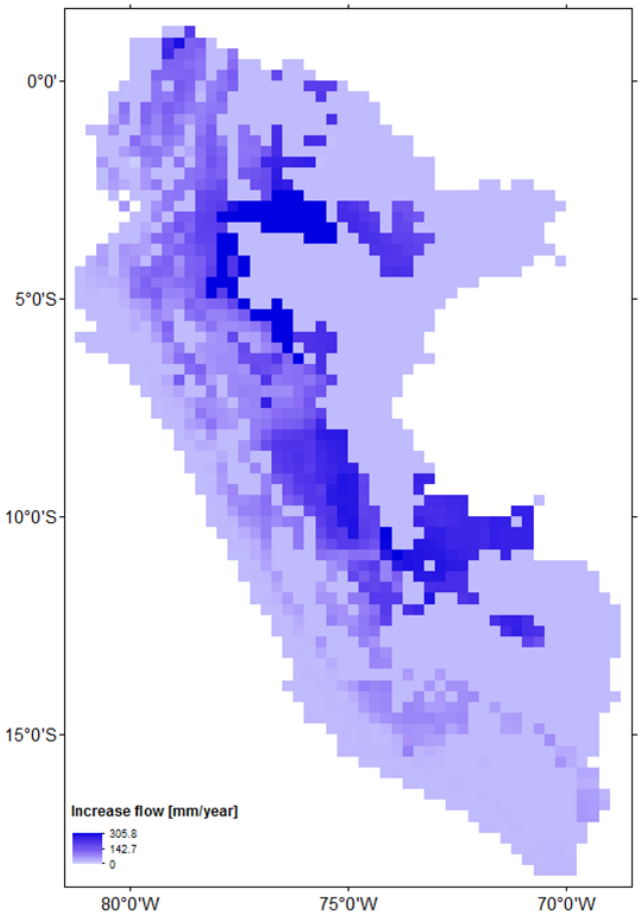

Figure 6.3 The difference in annual flow between the regional van Genuchten parameters and the locally modified soil parameters

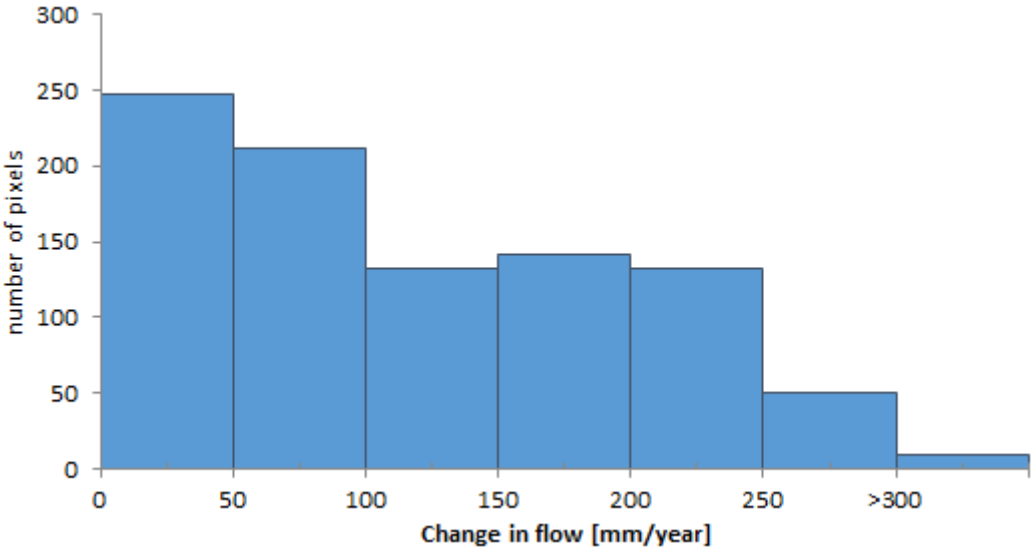

Figure 6.4 Histogram of the change in flow under the modified soil parameters

The modelled flow was further evaluated with the observation in 17 selected basins (Table 6.4). As shown in Figure 6.5, the modified soil parameters increase the water yield in EL TIGRE by 23 %. The increase of the flow is more significant in the dry season, as the BFI increased from 0.42 to 0.60 with the modification. The rainfall-runoff ratio is considerably increased. BELLAVISTA (Figure 6.6) is a wider forest covered catchment dominated by similar soil types. The simulated flow is lower than the observation, but the modified parameters result in simulated flow that is closer to the observed flow values. The higher model performance (NSE: 0.47 vs 0.33) is reflected in the good agreement between the BFI values (modelled: 0.89, observation: 0.92).

Four páramo covered catchments, ZAMBA, SALINAR, PUENTE ÑACARA, and PUENTE SANCHEZ CERRO, are classified with the same soil parameters as the dominant soil type in iMHEA site PIU. Doing so increases the model performance in ZAMBA (Figure 6.7) and SALINAR (Figure 6.8) as the modified soil parameters generated higher runoff.

The 11 catchments distributed in the Peruvian Andes have soils that are classified as Leptosols and Regosols, which is the same as the dominated soil type in iMHEA site HUA/HMT. The modelling results (Figure 6.11 - Figure 6.21) also show a noticeable improvement on the runoff generation compared to the use of the standard Van Genuchten parameters. The major gap in the hydrographs can be attributed to the uncertainties in the observations of both precipitation and streamflow. The deficiency in the observed precipitation and streamflow data is reflected in the rainfall-runoff ratio, which is as high as 1.32 in the EL TIGRE basin and far higher than the typical value in the range of 0.6 – 0.7 for the tropical environment (Zulkafli et al., 2013). Most likely this shows that the TRMM precipitation data still underpredict the precipitation in mountain areas, which can be attributed to the highly variable topography and mountain precipitation process such as orographic rainfall, which are not well captured in TRMM observations.

The modelling results in the selected basins show that the baseflow could be effectively generated by using the modified soil parameters, resulting in more precise flow estimates.

Table 6.4 The modelling results of the regional JULES. MODi: modelled flow with PTFs soil data; MODm: modelled flow with modified soil parameters; RR0/RR1/RR2: rainfall-runoff ratio of obs/MODi/MODm BFI0/BFI1/BFI2: baseflow index of obs/MODi/MODm; NSEi/NSEm: Nash–Sutcliffe model efficiency of MODi/MODm.

Station	Rainfall		OBS	MODi	MODm	RR0	RR1	RR2	BFI0	BFI1	BFI2	NSEi	NSEm
	[mm]	[m^3/s]	[m^3/s]	[m^3/s]	[m^3/s]								
EL TIGRE	937.9	142.1	187.6	50.9	62.5	1.32	0.36	0.44	0.73	0.42	0.6	0.15	0.16
BELLAVISTA	2891.9	9207.0	7269.6	5858.2	6162.4	0.79	0.64	0.67	0.92	0.85	0.89	0.33	0.47
ZAMBA	914.4	62.8	50.2	26.0	35.0	0.80	0.41	0.56	0.68	0.41	0.61	0.07	0.26
SALINAR	376.0	45.2	17.9	10.7	14.9	0.40	0.24	0.33	0.71	0.4	0.61	0.28	0.40
PUENTE ÑACARA	404.4	60.5	23.0	14.4	18.8	0.38	0.24	0.31	0.62	0.29	0.50	0.38	0.41
PUENTE SANCHEZ CERRO	544.6	130.4	96.8	31.4	38.2	0.74	0.24	0.29	0.66	0.33	0.50	0.35	0.36
BATAN	438.3	10.2	9.2	2.2	3.3	0.90	0.22	0.32	0.73	0.27	0.55	-0.08	0.01
YONAN	586.2	65.1	41.2	18.0	24.4	0.63	0.28	0.37	0.65	0.38	0.59	0.19	0.31
HUACAPONGO	304.1	9.2	2.2	1.7	2.3	0.24	0.18	0.25	0.55	0.28	0.52	0.15	0.21
CONDORCERRO	918.8	306.3	150.4	136.9	157.5	0.49	0.45	0.51	0.8	0.52	0.62	-0.13	-0.09
MALVADOS	337.6	16.5	6.3	4.2	5.7	0.38	0.26	0.35	0.74	0.36	0.58	0.17	0.33
CAHUA	684.1	67.8	41.9	24.1	31.1	0.62	0.35	0.46	0.82	0.48	0.64	-0.12	0.16
SANTO DOMINGO	446.7	26.4	23.1	7.5	10.8	0.87	0.29	0.41	0.78	0.40	0.62	-0.12	0.09
OBRAJILLO	533.1	7.6	6.8	2.4	3.6	0.90	0.32	0.47	0.80	0.41	0.64	-0.58	-0.15
CONTA	370.6	37.0	18.0	11.1	14.7	0.49	0.30	0.40	0.59	0.51	0.67	0.46	0.47
LETRAYOC	459.2	45.3	31.4	14.3	19.2	0.69	0.31	0.42	0.62	0.46	0.65	0.35	0.37
EGEMSA KM 105	1006.8	309.2	133.9	89.3	102.1	0.43	0.29	0.33	0.83	0.43	0.56	0.38	0.46

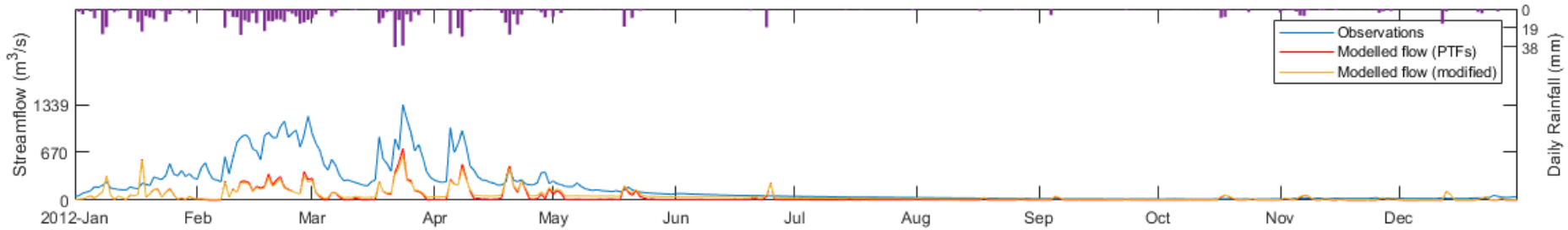

Figure 6.5 The regional modelling results in EL TIGRE

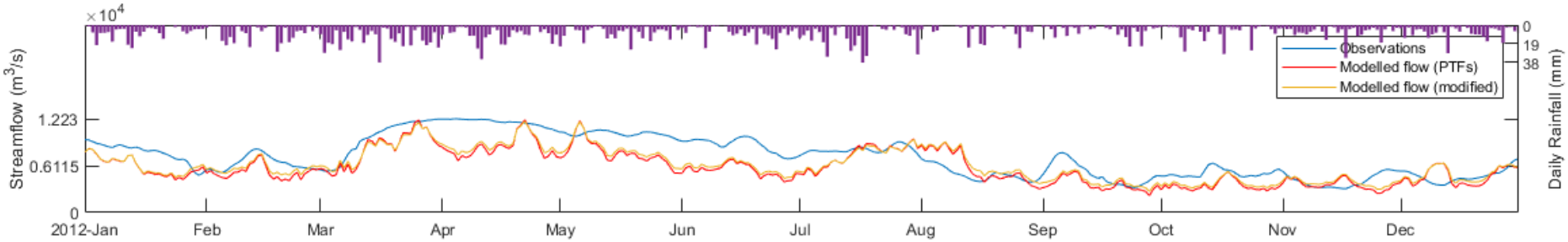

Figure 6.6 The regional modelling results in BELLAVISTA

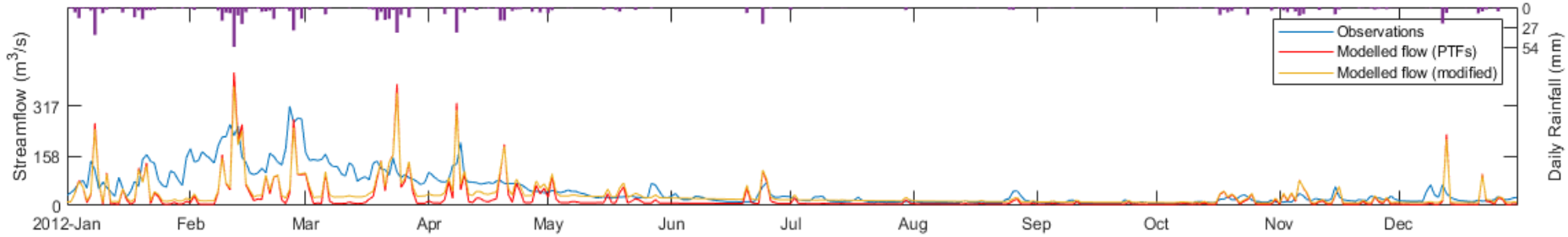

Figure 6.7 The regional modelling results in ZAMBA

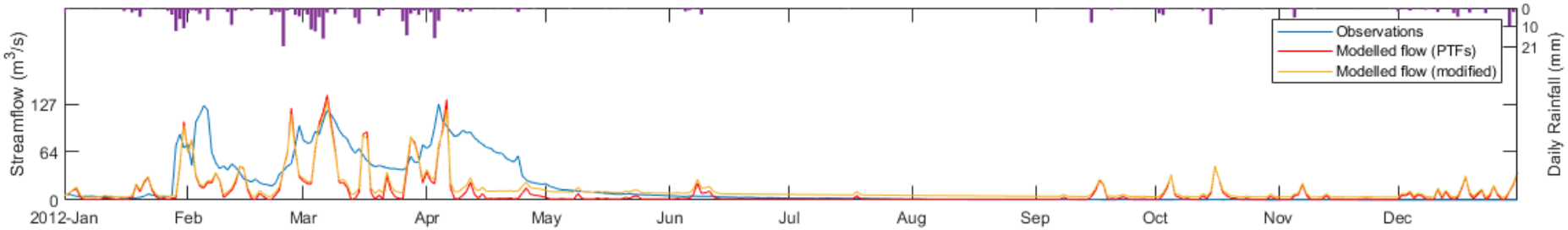

Figure 6.8 The regional modelling results in SALINAR

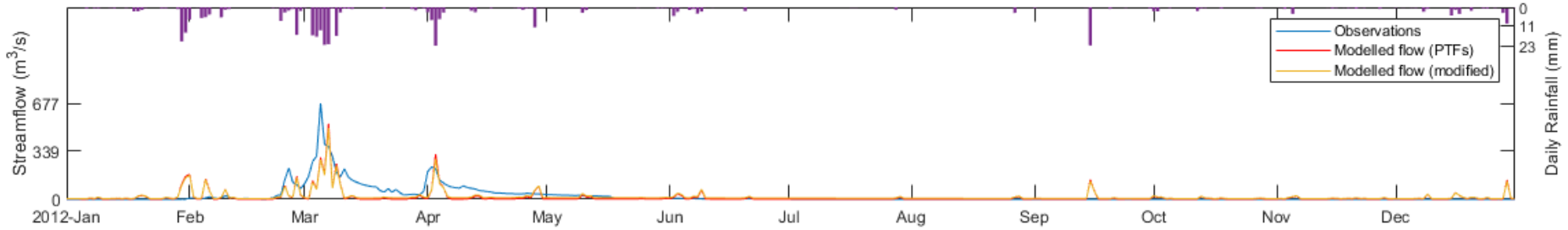

Figure 6.9 The regional modelling results in PUENTE ÑACARA

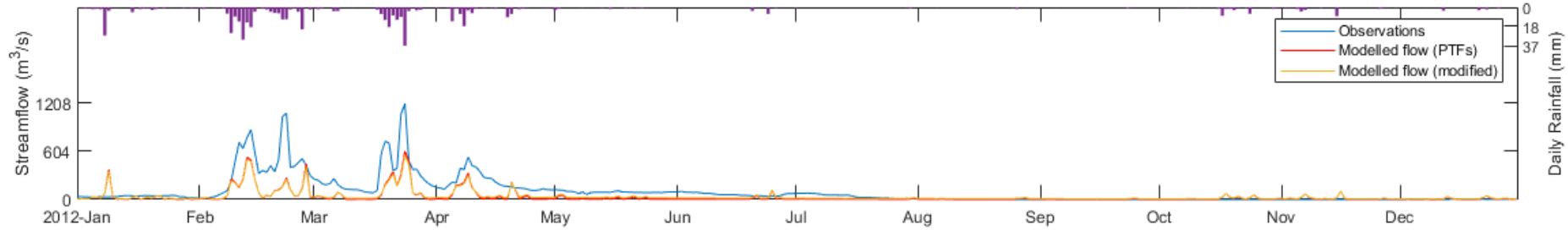

Figure 6.10 The regional modelling results in PUENTE SANCHEZ CERRO

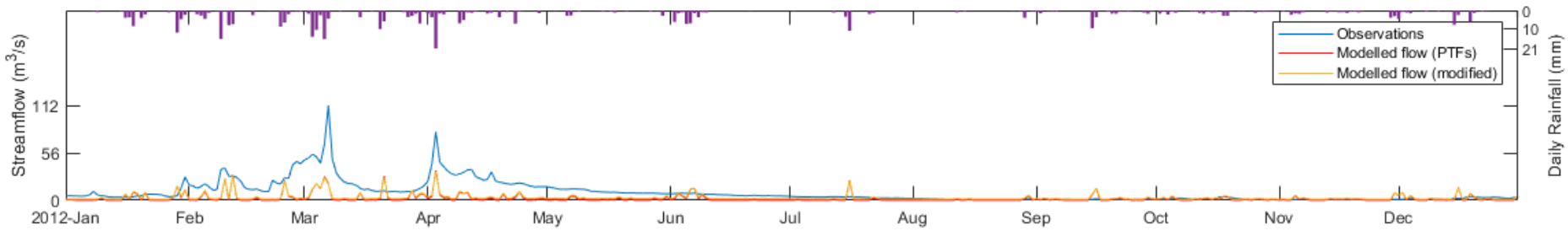

Figure 6.11 The regional modelling results in BATAN

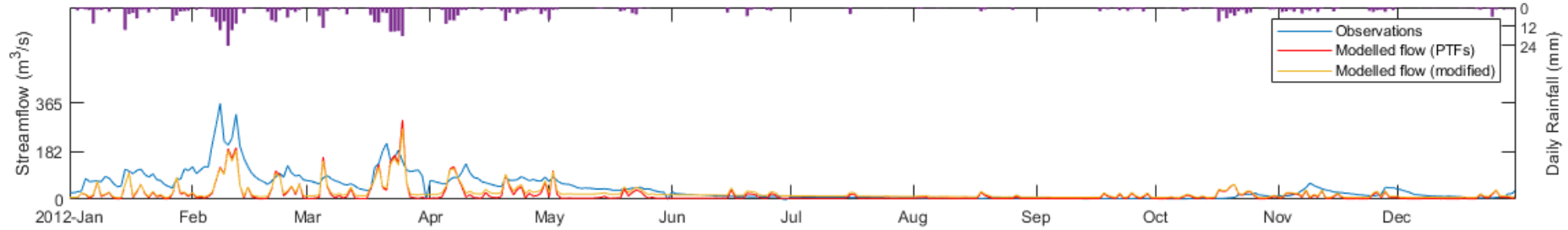

Figure 6.12 The regional modelling results in YONAN

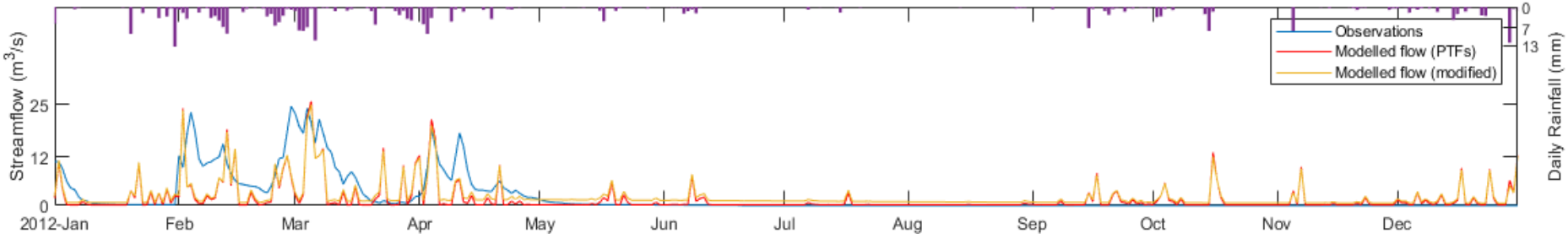

Figure 6.13 The regional modelling results in HUACAPONGO

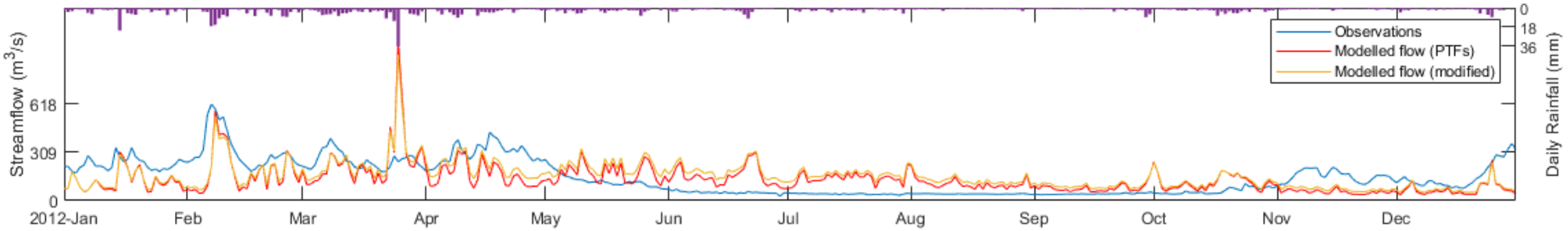

Figure 6.14 The regional modelling results in CONDORCERRO

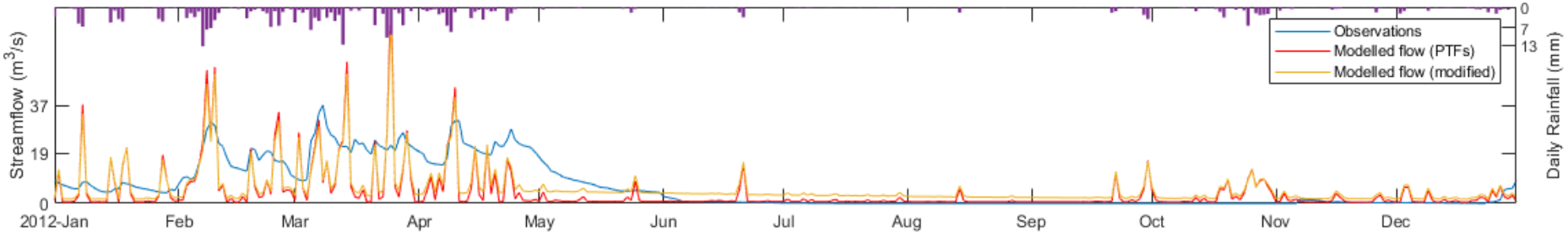

Figure 6.15 The regional modelling results in MALVADOS

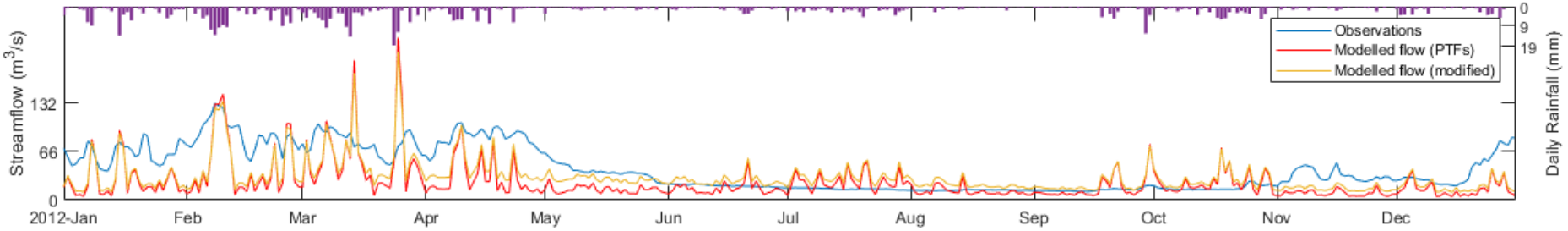

Figure 6.16 The regional modelling results in CAHUA

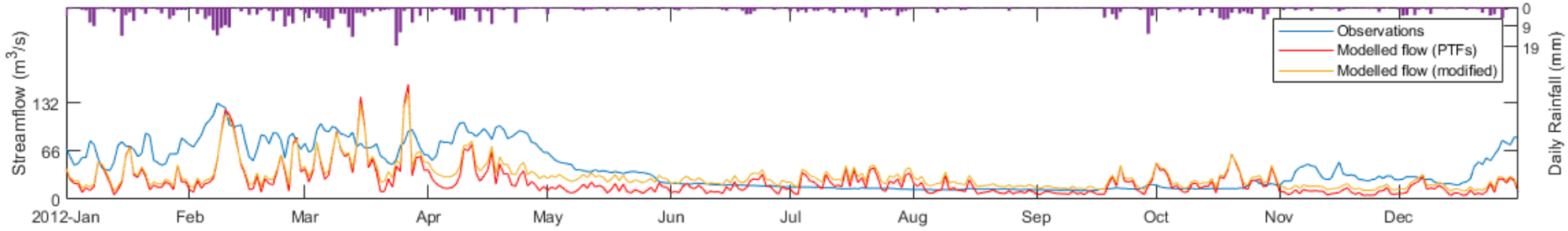

Figure 6.17 The regional modelling results in SANTO DOMINGO

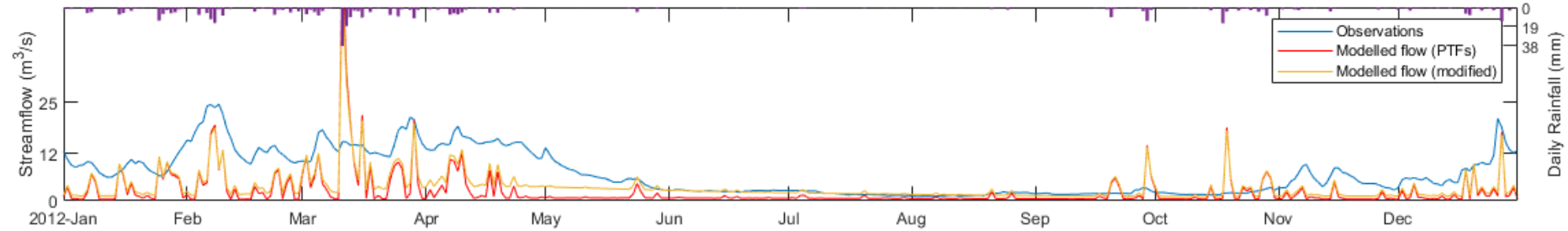

Figure 6.18 The regional modelling results in OBRAJILLO

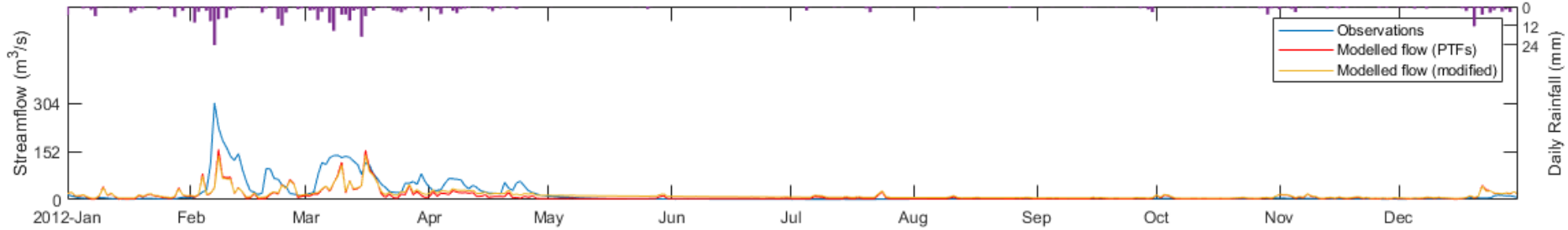

Figure 6.19 The regional modelling results in CONTA

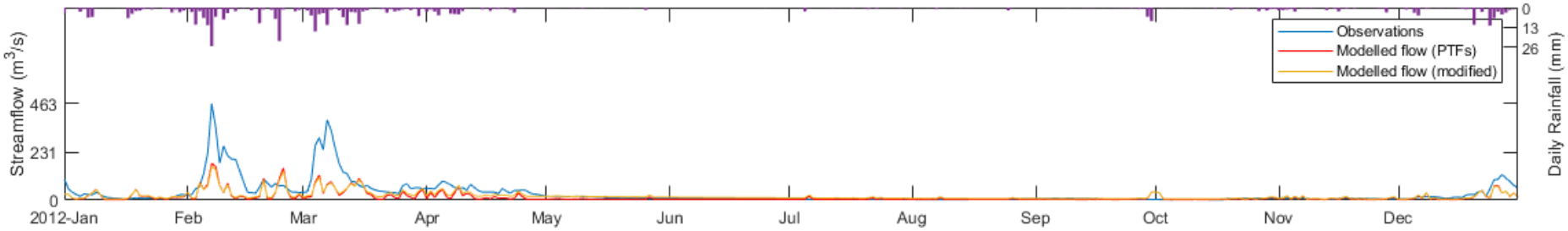

Figure 6.20 The regional modelling results in LETRAYOC

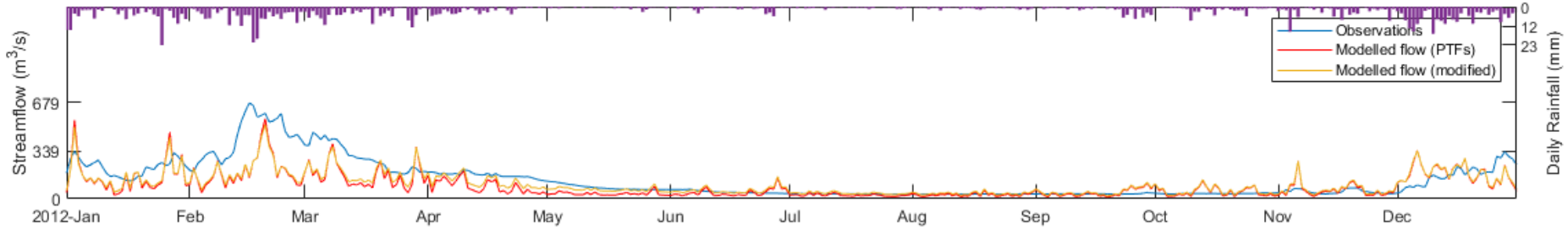

Figure 6.21 The regional modelling results in EGEMSA KM 105

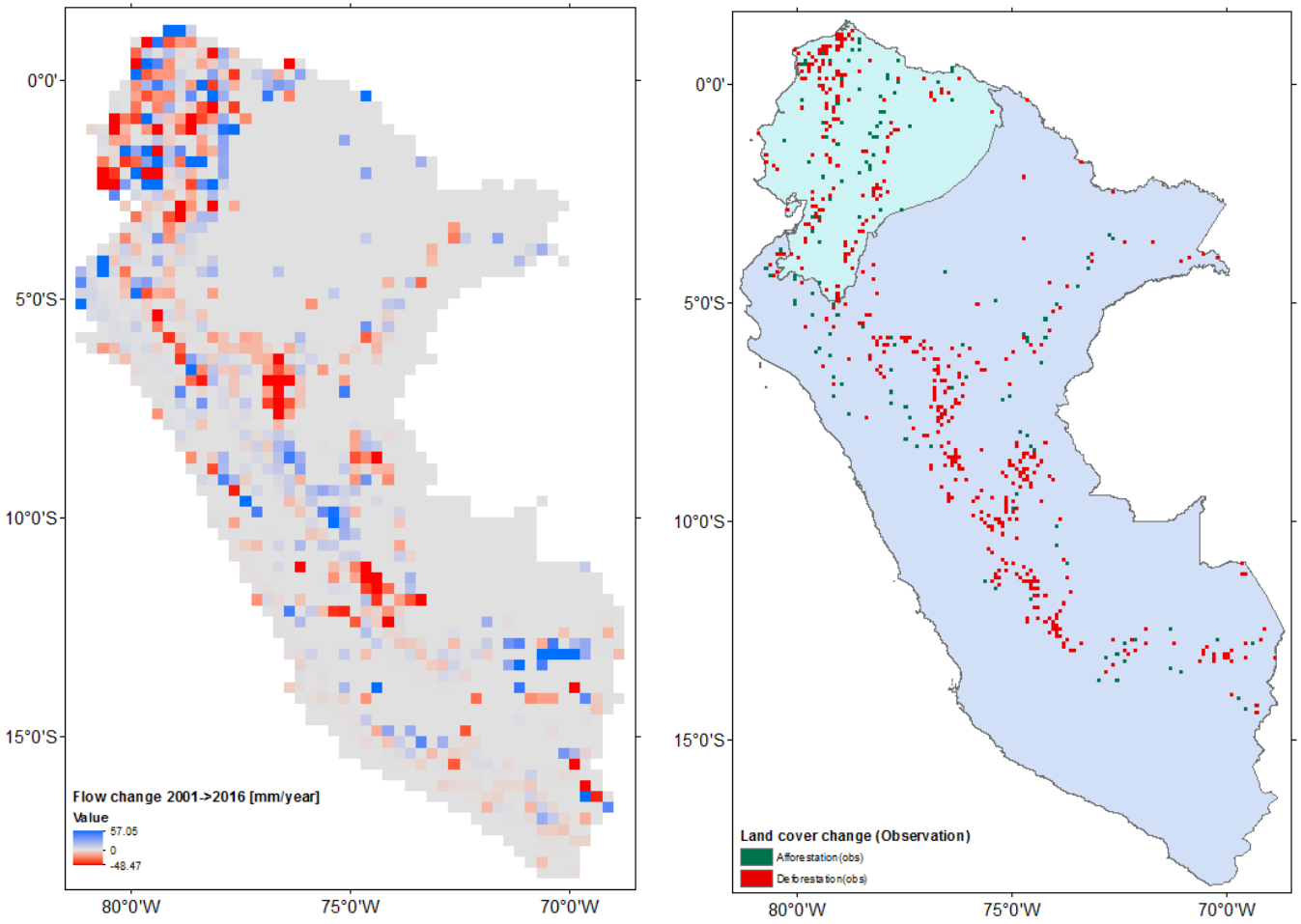

Figure 6.22 a) The change of annual runoff between the 2001 and the 2016 land cover b) Land cover change between 2001 and 2016

6.3.2 LUCC impacts on regional hydrology

The change in annual runoff was assessed in individual grid cells between the 2001 and the 2016 land use scenarios. Overall, 8.2% of land cover has been changed. Deforested areas have been mainly transformed to shrub and grasses (Table 5.3). Figure 6.22 shows that the change of annual runoff with the map indicated location of LUCC. The change in annual runoff ranges between +57.1 mm and -48.5 mm. The majority of the pixels experiences changes of less than 5 mm (Figure 6.23). The LUCC impacts on hydrology are strongly depended on the interaction with soil properties (see Chapter 4.2.2). No consistent change can be observed with the occurrence of deforestation, or afforestation between 2001 and 2016.

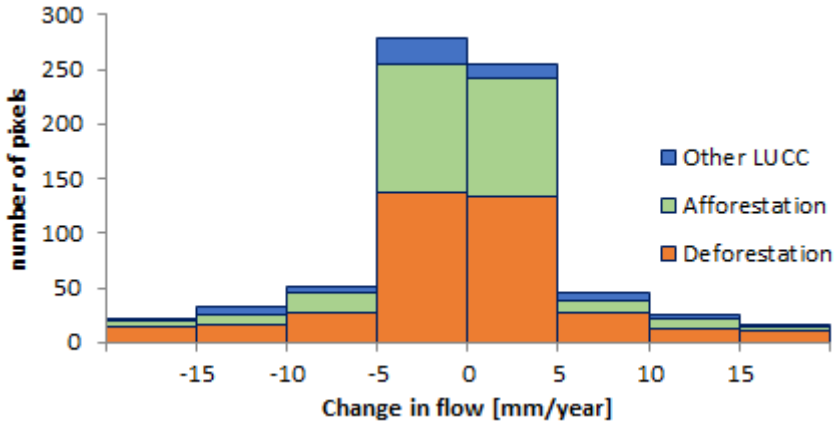

Figure 6.23 Histogram of the change in runoff [mm/year] for individual pixels between the 2001 and the 2016 land cover scenario subjected to deforestation.

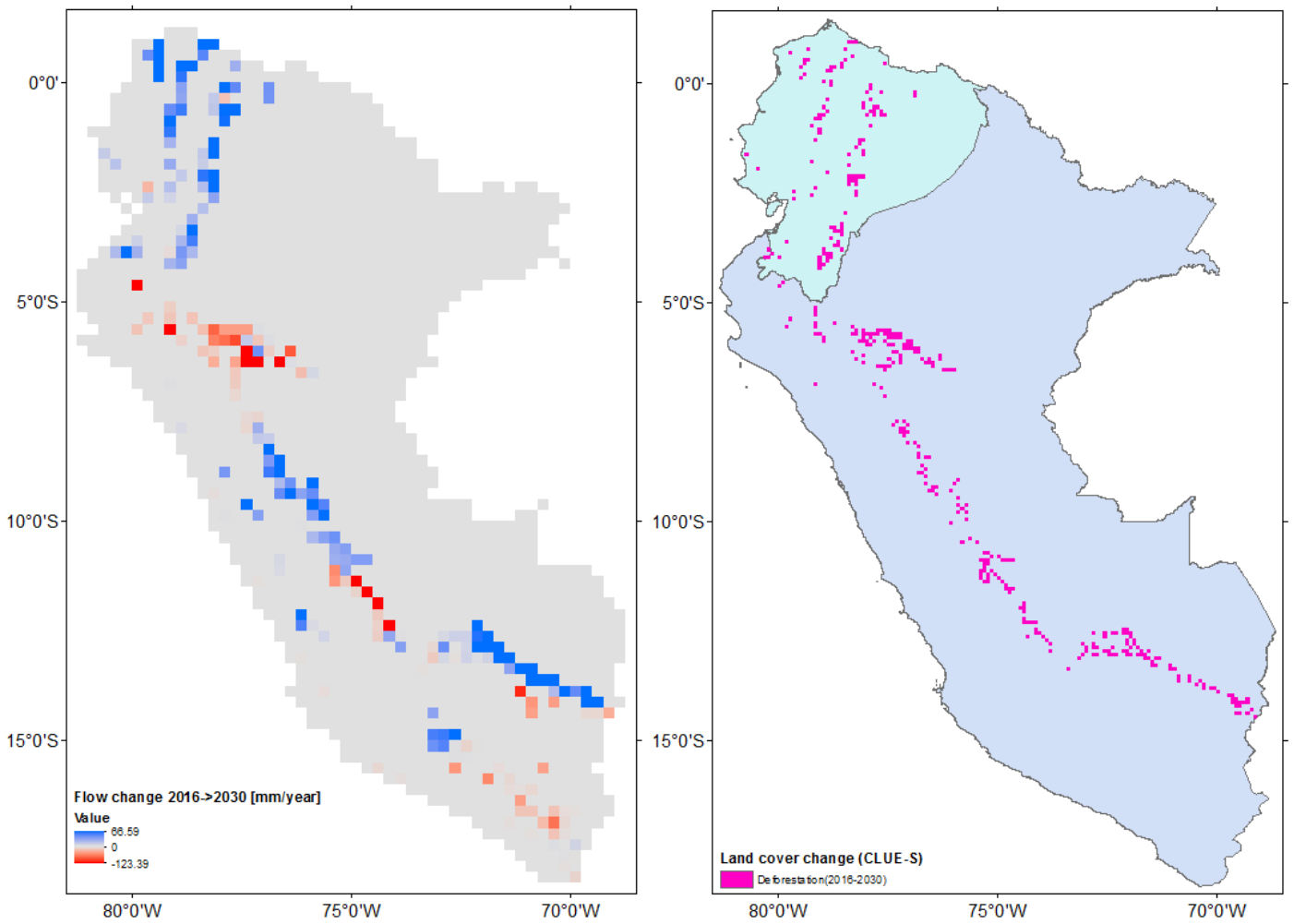

Figure 6.24 a) The change of annual runoff between 2016 and 2030 land cover b) Land cover change between 2016 and 2030

In Figure 6.24, the potential change of flow between 2016 and 2030 land use scenario was assessed with using land cover map simulated by lulcc R (CLUE-S). The change in runoff ranges between -123.4 mm/year and +66.6 mm/year when 3.7% of forest was transformed to shrub. In which, increasing runoff was observed in 61.4% of grid cells (Figure 6.25). The modelling result of JULES shows that LUCC impacts could be effectively detected by changing the land cover parameters (see Chapter 4).

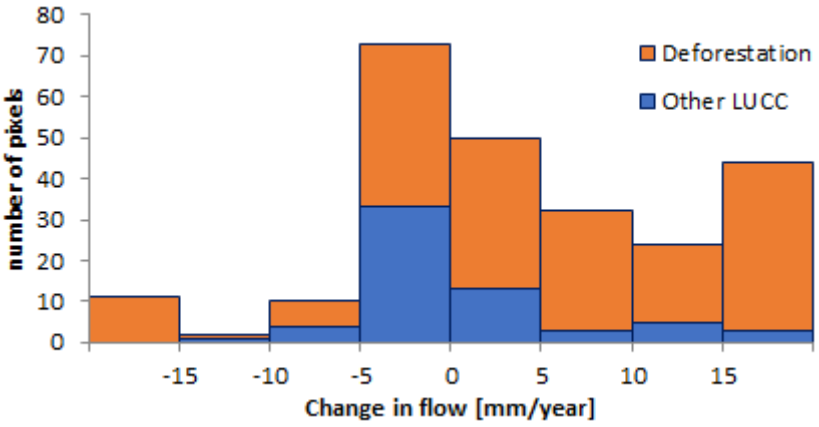

Figure 6.25 Histogram of the change in runoff [mm/year] between the 2016 and 2030 land cover scenarios.

6.4 Conclusions

In this chapter, the JULES model was implemented for the tropical Andes of Ecuador and Perú for hydrological assessment under a range of hydrological responses. The modelled flow was validated in 17 selected basins. The major gap between the simulation and observation can be attributed to the uncertainty in precipitation data as the rainfall-runoff ratio between the observed flow and TRMM precipitation ranges from 0.24 to 1.32, which results in clearly unrealistic values in several basins.

The initial simulation with the soil parameters generated by using the pedotransfer functions generally underestimates the baseflow generation. This can be improved effectively by modifying the soil parameters. The increased value of critical point estimates more accurately the water yield and baseflow ratio. The runoff volume is also increased by using the modified soil parameters. Overall, the modelled rainfall-runoff ratio increases from [0.27-0.62] to [0.37-0.67] and is closer to the observation in most catchments. The modelling results captured most of the hydrological response, which is reflected in increased NSE values.

The regional JULES model shows a potential to be used to assess the hydrology changes under long-term land use and land cover change. JULES is capable to simulate flow under various types of land cover. However, the LUCC occurring over the 15-year period is less the 10% in regional scale. No consistent change can be observed for specific LUCC (e.g. deforestation). It is more effective to combine the soil properties to attribute these changes.

7 Conclusions

7.1 Summary of contributions to knowledge

The Andean region is a hotspot of hydrological change, which needs to be studied because of its important role in regional water supply and vulnerability to human activities. This PhD research explores the changing Andean hydrology under land-use and land cover changes by integrating citizen science data, a land surface model, and a land use change model. The research has mainly contributed to knowledge generation in the context of exploring the use of new data, improving the hydrological simulation by model parameterisation, and consequently using this model for hydrological impact assessment.

Land surface models are increasingly used for hydrological assessment, given their advantage to map the modeller's knowledge about the hydrological impacts of land-use and land-cover change into physically meaningful parameters. However, these processes are hard to be interpolated into a model due to the high data requirement to represent the hydrological processes of a catchment. The iMHEA citizen science network has extended the hydrological monitoring in the upper regions of the tropical Andes, which is a regional hotspot of water resources, and not well covered by the traditional monitoring networks. These new sources of data provide new opportunities for hydrological studies. In Chapter 2, hydrological data obtained with citizen science approach were used to simulate the hydrological fluxes under a variety of land use conditions. I found that hydrological estimation at the headwater catchment scale can be improved by using participatory data, which addressed substantially the highly uncertainty in the large-scale reanalysis rainfall data.

Given that the JULES model is originally developed for larger scale meteorological purposes, the required data for modelling are commonly derived from large scale data

base. These data may not well represent the local hydrological fluxes. In this research, I focused particularly on the LUCC impact on soil properties, and the energy exchange as altered by the land cover parameters. I focused on improving the model for hydrological evaluation by complimenting the commonly used soil parameterisation with local experimental data. In Chapter 3, the water retention properties obtained from pedotransfer functions were adjusted with data from in-situ experiments in similar catchments. This modification represents better the soil water storage, which increased the generation of subsurface flow significantly, and simulates better the local flow.

In Chapter 4, a comparative analysis is performed, in which JULES is used to assess the hydrology under land use impact. The analysis simulates LUCC as the only contributor to affect the flow generation while other influencing factors such as climate influences have been kept constant, which reduces the uncertainty of catchment characteristics and meteorological drivers. The results show that a loss of water regulation ability with lower water yield and higher level of peak flow could be found in the areas with human interventions of grazing, cultivation, and afforestation.

In Chapter 5, a land use change model, lulcc R, is used to simulate the land use and land cover changes in Ecuador and Perú. Deforestation is the major type of land cover change in the region. These changes of land cover are allocated statistically based on the environment and social-economic variables. I find that the simulated land use map can allocate the major patterns of land cover adequately. The model is able to detect the main trends in land cover change and uses them to predict the location of future changes. It generates a simulated land cover map specifically under the projected development scenario, which allows the potential hydrological changes to be assessed by a predictive hydrological model.

This research has explored the use of the JULES land surface model to simulate

the hydrological fluxes from site (i.e. headwater catchment), to basin, and regional scale. In Chapter 6, the JULES model is extended to the several Andean basins which are monitored by the national observation network of Perú. Also, at this larger scale the low baseflow simulated by regional estimates of soil property can be improved effectively by using modified soil data obtained in representative experimental basins in the region. However, uncertainties present in the precipitation data remain the main source of the imperfect fit between the model and observation. Nevertheless, a reasonable estimation can be simulated by using the JULES model. This opens an opportunity to explore the potential hydrological change under land-use impacts in larger Andean region.

7.2 Pathways for future research

In this PhD thesis, I explored the use of JULES land surface model to simulate the hydrological flux under specific land use conditions in the tropical Andes. The fluxes are modelled grid-to-grid. Therefore, a river routing scheme is required for a meaningful comparison with the monitored river flow. In this research, the simply delay function provides reasonable estimation regards of the effects of topography. In the groundwater-dominated Andean region, groundwater storage (e.g. using linear reservoir) could be used to partition the surface flow, subsurface flow, and the interflow which was not considered in this study.

I found that there is considerable gap between using PTFs and experiment data in Andean region. The use of experiment data had greatly improved the model in site scale. However, the experiment data covering boarder region is still insufficient. The JULES model has an advantage to collaborated with various field of studies. In which, the setup of JULES-crop is used to simulate the hydrology under cultivated lands instead of using the C3/C4 grasses setup. Currently, the predominant crop types (e.g. potato and tubers) in the study regions are not parameterized in the JULES-crop model. The simulated results using the current setup has resulted in low transpiration. Thus, this implied that crop parameterisation could improve the model further.

The precipitation input was considered as unchanged when subjected to LUCC. However, the results had shown considerably change of evapotranspiration under different LUCC condition. Thus, the changes in local precipitation and other micro-climate factors should be considered in the setup to estimate the potential hydrological changes more effectively. For the long-term predictive model, there are potential to assess the hydrology under certain climate change scenarios (e.g. raising temperature and rainfall products), which is not discussed in this thesis.

References

Autoridad Nacional del Agua. (2019) *Sistema Nacional de Información de Recursos Hídricos Visor de Estaciones Convencionales.* Available from: http://snirh.ana.gob.pe/visors2/ [Accessed 30th June 2019].

Barber, C. P., Cochrane, M. A., Souza Jr, C. M. & Laurance, W. F. (2014) Roads, deforestation, and the mitigating effect of protected areas in the Amazon. *Biological Conservation.* 177 203-209.

Beck, E., Makeschin, F., Haubrich, F., Richter, M., Bendix, J. & Valerezo, C. (2008) *The ecosystem (Reserva Biológica San Francisco).* Springer, Berlin, Heidelberg.

Best, M. J., Pryor, M., Clark, D. B., Rooney, G. G., Essery, R., Ménard, C. B., Edwards, J. M., Hendry, M. A., Porson, A. & Gedney, N. (2011) The Joint UK Land Environment Simulator (JULES), model description–Part 1: energy and water fluxes. *Geoscientific Model Development.* 4 (3), 677-699.

Borrelli, P., Robinson, D. A., Fleischer, L. R., Lugato, E., Ballabio, C., Alewell, C., Meusburger, K., Modugno, S., Schütt, B. & Ferro, V. (2017) An assessment of the global impact of 21st century land use change on soil erosion. *Nature Communications.* 8 (1), 2013.

Boysen, L., Brovkin, V., Arora, V. K., Cadule, P., de Noblet-Ducoudré, N., Kato, E., Pongratz, J. & Gayler, V. (2014) Global and regional effects of land-use change on climate in 21st century simulations with interactive carbon cycle. *Earth System Dynamics.* 5 309-319.

Bradley, R. S., Vuille, M., Diaz, H. F. & Vergara, W. (2006) Threats to water supplies in the tropical Andes. *Science.* 312 (5781), 1755-1756.

Breuer, L., Vache, K. & Frede, H. (2006) *Hydrogeochemical modelling framework Project V3.2.* Estacion Cientifica San Francisco. Project description.

Brown, A. E., Zhang, L., McMahon, T. A., Western, A. W. & Vertessy, R. A. (2005) A review of paired catchment studies for determining changes in water yield resulting from alterations in vegetation. *Journal of Hydrology.* 310 (1-4), 28-61.

Buytaert, W. (2004) *The properties of the soils of the south Ecuadorian páramo and the impact of land use changes on their hydrology.* (Doctoral dissertation, Katholieke Universiteit Leuven).

Buytaert, W. & Beven, K. (2011) Models as multiple working hypotheses: hydrological simulation of tropical alpine wetlands. *Hydrological Processes.* 25 (11), 1784-1799.

Buytaert, W., Célleri, R., De Bièvre, B., Cisneros, F., Wyseure, G., Deckers, J. & Hofstede, R. (2006) Human impact on the hydrology of the Andean páramos. *Earth-Science Reviews.* 79 (1-2), 53-72.

Buytaert, W., Célleri, R. & Timbe, L. (2009) Predicting climate change impacts on water resources in the tropical Andes: Effects of GCM uncertainty. *Geophysical Research Letters.* 36 (7).

Buytaert, W., Cuesta-Camacho, F. & Tobón, C. (2011) Potential impacts of climate change on the environmental services of humid tropical alpine regions. *Global Ecology and Biogeography.* 20 (1), 19-33.

Buytaert, W. & De Bièvre, B. (2012) Water for cities: The impact of climate change and demographic growth in the tropical Andes. *Water Resources Research.* 48 (8).

Buytaert, W., Iniguez, V. & De Bievre, B. (2007) The effects of afforestation and cultivation on water yield in the Andean páramo. *Forest Ecology and Management.* 251 (1-2), 22-30.

Buytaert, W., Wyseure, G., De Bievre, B. & Deckers, J. (2005) The effect of land-use changes on the hydrological behaviour of Histic Andosols in south Ecuador. *Hydrological Processes: An International Journal.* 19 (20), 3985-3997.

Buytaert, W., Zulkafli, Z., Grainger, S., Acosta, L., Alemie, T. C., Bastiaensen, J., De Bièvre, B., Bhusal, J., Clark, J. & Dewulf, A. (2014) Citizen science in hydrology and water resources: opportunities for knowledge generation, ecosystem service management, and sustainable development. *Frontiers in Earth Science.* 2 26.

Célleri, R., Buytaert, W., De Bièvre, B., Tobón, C., Crespo, P., Molina, J. & Feyen, J. (2009) *Understanding the hydrology of tropical Andean ecosystems through an Andean Network of Basins.*

Célleri, R. & Feyen, J. (2009) The hydrology of tropical Andean ecosystems: importance, knowledge status, and perspectives. *Mountain Research and Development.* 29 (4), 350-356.

Centre for Ecology & Hydrology. (2018) *Hydro-JULES.* Available from: https://www.ceh.ac.uk/hydrojules [Accessed 31 Jan 2019].

Chahine, M. T. (1992) The hydrological cycle and its influence on climate. *Nature.* 359 (6394), 373.

Chapman, T. (1999) A comparison of algorithms for stream flow recession and baseflow separation. *Hydrological Processes.* 13 (5), 701-714.

Clark, D. B., Mercado, L. M., Sitch, S., Jones, C. D., Gedney, N., Best, M. J., Pryor, M., Rooney, G. G., Essery, R. & Blyth, E. (2011) The Joint UK Land Environment Simulator (JULES), model description–Part 2: carbon fluxes and vegetation dynamics. *Geoscientific Model Development.* 4 (3), 701-722.

Clark, D. B. & Gedney, N. (2008) Representing the effects of subgrid variability of soil moisture on runoff generation in a land surface model. *Journal of Geophysical Research: Atmospheres.* 113 (D10).

Cosby, B. J., Hornberger, G. M., Clapp, R. B. & Ginn, T. (1984) A statistical exploration of the relationships of soil moisture characteristics to the physical properties of soils. *Water Resources Research.* 20 (6), 682-690.

Cosgrove, B. A., Lohmann, D., Mitchell, K. E., Houser, P. R., Wood, E. F., Schaake, J. C., Robock, A., Marshall, C., Sheffield, J. & Duan, Q. (2003) Real-time and retrospective forcing in the North American Land Data Assimilation System (NLDAS) project. *Journal of Geophysical Research: Atmospheres.* 108 (D22).

Cox, P. M., Betts, R. A., Bunton, C. B., Essery, R., Rowntree, P. R. & Smith, J. (1999) The impact of new land surface physics on the GCM simulation of climate and climate sensitivity. *Climate Dynamics.* 15 (3), 183-203.

Crespo, P. J., Feyen, J., Buytaert, W., Bücker, A., Breuer, L., Frede, H. & Ramírez, M. (2011) Identifying controls of the rainfall–runoff response of small catchments in the tropical Andes (Ecuador). *Journal of Hydrology.* 407 (1-4), 164-174.

Dharssi, I., Vidale, P. L., Verhoef, A., Macpherson, B., Jones, C. & Best, M. (2009) New soil physical properties implemented in the Unified Model at PS18.

DIVA-GIS. (2019) *Free Spatial Data by Country.* Available from: https://www.diva-gis.org/gdata.

Dorel, M., Roger-Estrade, J., Manichon, H. & Delvaux, B. (2000) Porosity and soil water properties of Caribbean volcanic ash soils. *Soil use and Management.* 16 (2), 133-140.

Dunderdale, M., Muller, J. P. & Cox, P. (2000) Sensitivity of the Hadley Centre climate model to different earth observation and cartographically derived land surface data-sets. *The Contribution of POLDER and New Generation Spaceborne Sensors to Global Change Studies, Meribel, France.* pp.1–6.

Fao/Iiasa/Isric/Isscas/Jrc. (2012) Harmonized world soil database (version 1.2). *FAO, Rome, Italy and IIASA, Laxenburg, Austria.*

Farley, K. A., Jobbágy, E. G. & Jackson, R. B. (2005) Effects of afforestation on water yield: a global synthesis with implications for policy. *Global Change Biology.* 11 (10), 1565-1576.

Fischer, G., van Velthuizen, H. T. & Nachtergaele, F. O. (2000) Global agro-ecological zones assessment: methodology and results.

Fisher, D. K. & Gould, P. J. (2012) Open-source hardware is a low-cost alternative for scientific instrumentation and research. *Modern Instrumentation.* 1 (02), 8.

Foley, J. A., DeFries, R., Asner, G. P., Barford, C., Bonan, G., Carpenter, S. R., Chapin, F. S., Coe, M. T., Daily, G. C. & Gibbs, H. K. (2005) Global consequences of land use. *Science.* 309 (5734), 570-574.

Friedl, M. A. & Sulla-Menashe, D. (2015) *MCD12Q1 MODIS/Terra+Aqua Land Cover Type Yearly L3 Global 500m SIN Grid V006.* NASA EOSDIS Land Processes DAAC.

Fuchs, R., Herold, M., Verburg, P. H. & Clevers, J. (2012) A high-resolution and harmonized model approach for reconstructing and analyzing historic land changes in Europe.

Gura, T. (2013) Citizen science: amateur experts. *Nature.* 496 (7444), 259-261.

Guzha, A. C., Rufino, M. C., Okoth, S., Jacobs, S. & Nóbrega, R. (2018a) Impacts of land use and land cover change on surface runoff, discharge and low flows: Evidence from East Africa. *Journal of Hydrology: Regional Studies.* 15 49-67.

Guzha, A. C., Rufino, M. C., Okoth, S., Jacobs, S. & Nóbrega, R. (2018b) Impacts of land use and land cover change on surface runoff, discharge and low flows: Evidence from East Africa. *Journal of Hydrology: Regional Studies.* 15 49-67.

Haklay, M. (2013) Citizen Science and Volunteered Geographic Information: Overview and Typology of Participation. In: Anonymous *Crowdsourcing Geographic Knowledge.* 2012th edition. Dordrecht, Springer Netherlands. pp. 105-122.

Hansen, M. C., Potapov, P. V., Moore, R., Hancher, M., Turubanova, S., Tyukavina, A., Thau, D., Stehman, S. V., Goetz, S. J. & Loveland, T. R. (2013) High-resolution global maps of 21st-century forest cover change. *Science.* 342 (6160), 850-853.

Harden, C. P. (2006) Human impacts on headwater fluvial systems in the northern and central Andes. *Geomorphology.* 79 (3-4), 249-263.

Harper, A. B., Cox, P. M., Friedlingstein, P., Wiltshire, A. J., Jones, C. D., Sitch, S., Mercado, L. M., Groenendijk, M. & Reich, P. B. (2016) Improved representation of plant functional types and physiology in the Joint UK Land Environment Simulator (JULES v4. 2) using plant trait information. *Geoscientific Model Development.* 9 (7), 2415-2440.

Herschy, R. W. (2014) *Streamflow measurement.* CRC Press.

Hodnett, M. G. & Tomasella, J. (2002) Marked differences between van Genuchten soil water-retention parameters for temperate and tropical soils: a new water-retention pedo-transfer functions developed for tropical soils. *Geoderma.* 108 (3-4), 155-180.

Hou, A. Y., Kakar, R. K., Neeck, S., Azarbarzin, A. A., Kummerow, C. D., Kojima, M., Oki, R., Nakamura, K. & Iguchi, T. (2014) The global precipitation measurement mission. *Bulletin of the American Meteorological Society.* 95 (5), 701-722.

Houldcroft, C. J., Grey, W. M., Barnsley, M., Taylor, C. M., Los, S. O. & North, P. R. (2009) New vegetation albedo parameters and global fields of soil background albedo derived from MODIS for use in a climate model. *Journal of Hydrometeorology.* 10 (1), 183-198.

Huffman, G. J., Bolvin, D. T., Nelkin, E. J., Wolff, D. B., Adler, R. F., Gu, G., Hong, Y., Bowman, K. P. & Stocker, E. F. (2007) The TRMM multisatellite precipitation analysis (TMPA): Quasi-global, multiyear, combined-sensor precipitation estimates at fine scales. *Journal of Hydrometeorology.* 8 (1), 38-55.

JULES. (2018) *JULES version 5.3 Release Notes.* Available from: http://jules-lsm.github.io/vn5.3/release_notes/JULES5-3.html [Accessed 4th November 2018].

Kalnay, E., Kanamitsu, M., Kistler, R., Collins, W., Deaven, D., Gandin, L., Iredell, M., Saha, S., White, G. & Woollen, J. (1996) The NCEP/NCAR 40-year reanalysis project. *Bulletin of the American Meteorological Society.* 77 (3), 437-472.

Kanamitsu, M., Ebisuzaki, W., Woollen, J., Yang, S., Hnilo, J. J., Fiorino, M. & Potter, G. L. (2002) NCEP–DOE AMIP-II Reanalysis (R-2). *Bulletin of the American Meteorological Society.* 83 (11), 1631-1643. Available from: doi: 10.1175/BAMS-83-11-1631(2002)0832.3.CO;2.

Lambin, E. F. & Meyfroidt, P. (2011) Global land use change, economic globalization, and the looming land scarcity. *Proceedings of the National Academy of Sciences.* 108 (9), 3465-3472.

Le Maitre, D. C., Scott, D. F. & Colvin, C. (1999) Review of information on interactions between vegetation and groundwater.

Le Vine, N., Butler, A., McIntyre, N. & Jackson, C. (2016) Diagnosing hydrological limitations of a land surface model: application of JULES to a deep-groundwater chalk basin. *Hydrology and Earth System Sciences.* 20 (1), 143-159.

Lehner, B. & Grill, G. (2013) Global river hydrography and network routing: baseline data and new approaches to study the world's large river systems. *Hydrological Processes.* 27 (15), 2171-2186.

Lehner, B., Verdin, K. & Jarvis, A. (2008) New global hydrography derived from spaceborne elevation data. *Eos, Transactions American Geophysical Union.* 89 (10), 93-94.

Löffler-Mang, M. & Joss, J. (2000) An optical disdrometer for measuring size and velocity of hydrometeors. *Journal of Atmospheric and Oceanic Technology.* 17 (2), 130-139.

MacKellar, N. C., Dadson, S. J., New, M. & Wolski, P. (2013) Evaluation of the JULES land surface model in simulating catchment hydrology in Southern Africa. *Hydrology and Earth System Sciences Discussions.* 10 (8), 11093-11128.

Marthews, T. R., Quesada, C. A., Galbraith, D. R., Malhi, Y., Mullins, C. E., Hodnett, M. G. & Dharssi, I. (2014) High-resolution hydraulic parameter maps for surface soils in tropical South America. *Geoscientific Model Development.* 7 (3), 711-723.

Mas, J., Kolb, M., Paegelow, M., Olmedo, M. T. C. & Houet, T. (2014) Inductive pattern-based land use/cover change models: A comparison of four software packages. *Environmental Modelling & Software.* 51 94-111.

McIntyre, N., Ballard, C., Bruen, M., Bulygina, N., Buytaert, W., Cluckie, I., Dunn, S., Ehret, U., Ewen, J. & Gelfan, A. (2014) Modelling the hydrological impacts of rural land use change. *Hydrology Research.* 45 (6), 737-754.

Molina, A., Govers, G., Vanacker, V., Poesen, J., Zeelmaekers, E. & Cisneros, F. (2007) Runoff generation in a degraded Andean ecosystem: Interaction of vegetation cover and land use. *Catena.* 71 (2), 357-370.

Molina, A., Vanacker, V., Balthazar, V., Mora, D. & Govers, G. (2012) Complex land cover change, water and sediment yield in a degraded Andean environment. *Journal of Hydrology.* 472 25-35.

Moore, R. J. (1985) The probability-distributed principle and runoff production at point and basin scales. *Hydrological Sciences Journal.* 30 (2), 273-297.

Moulds, S., Buytaert, W. & Mijic, A. (2018) A spatio-temporal land use and land cover reconstruction for India from 1960–2010. *Scientific Data.* 5 180159.

Moulds, S., Buytaert, W. & Mijic, A. (2015) An open and extensible framework for spatially explicit land use change modelling: the lulcc R package. *Geoscientific Model Development.* 8 (10), 3215-3229.

Nash, J. E. & Sutcliffe, J. V. (1970) River flow forecasting through conceptual models part I—A discussion of principles. *Journal of Hydrology.* 10 (3), 282-290.

Ochoa-Tocachi, B. F., Buytaert, W. & De Bièvre, B. (2016) Regionalization of land-use impacts on streamflow using a network of paired catchments. *Water Resources Research.* 52 (9), 6710-6729.

Ochoa-Tocachi, B. F., Buytaert, W., De Bièvre, B., Célleri, R., Crespo, P., Villacís, M., Llerena, C. A., Acosta, L., Villazón, M. & Guallpa, M. (2016) Impacts of land use on the hydrological response of tropical Andean catchments. *Hydrological Processes.* 30 (22), 4074-4089.

Ochoa-Tocachi, B. F., Buytaert, W., Antiporta, J., Acosta, L., Bardales, J. D., Célleri, R., Crespo, P., Fuentes, P., Gil-Ríos, J. & Guallpa, M. (2018) High-resolution hydrometeorological data from a network of headwater catchments in the tropical Andes. *Scientific Data.* 5 180080.

Olden, J. D. & Poff, N. L. (2003) Redundancy and the choice of hydrologic indices for characterizing streamflow regimes. *River Research and Applications.* 19 (2), 101-121.

Osborne, T., Gornall, J. L., Hooker, J., Williams, K., Wiltshire, A., Betts, R. A. & Wheeler, T. (2015) JULES-crop: a parametrisation of crops in the Joint UK Land Environment Simulator. *Geoscientific Model Development.* 8 (4), 1139-1155.

Overdevest, C., Orr, C. H. & Stepenuck, K. (2004) Volunteer stream monitoring and local participation in natural resource issues. *Human Ecology Review.* 177-185.

Paul, J. D., Buytaert, W., Allen, S., Ballesteros-Cánovas, J. A., Bhusal, J., Cieslik, K., Clark, J., Dugar, S., Hannah, D. M. & Stoffel, M. (2018) Citizen science for hydrological risk reduction and resilience building. *Wiley Interdisciplinary Reviews: Water.* 5 (1), e1262.

Pitman, A. J., de Noblet-Ducoudré, N., Cruz, F. T., Davin, E. L., Bonan, G. B., Brovkin, V., Claussen, M., Delire, C., Ganzeveld, L. & Gayler, V. (2009) Uncertainties in climate responses to past land cover change: First results from the LUCID intercomparison study. *Geophysical Research Letters.* 36 (14), .

Pontius, R. G. & Parmentier, B. (2014) Recommendations for using the relative operating characteristic (ROC). *Landscape Ecology.* 29 (3), 367-382.

Poulenard, J., Podwojewski, P., Janeau, J. & Collinet, J. (2001) Runoff and soil erosion under rainfall simulation of Andisols from the Ecuadorian Páramo: effect of tillage and burning. *Catena.* 45 (3), 185-207.

Rosa, I. M., Ahmed, S. E. & Ewers, R. M. (2014) The transparency, reliability and utility of tropical rainforest land-use and land-cover change models. *Global Change Biology.* 20 (6), 1707-1722.

Royem, A. A., Mui, C. K., Fuka, D. R. & Walter, M. T. (2012) Proposing a low-tech, affordable, accurate stream stage monitoring system. *Transactions of the ASABE.* 55 (6), 2237-2242.

Scheffler, R., Neill, C., Krusche, A. V. & Elsenbeer, H. (2011) Soil hydraulic response to land-use change associated with the recent soybean expansion at the Amazon agricultural frontier. *Agriculture, Ecosystems & Environment.* 144 (1), 281-289.

Sheffield, J., Goteti, G. & Wood, E. F. (2006) Development of a 50-year high-resolution global dataset of meteorological forcings for land surface modeling. *Journal of Climate.* 19 (13), 3088-3111.

Silvertown, J. (2009) A new dawn for citizen science. *Trends in Ecology & Evolution.* 24 (9), 467-471.

Sing, T., Sander, O., Beerenwinkel, N. & Lengauer, T. (2005) ROCR: visualizing classifier performance in R. *Bioinformatics.* 21 (20), 3940-3941.

Singh, R., Wagener, T., Werkhoven, K. v., Mann, M. E. & Crane, R. (2011) A trading-space-for-time approach to probabilistic continuous streamflow predictions in a changing climate–accounting for changing watershed behavior. *Hydrology and Earth System Sciences.* 15 (11), 3591-3603.

Therneau, T. M. & Atkinson, E. J. (2019) *An introduction to recursive partitioning using the RPART routines.* Available from: https://cran.r-project.org/web/packages/rpart/vignettes/longintro.pdf .

Tomasella, J. & Hodnett, M. G. (1998) Estimating soil water retention characteristics from limited data in Brazilian Amazonia. *Soil Science.* 163 (3), 190-202.

Turner, B. L., Meyer, W. B. & Skole, D. L. (1994) Global land-use/land-cover change: towards an integrated study. *Ambio.Stockholm.* 23 (1), 91-95.

Turner, B. L., Lambin, E. F. & Reenberg, A. (2007) The emergence of land change science for global environmental change and sustainability. *Proceedings of the National Academy of Sciences.* 104 (52), 20666-20671.

Urrutia, R. & Vuille, M. (2009) Climate change projections for the tropical Andes using a regional climate model: Temperature and precipitation simulations for the end of the 21st century. *Journal of Geophysical Research: Atmospheres.* 114 (D2).

Van Genuchten, M. T. (1980) A closed-form equation for predicting the hydraulic conductivity of unsaturated soils 1. *Soil Science Society of America Journal.* 44 (5), 892-898.

Veldkamp, A. & Lambin, E. F. (2001) Predicting land-use change. *Agriculture, Ecosystems and Environment.* 85 (1), 1-6. Available from: https://www.sciencedirect.com/science/article/pii/S0167880901001992. Available from: doi: 10.1016/S0167-8809(01)00199-2.

Verburg, P. H., Soepboer, W., Veldkamp, A., Limpiada, R., Espaldon, V. & Mastura, S. S. (2002) Modeling the spatial dynamics of regional land use: the CLUE-S model. *Environmental Management.* 30 (3), 391-405.

Viviroli, D., Dürr, H. H., Messerli, B., Meybeck, M. & Weingartner, R. (2007) Mountains of the world, water towers for humanity: Typology, mapping, and global significance. *Water Resources Research.* 43 (7).

Williams, K., Gornall, J., Harper, A., Wiltshire, A., Hemming, D., Quaife, T., Arkebauer, T. & Scoby, D. (2017) Evaluation of JULES-crop performance against site observations of irrigated maize from Mead, Nebraska.

Wohl, E., Barros, A., Brunsell, N., Chappell, N. A., Coe, M., Giambelluca, T., Goldsmith, S., Harmon, R., Hendrickx, J. M. & Juvik, J. (2012) The hydrology of the humid tropics. *Nature Climate Change.* 2 (9), 655.

Zhang, L., Dawes, W. R. & Walker, G. R. (2001) Response of mean annual evapotranspiration to vegetation changes at catchment scale. *Water Resources Research.* 37 (3), 701-708.

Zhang, L., Walker, G. R. & Dawes, W. (1999) Predicting the effect of vegetation changes on catchment average water balance.

Zulkafli, Z., Buytaert, W., Onof, C., Lavado, W. & Guyot, J. (2013) A critical assessment of the JULES land surface model hydrology for humid tropical environments. *Hydrology and Earth System Sciences.* 17 (3), 1113-1132.